

The Mechanics of Earthquake Rupture.

J. R. RICE

Division of Engineering, Brown University - Providence, R. I. 02912

Published in: Physics of the Earth's Interior

(Proc. Int'l. School of Physics "E. Fermi", Course 78, 1979), eds. A. M. Dziewonski and E. Boschi, Italian Physical Society / North Holland Publ. Co., 1980.

I. - Introduction.

For purposes of this presentation it is convenient to divide considerations of the mechanics of earthquake rupture into three areas. These form the major parts of the paper. The areas are closely interrelated, and are:

i) *Representation of elastic field generated by earthquakes.* Here the concern is with relating the elastic field generated at points throughout the Earth to the location, orientation and relative motion along a fault. This is the main business of classical seismology. Its relevance to understanding the destructive effects of earthquakes is clear. Most importantly it enables in an inverse sense the interpretation of seismological observations in terms of the location and overall tectonic pattern of earthquake activity and, when observations can be made with sufficient accuracy over wide frequency ranges, of the time-dependent, and sometimes spatially discontinuous, processes by which rupture propagates in the Earth. An elegant general framework can be constructed for this representation based on classical elastodynamics. This is given in part I of the paper. However, the representation is essentially kinematical in nature. It enables the computation of elastic displacement fields generated by displacement discontinuities on faults and by distributed inelastic strains, or, in a limited inverse sense, the inference of such source processes from seismograph records. It does not address directly the rupture process itself.

ii) *Fundamentals of the rupture process in geological materials.* Earthquakes result from catastrophic reductions in the capacity of material to sustain stress. The concern in part II is with a fundamental description of this weakening process, *i.e.* of the fracture process. In part, this involves extension of the techniques and viewpoints of tensile crack mechanics to shear rupture. Also of interest is the inelastic and, ultimately, strain-softening response of stressed rock masses, the reductions of shear strength with ongoing slip of perhaps partially cemented fault surfaces in frictional contact, and the time or rate

dependence of these processes due, for example, to mechanical and chemical effects of infiltrating pore fluids. To the extent that deformation processes preceding seismic rupture lead to direct (*e.g.* accelerating creep, foreshocks) or indirect (*e.g.* acoustic, pore pressure, electrical or magnetic property alterations) manifestations, there is an obvious relevance of studies in this area to the prediction of impending rupture.

iii) *Processes on a tectonic scale leading to earthquake instabilities.* The concern in part III is with the description of the tectonic loading process itself. This includes the manner in which previous faulting has led to present concentrations of stress, and also the time dependence of these stress distributions that arises from overall tectonic motions and, for example, from accommodation to prior fault motions by viscous relaxation processes in the upper mantle. Such considerations are of importance to understanding the transmission of earthquake activity along plate boundaries, including the filling-in of seismic gaps, and hence to long-term aspects of earthquake prediction.

Briefly, area iii) is concerned with specifying the loading, area ii) with the inelastic response of fault regions to this loading and area i) with the resulting radiation of elastic disturbances.

The treatment of each area is necessarily limited in scope, and the reader will wish to consult a number of references for more detailed discussions. Some of the more central works are listed here; many others are cited in passing. What seems likely to become the standard reference for topic i) is a soon to be published book by AKI and RICHARDS [1] on quantitative seismology. This discusses Green's function and double-couple representations, ray theory and the relation of seismic spectra to the kinematics of fault motion. See also the related papers by BURRIDGE and KNOPOFF [2], KOSTROV [3] and DAS and AKI [4]. The book by ACHENBACH [5] is a general source on elastodynamics.

For topic ii), a basic source for crack mechanics is provided by an article by RICE [6]; also, FREUND [7] has summarized studies on the dynamics of crack propagation (AKI and RICHARDS [1] also discuss the dynamics of shear cracks) and RUDNICKI [8] has recently reviewed the application of fracture mechanics to the Earth's crust. Two recent special issues of journals, based essentially on U.S.G.S.-convened symposia, provide good summaries of current work on other aspects of topic ii): An issue of the *Journal of Geophysical Research* [9] is devoted to fault mechanics, and includes theoretical contributions on models for earthquake instabilities and related precursory processes, including those due to pore fluids, and on dynamic rupture propagation, as well as experimental studies of friction and fault formation. The latter topics are the major theme of an issue of *Pure and Applied Geophysics* [10] on rock friction and earthquake prediction, which is devoted mainly to experimental studies of rock deformation, friction and fracture. A summary of work on instability

models with emphasis on quasi-static processes precursory to rupture is given by RICE [11].

For topic iii) there appears to be less available in the way of general sources, although, of course, the vast literature on plate tectonics provides an overall framework. ANDERSON [12] has discussed the implications of a model of an elastic plate riding on a viscous asthenosphere for migration of earthquake activity along plate boundaries and earthquake recurrence times. Also, BUDIANSKY and AMAZIGO [13] and TURCOTTE *et al.* [14] analyze models for cyclic earthquake processes of stress release in crustal faulting followed by gradual stress build-up through viscoelastic relaxation at depth. A summary of observational studies of seismic gap zones and tectonic patterns of earthquake migration is provided by the report of a recent U.S.G.S. symposium [15].

PART I

Representation of elastic fields generated by faulting.

2. — General theory, Green's function and double-couple representations.

The equations of motion for a continuum are

$$(2.1) \quad \partial \sigma_{\alpha\beta} / \partial x_{\alpha} + f_{\beta} = \rho \partial^2 u_{\beta} / \partial t^2,$$

where f is the body force, u the displacement and σ the stress. In the case of linear elasticity σ is related to strain ϵ by

$$(2.2) \quad \sigma_{\alpha\beta} = C_{\alpha\beta\gamma\delta} \epsilon_{\gamma\delta} \quad \text{with } 2\epsilon_{\gamma\delta} = \partial u_{\gamma} / \partial x_{\delta} + \partial u_{\delta} / \partial x_{\gamma}.$$

The modulus tensor satisfies $C_{\alpha\beta\gamma\delta} = C_{\beta\alpha\gamma\delta} = C_{\alpha\beta\delta\gamma} = C_{\gamma\delta\alpha\beta}$ (the last following from existence of a strain energy function) so that the equations of motion are

$$(2.3) \quad \partial (C_{\alpha\beta\gamma\delta} \partial u_{\gamma} / \partial x_{\delta}) / \partial x_{\alpha} + f_{\beta} = \rho \partial^2 u_{\beta} / \partial t^2.$$

When the material is isotropic

$$(2.4) \quad C_{\alpha\beta\gamma\delta} \epsilon_{\gamma\delta} = 2G\epsilon_{\alpha\beta} + \Lambda\delta_{\alpha\beta}\epsilon_{\gamma\gamma},$$

where G is the shear modulus and $\Lambda + 2G/3$ is the bulk modulus.

The solution for a distribution of body force $f_{\beta}(\mathbf{x}, t)$ in a material with time-invariant elastic properties, that meets homogeneous boundary conditions (*e.g.* zero tractions on the Earth's surface), can be written as

$$(2.5) \quad u_{\nu}(\mathbf{x}, t) = \int_{-\infty}^t \int_V G_{\nu\beta}(\mathbf{x}, \mathbf{x}', t-t') f_{\beta}(\mathbf{x}', t) d^3\mathbf{x}' dt',$$

where V is the region occupied by the body and $G_{\nu\beta}$ is the Green's function. Plainly, $G_{\nu\beta}$ solves the problem, with homogeneous boundary conditions, of a unit impulsive point force applied at \mathbf{x}' , t' in direction β ; $G_{\nu\beta} = 0$ for $t < t'$. Frequently, in interpreting seismological records, it is convenient to deal with a Fourier transform of the received disturbance and if

$$(2.6) \quad \tilde{g}(\mathbf{x}, \omega) = \int_{-\infty}^{+\infty} g(\mathbf{x}, t) \exp[-i\omega t] dt$$

defines the transform operation, then

$$(2.7) \quad \tilde{u}_\nu(\mathbf{x}, \omega) = \int_V \tilde{G}_{\nu\beta}(\mathbf{x}, \mathbf{x}', \omega) \tilde{f}_\beta(\mathbf{x}', \omega) d^3 \mathbf{x}'$$

(the transform of a time convolution of two functions equals the product of their transforms).

Disturbances generated by the nonelastic deformation of matter can be represented by a distribution of « transformation » strain (e.g. [1, 16, 17]) $\boldsymbol{\varepsilon}^T(\mathbf{x}, t)$, such that $\boldsymbol{\varepsilon}^T$ is the strain corresponding instantaneously to the stress-free state, i.e.

$$(2.8) \quad \sigma_{\alpha\beta}^T = C_{\alpha\beta\gamma\delta}(\varepsilon_{\gamma\delta} - \varepsilon_{\gamma\delta}^T).$$

When this is substituted into the equations of motion (2.1), with $\mathbf{f} = 0$, there results equations for \mathbf{u} in the same form as (2.3) but with \mathbf{f} replaced by an « effective » body force

$$(2.9) \quad f_\beta^{\text{eff}} = -\partial(C_{\alpha\beta\gamma\delta}\varepsilon_{\gamma\delta}^T)/\partial x_\alpha.$$

The quantity in parentheses plays a fundamental role in the theory of seismic sources. We define it as the « seismic moment density tensor » $m_{\alpha\beta}$, i.e.

$$(2.10) \quad m_{\alpha\beta}(\mathbf{x}, t) = C_{\alpha\beta\gamma\delta}(\mathbf{x}) \varepsilon_{\gamma\delta}^T(\mathbf{x}, t),$$

and the « seismic moment » tensor $M_{\alpha\beta}$ is defined as

$$(2.11) \quad M_{\alpha\beta}(t) = \int_V m_{\alpha\beta}(\mathbf{x}, t) d^3 \mathbf{x}.$$

(The concept of a moment tensor is due to KOSTROV [3], who dealt with the special case to which (2.10), (2.11) will be seen to reduce when the transformation is generated by a surface of displacement discontinuity; the generalization to distributed volume sources is due to BACKUS and MULCAHY [17].)

Substitution of f_{β}^{eff} of (2.9) into (2.5) shows, after an integration by parts (in which we assume that ϵ^T vanishes on the surface of the body), that the displacement field generated by ϵ^T is

$$(2.12) \quad u_{\nu}(\mathbf{x}, t) = \int_{\mathcal{V}} \int_{-\infty}^t [\partial G_{\nu\beta}(\mathbf{x}, \mathbf{x}', t-t') / \partial x'_{\alpha}] m_{\alpha\beta}(\mathbf{x}', t') dt' d^3\mathbf{x}' .$$

2'1. *Double couples.* - The derivative $\partial G_{\nu\beta} / \partial x'_{\alpha}$ which appears here is the response u_{ν} to a certain impulsive force dipole or couple. This response is generated, in the limit as $h \rightarrow 0$, by a pair of oppositely directed impulses of the same magnitude $1/h$, one in the negative β -direction at point \mathbf{x}' and the other in the positive β -direction at a point removed from \mathbf{x}' by distance h in the α -direction. Examples of generating impulses are shown in fig. 1a), b).

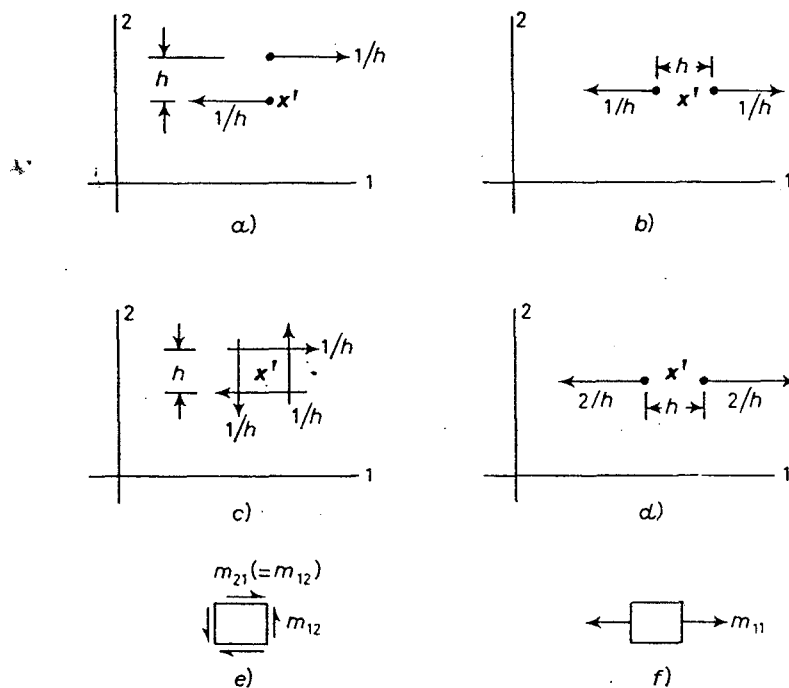


Fig. 1. - a, b) Impulse couples: a) $u_{\nu} = \partial G_{\nu 1} / \partial x'_{2}$, b) $u_{\nu} = \partial G_{\nu 1} / \partial x'_{1}$. c, d) Double couples without moment: c) $u_{\nu} = H_{\nu 12}(=H_{\nu 21})$, d) $u_{\nu} = H_{\nu 11}$. e, f) Relation to release of constraint stresses.

However, because $C_{\alpha\beta\gamma\delta} = C_{\beta\alpha\gamma\delta}$ (i.e. because the stress tensor is symmetric), $m_{\alpha\beta}$ is symmetric, and hence these dipole responses never occur singly but rather as the combination of terms

$$(2.13) \quad H_{\nu\alpha\beta}(\mathbf{x}, \mathbf{x}', t-t') = \partial G_{\nu\beta} / \partial x'_{\alpha} + \partial G_{\nu\alpha} / \partial x'_{\beta} .$$

$H_{\nu\alpha\beta}$ is referred to as the response u_ν to a double couple without moment, because it is generated by a pair of impulsive force dipoles of the type just described, which are such that their net moment is zero. Examples are shown in fig. 1c) and d).

Hence (2.12) can be written as

$$(2.14) \quad u_\nu(\mathbf{x}, t) = \frac{1}{2} \int_V \int_{-\infty}^t H_{\nu\alpha\beta}(\mathbf{x}, \mathbf{x}', t-t') m_{\alpha\beta}(\mathbf{x}', t') dt' d^3\mathbf{x}' .$$

The formula has a simple logic which can be explained in terms of Eshelby's [16] approach to transformation problems. At each instant of time one could identify a set of constraining stresses which would have the effect of annulling $\boldsymbol{\epsilon}^T$ by elastic deformation, *i.e.* of making $\boldsymbol{\epsilon} = 0$, if they were the only stresses acting. From (2.8) and (2.10), this constraining stress field is just $-m_{\alpha\beta}$. But there is no source for such constraining stresses and hence we may regard the displacement field as being generated by application to the body of an effective force system equivalent to their removal, as in fig. 1e) and f), and the association with corresponding types of double-couple response is clear.

2.2. Surfaces of displacement discontinuity. — Typically rupture is modelled as the development of a displacement discontinuity $\Delta\mathbf{u}(\mathbf{x}, t)$ on a surface or collection of surfaces S . Let the sides of S be noted $+$ and $-$, so that $\Delta\mathbf{u} = \mathbf{u}^+ - \mathbf{u}^-$, and let \mathbf{n} be the local unit normal to S , directed from $-$ to $+$. We can deal with this case as the zero-thickness limit of transformation strain in a thin layer coinciding with S ; $\boldsymbol{\epsilon}^T$ must be of order $\Delta\mathbf{u}$ divided by the layer thickness, and hence become Dirac singular in the limit. In particular, if δV is some small volume element intersected by δS of the surface,

$$(2.15) \quad \int_{\delta V} \boldsymbol{\epsilon}_{\alpha\beta}^T d^3\mathbf{x} = \frac{1}{2}(n_\alpha \Delta u_\beta + n_\beta \Delta u_\alpha) \delta S .$$

Hence, along S we write

$$(2.16) \quad m_{\alpha\beta}(\mathbf{x}, t) = C_{\alpha\beta\gamma\delta}(\mathbf{x}) \epsilon_{\gamma\delta}(\mathbf{x}, t) = C_{\alpha\beta\gamma\delta}(\mathbf{x}) n_\gamma(\mathbf{x}) \Delta u_\delta(\mathbf{x}, t) \delta_D(S) ,$$

where $\delta_D(S)$ is a surface Dirac function, converting any volume integral over a region intersected by some part of S to a surface integral over that part of S . Thus, for example, when transformations are limited to such surface discontinuities, (2.12) becomes

$$(2.17) \quad u_\nu(\mathbf{x}, t) = \int_{-\infty}^t \int_S \frac{\partial G_{\nu\beta}}{\partial x'_\alpha}(\mathbf{x}, \mathbf{x}', t-t') C_{\alpha\beta\gamma\delta}(\mathbf{x}') n_\gamma(\mathbf{x}') \Delta u_\delta(\mathbf{x}', t') d^2\mathbf{x}' dt' .$$

For simplicity of presentation, however, \mathbf{u} is generally written in the volume

integral form of (2.12) or (2.14), where we understand that m may contain both volume and (Dirac singular) surface contributions.

An alternate way of deriving (2.17) (the alternate derivation could also be extended to volume sources) is due to DEHOOP [18] and is discussed by AKI and RICHARDS [1]. It involves two applications of elastic reciprocity (actually, these are essentially self-cancelling; as shown by the above derivation, the result does not rely on the source of the reciprocal theorem, namely that $C_{\alpha\beta\gamma\delta} = C_{\gamma\delta\alpha\beta}$, and would be valid even if this condition were not met). The first relates the worklike convolution integral of a concentrated force at x with the displacement produced by the motion Δu on S to the convolution of stresses produced by the concentrated force on the motion Δu at points x' of S . The second uses source point-receiver point symmetry of $G_{r\beta}$, stemming from reciprocity, to put the source points of $G_{r\beta}$ along S and the field point at x . The method adopted here, based on [17], is a simple generalization of the Duhamel analogy in thermoelasticity (*e.g.* [19]), in which thermal strains are regarded as the source of effective body forces and, as remarked, is similar in concept to a formulation by ESHELBY [16] of the elastostatic problem of an inclusion undergoing a shape transformation, as well as to various formulations of elastic-plastic stress analysis. The static version of (2.17) for a homogeneous medium stems from the early work of Volterra and has been used widely in the theory of crystal dislocations (in which case typically Δu is constant and S is flat, so that the representation can be reduced to a line integral around the boundary of S). NABARRO [20] gave the corresponding dynamical version of (2.17) for moving crystal dislocations, and this was first adapted to the earthquake context by VVEDENSKAYA [21], who showed the double-couple equivalence of point sources of slip, later discussed in the context of the representation (2.17) by BURRIDGE and KNOPOFF [2]. STEKETEE [22] made use of static dislocation representations for displacements produced by faulting.

2'3. *Point source representation; fault plane solutions.* — Equation (2.14) may be written analogously to (2.7) as a relation between Fourier transforms of u and the source field m . When the receiver point is distant from the source region, and when sufficiently low frequencies are considered (*i.e.* associated with wavelengths that are large compared to source dimensions), one may take any representative point within the source zone for x' and take $\tilde{H}_{r\alpha\beta}$ outside of the integral. This is equivalent to a point source representation and one obtains

$$(2.18) \quad \tilde{u}_r(\mathbf{x}, \omega) = \frac{1}{2} \tilde{H}_{r\alpha\beta}(\mathbf{x}, \mathbf{x}', \omega) \tilde{M}_{\alpha\beta}(\omega),$$

where $M_{\alpha\beta}(t)$ is defined by (2.11); specifically,

$$(2.19) \quad M_{\alpha\beta} = \int_S C_{\alpha\beta\delta\gamma} n_\gamma \Delta u_\delta d^2 x' + \int_V C_{\alpha\beta\gamma\delta} \epsilon_{\gamma\delta}^T d^3 x',$$

when the surface and volume contributions are written out explicitly. In typical cases the rupture propagates at speeds comparable to an elastic-wave speed, so that motion in the source region has effectively stopped at times comparable to the long periods for which the above point source representation is valid. Hence what is effectively measured from the low-frequency portion of the spectrum received at distant stations is the value of $M_{\alpha\beta}$ at the completion of the rupture process, and frequently the term seismic moment is reserved for this long-time value. It is the basic observable from distant low-frequency recordings and, of course, contains only limited information about the rupture process.

For the special case when the medium is isotropic and the motion consists of slip Δu on S (*i.e.* $n \cdot \Delta u = 0$)

$$(2.20) \quad M_{\alpha\beta} = \int_S G(n_\alpha \Delta u_\beta + n_\beta \Delta u_\alpha) dS.$$

When S is flat, $M_{\alpha\beta}$ has components relative to a set of axes with x_1 in the average slip direction (*i.e.* direction of $\int_S G \Delta u dS$) and x_2 in the direction of n which are

$$(2.21) \quad (M_{\alpha\beta}) = \begin{pmatrix} 0 & M & 0 \\ M & 0 & 0 \\ 0 & 0 & 0 \end{pmatrix}, \quad M = \int_S G \Delta u_1 dS.$$

The result is illustrated in fig. 2a), where (see sect. 3) directions of the displacement radiation are shown.

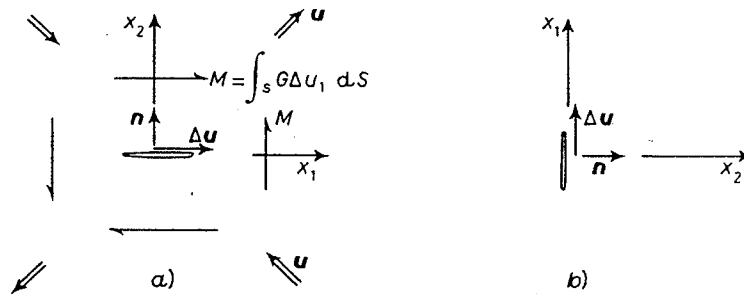


Fig. 2. - a) Nonvanishing components of seismic moment tensor ($M_{12} = M_{21} = M$) and pattern of displacement for a point source model of a slipping fault. b) Indistinguishable fault event for point source model.

Since the components of $M_{\alpha\beta}$ (on some fixed set of axes) can in principle be determined from far-field seismological observations based on (2.18), these observations suffice to determine M and two candidate directions for x_1 and x_2 , although the observations, interpreted in terms of the point source model,

do not determine which of these coincides with \mathbf{n} and which with the average slip direction (compare fig. 2*a*) and *b*). The process is referred to as the determination of the earthquake mechanism solution, or the fault plane solution, and has been reviewed by BALAKINA *et al.* [23] and KHATTRI [24]. In practice the Green's function cannot be fully constructed. Instead a homogeneous, isotropic material model is used for the near field and corrected for inhomogeneities over large propagation distances by methods of ray theory. These latter methods are not discussed here. The reader is referred to the account by STACEY [25] for elements of the ray method and travel time results for the Earth, to AKI and RICHARDS [1] and ACHENBACH [5] for the underlying theory and limitations of ray calculations, and to KHATTRI [24] for their use in determining fault plane solutions from distant seismological observations. Values of M for approximately 60 great earthquakes are summarized by KANAMORI [26], in connection with an earthquake magnitude scale based on $\log M$. (Actually, KANAMORI proposes an earthquake energy parameter as the fundamental basis for this scale, but the energy parameter is not directly measurable and, in the end, is simply assumed to be proportional to M .)

3. - Results for homogeneous isotropic solids.

For homogeneous unbounded bodies $G_{\nu\beta}(\mathbf{x}, \mathbf{x}', t - t') = G_{\nu\beta}(\mathbf{x} - \mathbf{x}', t - t')$, and this also applies for finite bodies at times prior to wave reflections from boundaries. Further, when the material is isotropic ($C_{\alpha\beta\gamma\delta}$ given by eq. (2.4)), $G_{\nu\beta}(\mathbf{x}, t)$ satisfies eq. (2.3) in the Navier form

$$(3.1) \quad (\Lambda + G) \partial^2 G_{\nu\beta} / \partial x_\nu \partial x_\alpha + G \nabla^2 G_{\alpha\beta} + \delta_D(t) \delta_D(\mathbf{x}) \delta_{\alpha\beta} = \rho \partial^2 G_{\alpha\beta} / \partial t^2,$$

where δ_D denotes the Dirac function. Defining the full space-time Fourier transform by

$$(3.2) \quad \bar{g}(\mathbf{k}, \omega) = \int_{-\infty}^{+\infty} g(\mathbf{x}, t) \exp[-i\mathbf{k} \cdot \mathbf{x} - i\omega t] dt d^3\mathbf{x}$$

and operating on the equation for $G_{\nu\beta}$, we obtain

$$(3.3) \quad [\rho(c_a^2 - \omega^2/k^2)k_\alpha k_\nu + \rho(c_s^2 - \omega^2/k^2)(\delta_{\alpha\nu}k^2 - k_\alpha k_\nu)] \bar{G}_{\nu\beta} = \delta_{\alpha\beta},$$

where

$$(3.4) \quad c_a = \sqrt{(\Lambda + 2G)/\rho}, \quad c_s = \sqrt{G/\rho}$$

define the dilational and shear wave speeds. The solution for $\bar{G}_{\nu\beta}$ can be written as

$$(3.5) \quad \bar{G}_{\nu\beta} = \bar{G}_{\nu\beta}^a + \bar{G}_{\nu\beta}^s,$$

where

$$(3.6) \quad \begin{cases} \bar{G}_{\nu\beta}^d = k_\nu k_\beta / \rho k^2 (c_a^2 k^2 - \omega^2), \\ \bar{G}_{\nu\beta}^s = (\delta_{\nu\beta} k^2 - k_\nu k_\beta) / \rho k^2 (c_s^2 k^2 - \omega^2). \end{cases}$$

If we now recognize that $k_\nu k_\beta \bar{g}$ is the transform of $-\partial^2 g / \partial x_\nu \partial x_\beta$, the solution for the parts $G_{\nu\beta}^d$ and $G_{\nu\beta}^s$ of $G_{\nu\beta}$ is

$$(3.7) \quad \begin{cases} G_{\nu\beta}^d = -(\partial^2 / \partial x_\nu \partial x_\beta) h(r, t; c_a), \\ G_{\nu\beta}^s = -(\nabla^2 \delta_{\nu\beta} - \partial^2 / \partial x_\nu \partial x_\beta) h(r, t; c_s), \end{cases}$$

where $h(r, t; c)$ is the function whose transform is

$$(3.8) \quad \bar{h}(k, \omega; c) = 1 / \rho k^2 (c^2 k^2 - \omega^2)$$

and, as the notation suggests, this function depends only on the magnitude r of \mathbf{x} .

Using the Fourier inversion theorem and noting that $\mathbf{k} \cdot \mathbf{x} = kr \cos \varphi$, where φ is the angle between \mathbf{k} and \mathbf{x} , and that for the present case one may write « volume » elements in \mathbf{k} space as

$$(3.9) \quad d^3 \mathbf{k} = (2\pi k \sin \varphi) (k d\varphi) dk,$$

we have

$$(3.10) \quad \begin{aligned} h(r, t; c) &= \left(\frac{1}{2\pi}\right)^4 \int_{-\infty}^{+\infty} \int_0^\infty \int_0^\pi \frac{\exp[ikr \cos \varphi + i\omega t]}{\rho k^2 (c^2 k^2 - \omega^2)} (2\pi k^2 \sin \varphi) d\varphi dk d\omega = \\ &= \frac{2}{(2\pi)^3} \int_{-\infty}^{+\infty} \int_0^\infty \frac{\sin(kr) \exp[i\omega t]}{\rho kr (c^2 k^2 - \omega^2)} dk d\omega = \frac{1}{(2\pi)^2 \rho cr} \int_0^\infty \frac{\sin(kr) \sin(kct)}{k^2} dk = \\ &= \begin{cases} t/4\pi cr, & r > ct, \\ 1/4\pi ce, & r < ct. \end{cases} \end{aligned}$$

It is surprising at first sight that this function is nonzero (or nonconstant) for $r > ct$. However, a term in h of the form $t/4\pi cr$ contributes equal but opposite displacements to both $G_{\nu\beta}^d$ and $G_{\nu\beta}^s$ in (3.7), *i.e.* no net displacement, since $\nabla^2(1/r) = 0$. Thus, with no loss of validity of the representation in (3.7), we may *redefine* h by subtracting such a term from it, so that

$$(3.11) \quad h(r, t; c) = -\frac{1}{4\pi cr} (t - r/c) U(t - r/c),$$

where U is the unit step function, and this has the desirable property of making both contributions to $G_{\nu\beta}$ vanish separately when $r > c_a t$. In fact, $G_{\nu\beta}$ also vanishes for $r < c_s t$, has delta-function singularities at $r = c_s t$ and $r = c_a t$, and has a variable structure with r (contributed only by $G_{\nu\beta}^d$) between these outgoing wave fronts.

3.1. *Displacement field generated by rupture.* — For the representation of displacement fields due to earthquake rupture, we are interested in derivatives of $G_{\nu\beta}$ as combined in $H_{\nu\alpha\beta}$ of (2.13) to represent double-couple response. Since $\partial G_{\nu\beta}/\partial x'_\alpha = -\partial G_{\nu\beta}/\partial x_\alpha$ for a homogeneous medium,

$$(3.12) \quad H_{\nu\alpha\beta} = -\partial G_{\nu\alpha}/\partial x_\beta - \partial G_{\nu\beta}/\partial x_\alpha.$$

Thus we may write $H_{\nu\alpha\beta}$ in terms of « d » and « s » contributions,

$$(3.13) \quad H_{\nu\alpha\beta} = H_{\nu\alpha\beta}^d + H_{\nu\alpha\beta}^s,$$

and from (3.7) one finds

$$(3.14) \quad \begin{cases} H_{\nu\alpha\beta}^d = 2(\partial^3/\partial x_\nu \partial x_\alpha \partial x_\beta)h(r, t; c_d), \\ H_{\nu\alpha\beta}^s = [(\delta_{\nu\beta} \partial/\partial x_\alpha + \delta_{\nu\alpha} \partial/\partial x_\beta) \nabla^2 - 2(\partial^3/\partial x_\nu \partial x_\alpha \partial x_\beta)]h(r, t; c_s). \end{cases}$$

Using the representation for $u_\nu(\mathbf{x}, t)$ of (2.14), the result of (3.14) for the double-couple response and symmetry of the seismic moment density tensor, we now obtain the following results for the displacement field:

$$(3.15) \quad u_\nu(\mathbf{x}, t) = u_\nu^d(\mathbf{x}, t) + u_\nu^s(\mathbf{x}, t),$$

where

$$(3.16) \quad \begin{cases} u_\nu^d(\mathbf{x}, t) = \partial^3 \mu_{\alpha\beta}(\mathbf{x}, t; c_d) / \partial x_\nu \partial x_\alpha \partial x_\beta, \\ u_\nu^s(\mathbf{x}, t) = \nabla^2 [\partial \mu_{\nu\beta}(\mathbf{x}, t; c_s) / \partial x_\beta] - \partial^3 \mu_{\alpha\beta}(\mathbf{x}, t; c_s) / \partial x_\nu \partial x_\alpha \partial x_\beta, \end{cases}$$

and where $\mu_{\alpha\beta}(\mathbf{x}, t; c)$ is a tensor set of potentials associated with corresponding members of the moment density tensor, and given by

$$(3.17) \quad \mu_{\alpha\beta}(\mathbf{x}, t; c) = \int_V \int_{-\infty}^t h(r, t-t'; c) m_{\alpha\beta}(\mathbf{x}', t') dt' d^3 \mathbf{x}'$$

with $r = |\mathbf{x} - \mathbf{x}'|$ and h given by (3.11).

The result can also be written in terms of the Fourier transform on time, so that $\tilde{u}_\nu(\mathbf{x}, \omega)$ is given by (3.15), (3.16) in terms of transformed potentials $\tilde{\mu}_{\alpha\beta}$, where

$$(3.18) \quad \tilde{\mu}_{\alpha\beta}(\mathbf{x}, \omega; c) = \int_V \tilde{h}(r, \omega; c) m_{\alpha\beta}(\mathbf{x}', \omega) d^3 \mathbf{x}'$$

and \tilde{h} is the transform of h in (3.11), that is

$$(3.19) \quad \tilde{h}(r, \omega; c) = \exp[-i\omega r/c] / 4\pi\rho\omega^2 r.$$

Equations (3.15)-(3.19) for the displacement field are given in a somewhat different but equivalent form in [1] and other references.

3.2. *Far-field displacements.* — The wavelength λ associated with a Fourier component of frequency ω is $2\pi c/\omega$. Thus the exponential term in (3.19) can be written as $\exp[-2\pi ir/\lambda]$, and, at distances r that are large compared to λ , this term changes much more rapidly than $1/r$. Hence the third-order derivative operations in (3.16), when used in computing \tilde{u}_ν , effectively act only on the exponential of (3.19) at large r , that is

$$(3.20) \quad \frac{\partial^3}{\partial x_\nu \partial x_\alpha \partial x_\beta} \left(\frac{\exp[-i\omega r/c]}{r} \right) = \frac{i\gamma_\nu \gamma_\alpha \gamma_\beta \omega^3}{rc^3} \exp[-i\omega r/c] \left[1 + O\left(\frac{\lambda}{2\pi r}\right) \right],$$

where

$$(3.21) \quad \gamma_\nu = \partial r / \partial x_\nu = (x_\nu - x'_\nu) / r$$

are components of the unit vector from source point to receiver point. Further, if the origin of co-ordinates is set somewhere in the source region, and if r is large compared to source dimensions,

$$(3.22) \quad r = (r_0 - \boldsymbol{\gamma} \cdot \mathbf{x}') [1 + O(\boldsymbol{\gamma} \cdot \mathbf{x}' / r_0)],$$

where $r_0 \stackrel{\Delta}{=} |\mathbf{x}|$.

Thus eqs. (3.16), (3.18), (3.19) lead to the far-field displacements, *i.e.* at distances r_0 that are large compared to λ and source dimensions,

$$(3.23) \quad \begin{cases} \tilde{u}_\nu^d = \frac{i\omega}{4\pi Q r_0^3 c_d^3} \exp[-i\omega r_0/c_d] \gamma_\nu \gamma_\alpha \gamma_\beta \int_V \tilde{m}_{\alpha\beta}(\mathbf{x}', \omega) \exp[i\omega \boldsymbol{\gamma} \cdot \mathbf{x}' / c_d] d^3 \mathbf{x}', \\ \tilde{u}_\nu^s = \frac{i\omega}{4\pi Q r_0^3 c_s^3} \exp[-i\omega r_0/c_s] \left[\frac{1}{2} (\delta_{\nu\alpha} \gamma_\beta + \delta_{\nu\beta} \gamma_\alpha) - \gamma_\nu \gamma_\alpha \gamma_\beta \right] \cdot \\ \quad \cdot \int_V \tilde{m}_{\alpha\beta}(\mathbf{x}', \omega) \exp[i\omega \boldsymbol{\gamma} \cdot \mathbf{x}' / c_s] d^3 \mathbf{x}', \end{cases}$$

where now, to the order of accuracy of the far-field approximation, $\boldsymbol{\gamma} = \mathbf{x}/r_0$.

Since $i\omega \tilde{m}_{\alpha\beta}(\mathbf{x}', \omega)$ is the transform of $\dot{m}_{\alpha\beta}(\mathbf{x}', t)$, corresponding results in the time domain are

$$(3.24) \quad \begin{cases} u_\nu^d = \frac{1}{4\pi Q r_0^3 c_d^3} \gamma_\nu \gamma_\alpha \gamma_\beta \int_V \dot{m}_{\alpha\beta}(\mathbf{x}', t - r_0/c_d + \boldsymbol{\gamma} \cdot \mathbf{x}' / c_d) d^3 \mathbf{x}', \\ u_\nu^s = \frac{1}{4\pi Q r_0^3 c_s^3} \left[\frac{1}{2} (\delta_{\nu\alpha} \gamma_\beta + \delta_{\nu\beta} \gamma_\alpha) - \gamma_\nu \gamma_\alpha \gamma_\beta \right] \cdot \\ \quad \cdot \int_V \dot{m}_{\alpha\beta}(\mathbf{x}', t - r_0/c_s + \boldsymbol{\gamma} \cdot \mathbf{x}' / c_s) d^3 \mathbf{x}'. \end{cases}$$

Observe from the angular dependences here and in (3.23) that \mathbf{u}^d is in the direction of $\boldsymbol{\gamma}$, whereas \mathbf{u}^s is perpendicular to $\boldsymbol{\gamma}$. The retarded times in (3.24), associated with the exponential terms in (3.23), represent time delays due to « d » and « s » wave propagation between motions in the source region and the reception of their effects at the receiver point.

In the case of a shear fault (*e.g.* $m_{12} = m_{21}$ are the only nonzero $m_{\alpha\beta}$) the maximum magnitude of the orientation terms (*i.e.* the terms outside the integrals that depend on $\boldsymbol{\gamma}$) is the same for both the d and s fields. Hence the magnitude ratio of the d and s far-field contributions to \mathbf{u} is essentially the ratio $c_s^3/c_d^3 \approx 0.19$ (when $A = G$, *i.e.* when the Poisson ratio $\nu = 0.25$), so that the later-arriving s waves are of the order of 5 times greater in displacement amplitude.

A point source representation was presented in subsect. 2'3. This corresponds to considering sufficiently low frequencies ω that the exponentials within the integrals of (3.23) can be approximated by unity (*i.e.* the associated wavelengths λ are large compared to source dimensions) or, equivalently, that the time delays $\boldsymbol{\gamma} \cdot \mathbf{x}'/c$ between different points in the source region can be neglected in (3.24). Thus the integrals in (3.23), (3.24) simply define the moment tensor in this limit and, for example,

$$(3.25) \quad \tilde{u}_r^d = \frac{\exp[-i\omega r_0/c_d]}{4\pi\rho c_d^3 r_0} \gamma_r \gamma_\alpha \gamma_\beta [i\omega \tilde{M}_{\alpha\beta}(\omega)],$$

$$(3.26) \quad u_r^d = \frac{1}{4\pi\rho c_d^3 r_0} \gamma_r \gamma_\alpha \gamma_\beta \dot{M}_{\alpha\beta}(t - r_0/c_d).$$

Since the short-time motion in an earthquake source can be regarded as essentially complete for periods associated with the low-frequency range considered (slow, aseismic fault slip or inelastic deformation may continue over much longer time scales), $\tilde{M}_{\alpha\beta}(\omega)$ is to be regarded as being essentially the transform of a constant, $M_{\alpha\beta}(t_r)$, where t_r is the time of completion of seismic rupture. Hence

$$(3.27) \quad \tilde{M}_{\alpha\beta}(\omega) \approx M_{\alpha\beta}(t_r)/i\omega$$

in the frequency range for which the above formulae are valid, which means that the amplitude of the Fourier spectrum of \mathbf{u} is flat (*i.e.* independent of ω) at low frequencies, and is characterized entirely by the location of the source and its moment tensor $M_{\alpha\beta}(t_r)$ at completion of rupture.

If we consider the slipping source of fig. 2, with moment tensor given by (2.21), the radial component of displacement $u \equiv \boldsymbol{\gamma} \cdot \mathbf{u}$ (to which only \mathbf{u}^d contributes) is

$$u = \frac{\dot{M}(t - r_0/c_d)}{2\pi\rho c_d^3 r_0} \gamma_1 \gamma_2.$$

This is the form of the displacement pattern illustrated in fig. 2*a*). It vanishes on the nodal planes $x_1 = 0$, $x_2 = 0$, and takes extrema (positive or negative) at the mid-angle of each quadrant. It is this angular signature, determined after corrections for distortion of ray paths by heterogeneity, that leads to the fault plane solutions discussed in subsect. 2'3.

4. - Propagating shear rupture.

As has been seen, the low-frequency portion of the seismic spectrum is flat and its amplitude measures the seismic moment at completion of rupture. Information on details of the rupture propagation process and the size of the rupture zone is contained only in higher-frequency portions of the spectrum and this is discussed here, again with reference to the far field. For simplicity we consider a plane fault on $x_2=0$ sustaining a shearing displacement $\Delta u(x_1, x_3, t)$ in the x_1 -direction only, *i.e.* as in fig. 2*a*). (There will in general be at least minor slips in the orthogonal direction, x_3 , in ruptures which propagate under limiting friction-type boundary conditions, particularly in the process of arresting motion.) For the case considered the moment density tensor has the form

$$(4.1) \quad m_{\alpha\beta} = (\delta_{\alpha 1} \delta_{\beta 2} + \delta_{\beta 1} \delta_{\alpha 2}) G \Delta u \delta_D(S)$$

and the integral involving $\dot{m}_{\alpha\beta}$ in the far-field representations of (3.24) is

$$(4.2) \quad \int_V \dot{m}_{\alpha\beta}(\mathbf{x}', t - r_0/c + \boldsymbol{\gamma} \cdot \mathbf{x}'/c) d^3 \mathbf{x}' = G(\delta_{\alpha 1} \delta_{\beta 2} + \delta_{\beta 1} \delta_{\alpha 2}) \Omega(\boldsymbol{\gamma}, t - r_0/c),$$

where

$$(4.3) \quad \Omega(\boldsymbol{\gamma}, t) = \int_S \Delta \dot{u}[x_1, x_3, t + (\gamma_1 x_1 + \gamma_3 x_3)/c] dx_1 dx_3.$$

For a given orientation $\boldsymbol{\gamma}$ of the receiving point the time history of the displacement signal is thus characterized completely by the function Ω , evaluated for $c = c_a$ and $c = c_s$. The definition of Ω differs from that of Aki and Richards [1], who review various evaluations of it, only in that here t is advanced by the travel time r_0/c from the co-ordinate origin in the source region.

The transformed function, giving the spectral content of \mathbf{u} , is

$$(4.4) \quad \tilde{\Omega}(\boldsymbol{\gamma}, \omega) = \int_S \Delta \tilde{u}(x_1, x_3, \omega) \exp [i\omega(x_1 \gamma_1 + x_3 \gamma_3)/c] dx_1 dx_3,$$

where $\Delta \tilde{u} = i\omega \Delta \tilde{u}(x_1, x_3, \omega)$. This function amounts to the complete space-time Fourier transform of the function $\Delta \dot{u}$ for wave numbers $k_1 = -\gamma_1 \omega/c$,

$k_3 = -\gamma_3\omega/c$. Because the k 's and ω are linked in this way, and the γ 's must lie between -1 and $+1$, far-field observations (say, over a range of orientations γ) cannot in principle suffice for a full determination of $\Delta\dot{u}$. That is, the spatial structure along the fault plane of a given frequency component of $\Delta\dot{u}$ is resolvable only over the range of wave numbers that are smaller in magnitude than ω/c ; shorter-wavelength information is not transmitted to the far field and, evidently, results in motions that are confined to the near field of the source region. A good way of presenting the overall radiation pattern is to plot contour surfaces of $|\bar{\Omega}(k_1, k_3, \omega)|$ in (k_1, k_3, ω) -space, where $\bar{\Omega}$ is the full space-time Fourier transform of $\Delta\dot{u}(x_1, x_3, t)\delta_D(S)$. Then $|\bar{\Omega}(\gamma, \omega)|$ is given as a function of ω by the contour levels of $|\bar{\Omega}(k_1, k_3, \omega)|$ that are traversed along the ray $k_1 = -\gamma_1\omega/c$, $k_3 = -\gamma_3\omega/c$. DAS and AKI [4] give several two-dimensional examples of this procedure in a (k_1, ω) -plane, *i.e.* corresponding to receiving stations located on the plane $x_3 = 0$ through the source region.

4.1. *Properties of earthquake spectra.* — It is reasonable to expect that $\Delta u \geq 0$ during the rupture (reverse slip inhibited by friction), which requires that $\Omega(\gamma, t) \geq 0$ and hence that the magnitude of $\bar{\Omega}(\gamma, \omega)$, *i.e.* $|\bar{\Omega}(\gamma, \omega)|$, be greatest at $\omega = 0$. This greatest magnitude is just M/G , where M is the seismic moment at completion of rupture. Characteristics of the spectrum at high frequencies depend on details of rupture propagation, that is on the way that the rupture front spreads in time over S , on the time dependence of Δu at a point within the ruptured zone (*e.g.* different for « crack » *vs.* « dislocation » models), on whether the rupture front moves continuously or skips over nonslipping barrier regions [4] and on the details of spreading back over the fault of the final arrest process.

There are many studies of spectral structure in relation to these factors, and the area is currently one of active research. Only a brief review is given here.

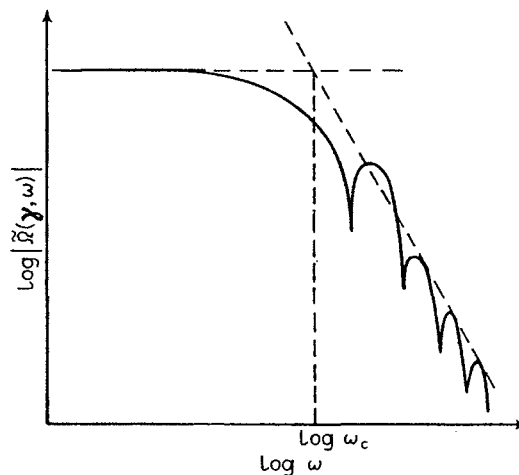


Fig. 3. — Schematic illustration of earthquake amplitude spectrum; ω_c is the « corner frequency ».

Figure 3 shows, schematically, an amplitude spectrum for $\tilde{\Omega}(\boldsymbol{\gamma}, \omega)$. This is drawn to show the general features predicted by theoretical fault models. The most striking feature is the oscillation in amplitude as the general level of $\log |\tilde{\Omega}|$ decays at high frequencies (in some models this oscillation appears only as a small ripple on a decaying curve).

Some insight into the origin of this structure is given by examining a simple version of Haskell's [27] dislocation fault model, although the model is certainly unsuitable in several respects. In this model S is a rectangle of length L (in the x_1 -direction) and width W (in the x_3 -direction) (fig. 4a). Rupture propagates

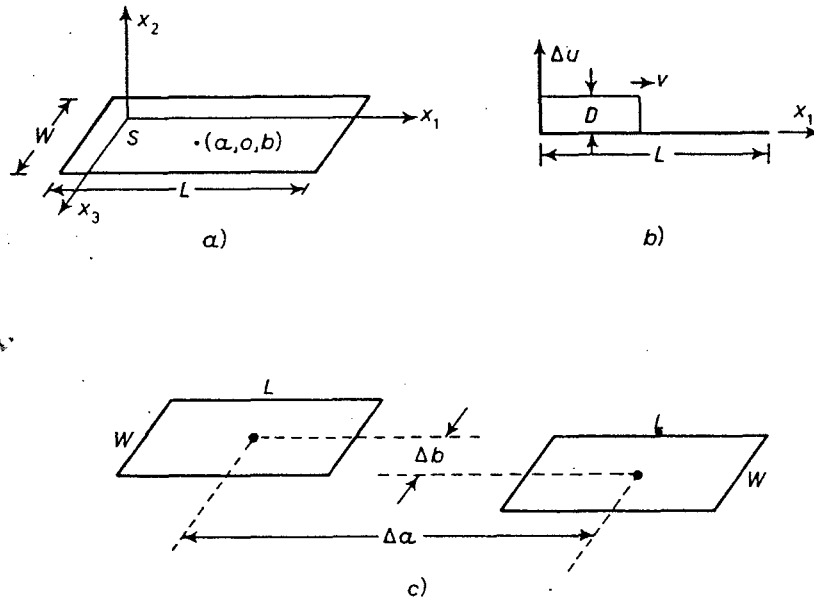


Fig. 4. - a, b) Propagation of concentrated dislocation, with slip offset D , at uniform speed along a rectangular fault. c) Adjacent fault segments separated by nonslipping region.

at uniform speed v in the x_1 -direction (fig. 4b)) from one end of the fault to the other, as a concentrated dislocation line, so that a fixed slip offset $\Delta u = D$ is attained at all points traversed by the dislocation. That is

$$(4.5) \quad \Delta u(x_1, x_3, t) = D U(t - t_0 - x_1/v),$$

where U is the unit step function and t_0 is the time at which a disturbance of this type would pass $x_1 = 0$ (if $x_1 = 0$ lies on the fault). Hence

$$(4.6) \quad \Delta \tilde{u}(x_1, x_3, \omega) = \int_{-\infty}^{+\infty} D \delta_D(t - t_0 - x_1/v) \exp[-i\omega t] dt = D \exp[-i\omega(t_0 + x_1/v)],$$

and, if the fault is centered at $x_1 = a$, $x_3 = b$,

$$(4.7) \quad \tilde{\Omega}(\gamma, \omega) = \int_{a-L/2}^{a+L/2} \int_{b-W/2}^{b+W/2} D \exp[-i\omega(t_0 + x_1/v) + i\omega(\gamma_1 x_1 + \gamma_3 x_3)/c] dx_3 dx_1 = \\ = DWL \exp[-i\omega\varphi] \frac{\sin(\pi\omega/\omega_1) \sin(\pi\omega/\omega_3)}{\pi^2 \omega^2 / \omega_1 \omega_3},$$

where

$$(4.8) \quad \begin{cases} 2\pi/\omega_1 = L/v - \gamma_1 L/c, & 2\pi/\omega_3 = \gamma_3 W/c, \\ \varphi = t_0 + a/v - (\gamma_1 a + \gamma_3 b)/c. \end{cases}$$

Although the model is a severely simplified description of rupture, it suffices for a discussion of the following features exhibited by the amplitude spectrum of $\tilde{\Omega}$:

i) At low frequencies $|\tilde{\Omega}|$ is proportional to DWL , which is just the moment M divided by shear modulus G , as expected.

ii) At high frequencies $|\tilde{\Omega}|$ is oscillatory and, for this model, it vanishes at $\omega = \frac{1}{2} \omega_1, \pm 2\omega_1, \dots, \pm \omega_3, \pm 2\omega_3, \dots$, while its peak amplitude decays as a negative power of ω , in this case as ω^{-2} in general and as ω^{-1} when $\gamma_3 = 0$ (decay results are somewhat model dependent).

iii) The oscillations are affected by rupture propagation, but would be exhibited even if the rupture displacement occurred simultaneously everywhere over S (simulated by setting $v = \infty$ in the preceding formulae). This occurs because the signal received at the recording station emanates from all of the fault, and phase differences owing to variations in travel times can lead to constructive and destructive interference of signals.

iv) The effect of propagation of the rupture is to give directivity to the spectrum (*e.g.* see [1, 28]); for a receiver station with γ_1 positive, ω_1 of (4.8) is larger, and hence the oscillations of $|\tilde{\Omega}|$ of (4.7) set in later and are more widely spaced along the ω -axis, than for a station with γ_1 negative. This is a pronounced effect near $\gamma_1 = \pm 1$, especially for s waves, because the speed of propagation seems typically to be a large fraction of c_s , and the corresponding differences in ω_1 are great.

v) The phase factor φ of (4.8) has no effect on $|\tilde{\Omega}|$ for a single rupture. However, if we consider the rupture process to spread discontinuously in space over, say, two identically shaped and oriented rectangular sectors (fig. 4c), and for simplicity take the speed of propagation to be uniform so that (4.5) for Δu applies within each sector (with the second rectangle beginning to rupture only when the disturbance of speed v has reached it), then $\tilde{\Omega}$ is given by the sum of two terms of the type in eq. (4.7). These two terms differ only in that φ

differs for the two rectangles because the center locations differ. Hence one easily computes

$$(4.9) \quad \tilde{Q} = 2DWL \exp[-i\omega\bar{\varphi}] \cos \left[\pi\omega \left(\frac{\Delta a}{L\omega_1} - \frac{\Delta b}{W\omega_3} \right) \right] \frac{\sin(\pi\omega/\omega_1) \sin(\pi\omega/\omega_3)}{\pi^2 \omega^2 / \omega_1 \omega_3},$$

where $\bar{\varphi}$ is the average of φ of (4.8) for the two rectangles and where Δa , Δb denote differences between their center locations (fig. 4c)). This shows the perhaps obvious result that the oscillatory structure of the spectrum is increased by discontinuous (or multifocus) rupture events. This is discussed later and has been emphasized in recent work of Das and Aki [4].

Now, a concentrated dislocation model of the type described by (4.5) and fig. 4b) is objectional on several grounds. Indeed, *any* « dislocation » model in which Δu is prescribed without reference to the associated stress drops on the rupture surface (which should, in principle, be related in a constitutive sense to Δu) is certainly an incomplete description of rupture. However, the model described should, at minimum, be given a finite « rise time » (as was actually done in Haskell's [27] work) to achieve the final offset D , and allow for the possibility that rupture emanates from a point and spreads out in two directions over the fault. As SAVAGE [29] observed in a review of some of the earlier dislocation models, « smoothing » features make the spectrum decay more rapidly at higher frequencies, and this is the effect of a time-dependent $D(t)$, although bilateral rupture alone does not seem to affect the decay rate.

A feature which arose from these early investigations is Brune's [30] concept of a « corner frequency » (see also [29]). This is illustrated in fig. 3, where the high-frequency asymptote has been extrapolated to the low-frequency level of the spectrum to define the corner frequency ω_c . This is essentially a model-dependent parameter (and, for a given model, the particular value obtained for ω_c will depend on the orientation γ of the receiver and the wave type on which it is based). Nevertheless, for simple fault models involving the spreading of rupture at a uniform rate (independent of fault size) over a single continuous, deeply buried rupture surface, it is required by dimensional considerations that ω_c should scale in inverse proportion to the size of the rupture region.

This kind of correlation has been explored widely. In a recent review BRUNE *et al.* [31] have examined estimates of ω_c from « s » wave radiation according to the results of several authors for the spread of rupture at $v = 0.9c_s$ (near the Rayleigh speed; see part II) over a circular region of radius r . Most of the results are for dislocation models, although recent work by MADARIAGA [32] on a cracklike model with fixed stress drop behind the rupture front is also included. BRUNE *et al.* conclude that

$$(4.10) \quad \omega_c/2\pi \approx (c_s/3r)(1 \pm 0.5),$$

where ± 0.5 accounts for variations among models and receiver station locations. These authors also give parameters equivalent to r for surface-breaking faults and buried rectangular faults, and present results for a variety of calculated model spectra and observed spectra. In general, the latter are much more « jagged ». Of course, ω_c also can be associated with a dominant period of the time signal of the rupture.

It is important to observe that the correlation between ω_c and r is based on simple models for continuously progressing rupture, with a single characteristic dimension. There is no guarantee that the estimates of r made in this way from observed spectra will have much accuracy in characterizing actual rupture size. Indeed, to the extent that discontinuous propagation occurs in Nature, dominant time features of the radiated pulse cannot be expected to scale directly with size. Also, the simple example of eq. (4.9) and work discussed in the next section suggest that the spectrum may then be modified in the early stages of decay, which, in practical implementations of the corner frequency procedure [31], would seem capable of influencing significantly the result obtained.

4.2. *Crack models; continuous versus discontinuous rupture propagation.* — Recent work on rupture propagation in relation to seismic spectra (e.g. [4, 32-35]) has been based on crack models, in which the motion $\Delta u(x_1, x_3, t)$ is calculated in such a way that the ruptured surface sustains a uniform drop in shear stress while slipping, and is prohibited from reverse slip. In some cases the rupture propagation speed v is prescribed [32, 33, 34] (typically as $0.9c_s$, to simulate the Rayleigh velocity); in others [4, 35] (see also [7, 36, 37]) it is calculated according to some fracture criterion, as discussed in part II.

Madariaga's model [32, 33] of a circular shear rupture that spreads at uniform speed v to a final radius r , and then stops, is illustrated in fig. 5a), and a schematic representation of the associated time pulse of $\Omega(\gamma, t)$ is shown in fig. 5b), for an observation station in the plane $x_3 = 0$ (plane defined by fault plane normal and slip direction); because the ratios γ/c are different for d and s waves, the shape of $\Omega(\gamma, t)$ will be somewhat different in the two cases. The rupture stops propagating at $t = r/v$, and this shows at the receiving station at

$$(4.11) \quad t_1 = r/v - \gamma_1 r/c = r/v - \cos \theta r/c,$$

where the correction $\gamma_1 r/c$ arises because the nearest extremity of the stopped tip is closer to the station (recall that the propagation time from the fault center has been removed from t). For $t < t_1$ the signal Ω is accelerating upward, but at $t = t_1$ an inflection point occurs as the information that propagation has stopped is transmitted. Later at $t = t_2$, where

$$(4.12) \quad t_2 = r/v + \gamma_1 r/c = r/v + \cos \theta r/c,$$

the information that the opposite crack extremity has stopped reaches the station, causing another inflection point after which the signal decays somewhat more slowly to zero. It does not drop immediately to zero, as in dislocation models, since the information that rupture propagation has stopped has to be transmitted back from the crack extremities towards its center to arrest slip motion. These effects at $t = t_1, t_2$ are referred to as «stopping phases», and

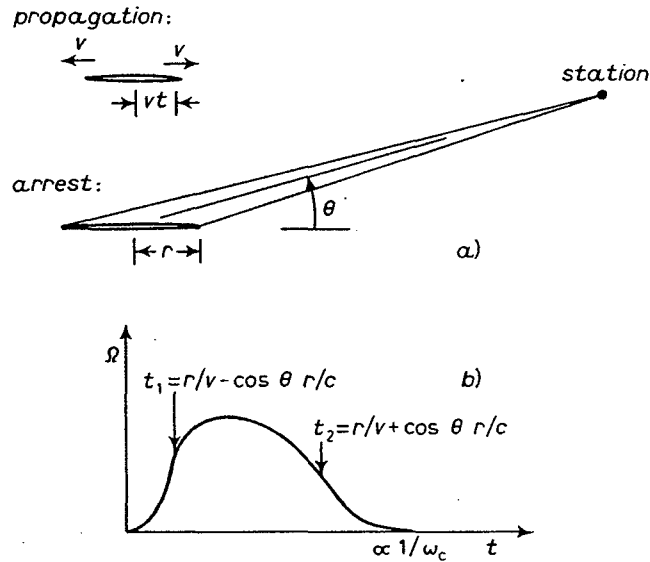


Fig. 5. — Cracklike circular rupture spreading at uniform speed v and arresting at radius r ; times t_1, t_2 indicate arrival of stopping phases, t_1 from the near crack extremity and t_2 from the far extremity.

they determine the characteristic time duration of the pulse. (Actual signals received will be more oscillatory than in fig. 5b) due to various sources of dispersion and boundaries in the Earth's structure, and to recorder-signal interactions.) MADARIAGA finds that the pulse width varies in inverse proportion to the corner frequency of the associated spectrum, with a coefficient that is approximately independent of the location of the recording station.

The time history of Δu in Madariaga's numerical solution [32] agrees closely with Kostrov's [38] solution for self-similar crack growth,

$$(4.13) \quad \Delta u = (\beta \Delta \sigma / G) \sqrt{v^2 t^2 - \varrho^2},$$

up to the intervention of stopping phases, where ϱ is distance measured from the fault center, $\Delta \sigma$ is the stress drop, and β is a speed-dependent coefficient which varies (for Poisson ratio $\nu = 1/4$) from 1.09 at $v = 0$ to 0.89 at $v = c_R$, the Rayleigh speed. The value of Ω corresponding to motion without arrest («starting phases») is [33]

$$(4.14) \quad \Omega(\gamma, t) = 2\pi\beta \Delta \sigma v^3 t^2 / [1 - v^2(\gamma_1^2 + \gamma_3^2)/c^2]_1^2,$$

which is the source of the initial parabolic rise in fig. 5b). For the associated contribution of starting phases to the spectrum, $\tilde{Q}(\gamma, \omega)$ is given by this expression with t^2 replaced by $2/(i\omega)^3$.

But the actual high-frequency decay of $\tilde{Q}(\gamma, \omega)$ is dominated by the stopping phases, and MADARIAGA [33] develops an asymptotic analysis of this by ray theory methods, which are valid in the high-frequency limit. He observes that the singular slip velocity $\Delta \dot{u}$ at the crack tip is the source of high-frequency radiation, and that the discontinuity there associated with sudden stopping of the crack is the source of the dominant high-frequency contribution. Using Freund's [39] general solutions for crack propagation at variable velocity, in this case for a sudden decrease of velocity to zero, to construct the near tip fields immediately after stopping, and employing ray calculations based on the resulting circular distribution of sources along the crack front, MADARIAGA [33] shows that $\tilde{Q}(\gamma, \omega)$ decays as ω^{-2} according to this model, which is in agreement with his numerical calculations [32].

However, there is evidence that rupture does not always propagate continuously over a single rupture surface. This has important consequences for the high-frequency structure of the spectrum and shape of time pulses, and also for the practical estimation of stress drops (subsect. 4.3) from corner frequency or other estimates of nominal rupture area. DAS and AKI [4] cite examples in which multifocus earthquakes are suggested by seismological records, and note geological evidence for discontinuous surface breaks of fault traces (in some but probably not all cases these may be a consequence of properties peculiar to near-surface material). They conclude that frequently earthquakes propagate discontinuously, leaving « barrier » segments between segments of shear rupture, with these barriers sometimes remaining coherent and sometimes finally rupturing at later stages in the earthquake process. MADARIAGA [40] cites additional evidence for discontinuous rupture propagation, and MCGARR *et al.* [41] show by evacuation of a (presumably) freshly formed fault near a mine opening that shear rupture is, indeed, discontinuous in this case on the scale of a few meters. Segments of shear failure form an *en échelon* pattern with short fissures, probably due to local tensile fracture at the ends of the shear zones, joining one zone to another. (The large-scale surface breaks cited by DAS and AKI [4] are typically discontinuous on a much larger scale of 10 to 20 km.)

Progress toward the fundamental understanding of shear failure has not yet advanced in such a way that these features can be predicted from first principles and incorporated into rupture propagation models. The more *ad hoc* approach of Das and Aki [4, 35] introduces the concept of barriers within a two-dimensional finite-difference code for shear crack propagation. Their barriers consist of segments along the prospective rupture surface which require an unusually high average stress to initiate slip (which is assumed to take place subsequently under a fixed stress drop level), and they give examples

of fault surface motion for strong barriers, which remain unbroken, and somewhat weaker barriers which ultimately fail. MADARIAGA [40] reports similar three-dimensional calculations, in which no fracture criterion is adopted but rupture is assumed to propagate across disconnected coplanar fault segments, as in fig. 4c) with $\Delta b = 0$, in such a way that a uniform stress drop results. Both DAS and AKI [4] and MADARIAGA [40] report far-field amplitude spectrum results, and, as anticipated by the simpler model for discontinuous rupture discussed earlier (fig. 4c) and eq. (4.9)), the general effect is to amplify the size of the high-frequency oscillations, especially of the first peak, and the corresponding time functions $\Omega(\gamma, t)$ show a two-peak structure consistent with time-separated discontinuous foci. MADARIAGA [40] finds similar features for a long continuous fault with a central segment on which the stress drop is taken as zero.

4.3. *Stress drops associated with shear rupture.* — Many estimates of earthquake stress drops are given in the literature (*e.g.* see [26] for a summary). It is important to understand the manner in which these numbers are obtained and the uncertainties of the process. They should perhaps be referred to as nominal stress drops, because in complex faulting processes as just considered they may have no simple relation to, and sometimes greatly underestimate, actual stress drops on shear rupture surfaces.

In the development of sect. 2 stresses are measured relative to the state of the body before rupture. That is, if σ^0 is the (generally position dependent) initial stress field in the body, then the « stress » associated with the displacement field u is $\sigma - \sigma^0$, where σ is the actual local stress. Hence stress drops $\Delta\sigma$ are defined by $\sigma^0 - \sigma$ and, in particular,

$$\Delta\sigma_{21} = \sigma_{21}^0 - \sigma_{21} \quad \text{and} \quad \Delta\sigma_{23} = \sigma_{23}^0 - \sigma_{23}$$

are components of (shear) stress drop along a fault surface on $x_2 = 0$ as in fig. 2a) and 4. The static elasticity solution for the displacement discontinuity along a deeply buried circular shear fault of radius r that sustains a uniform stress drop is (*e.g.* [42])

$$(4.15) \quad \Delta u = [8(1 - \nu) \Delta\sigma / (2 - \nu)\pi G] \sqrt{r^2 - \rho^2}$$

for an isotropic material. The direction of slip is coaxial with the direction of the shear stress drop, which is also true of Kostrov's [38] self-similar dynamic solution. (This solution and corresponding results for planar elliptical shear cracks can be obtained by specialization of results for ellipsoidal voids by ESHELBY [16].) Hence the long-term seismic moment of a buried circular

rupture sustaining a uniform stress drop is

$$(4.16) \quad M = \int_S G \Delta u \, dS = [16(1-\nu)/3(2-\nu)] \Delta \sigma r^3 = (16/7) \Delta \sigma r^3 \quad \text{for } \nu = 0.25.$$

Thus, if an effective radius r can be determined, either from corner frequency estimates based on (4.10), or by using the size of the aftershock zone following large earthquakes (writing its area S as πr^2), or from information based on surface-breaking ruptures and associated ground motion, then a knowledge of M (or of the average Δu from surface observations) leads to a nominal $\Delta \sigma$. According to the summary by KANAMORI [26], these nominal stress drops are rather variable (10 to 100 bar, with much of the data falling in the range of 20 to 60 bar), but their distribution of values within these ranges seems to have little dependence on the size of the earthquake.

The size range is somewhat puzzling. Laboratory friction experiments are generally interpreted (see part II) as requiring much higher values, although recent experiments by DIETERICH [43], in which stick-slip instabilities are confined to a portion of a fault plane and do not spread to specimen boundaries, suggest that the disparity may be somewhat less than previously thought. Certainly, in the case of fresh shear rupture of rock, much higher stress drops are expected locally on rupture surfaces [41].

In fact, by measuring directly the slip along shear segments of the fault which they excavate, and estimating its size r by using the seismically inferred moment of the event, MCGARR *et al.* [41] calculate a stress drop from (4.16) of approximately 700 bar (which is consistent with laboratory strength drop data for initially coherent rock at similar confining pressure). By contrast, the conventional corner frequency procedure led to a much larger value of r , which, given the value of M , greatly underestimated the observed slip and led to an inference of stress drops from (4.16) in the range of 5 to 50 bar.

As a separate issue, DAS and AKI [4] and MADARIAGA [40] suggest, from their solutions for discontinuous rupture propagation, that the actual local stress drop can be significantly larger, for a given M , than the nominal value based on the net area of rupture. This occurs because, for a given stress drop on a collection of surfaces S , the value of $\int \Delta u \, dS$ is smaller for disconnected surfaces than for a single coherent surface of the same area.

An estimate of the effect can be made from the following two-dimensional model for a long series of *en échelon* shear faults, each sustaining a uniform stress drop $\Delta \sigma$. The array is shown in fig. 6a) and approximated in fig. 6b) as a periodic array of collinear cracks in plane strain, with center-to-center spacings $2b$ and individual lengths $2a$. The strain energy loss of the body, on a unit-thickness basis, per crack is

$$(4.17) \quad \Delta U = \frac{1}{2} \Delta \sigma \int_{-a}^{+a} \Delta u \, dx.$$

This can also be calculated as the integral of the energy release rate \mathcal{J} , where

$$(4.18) \quad \mathcal{J} = \frac{1-\nu}{2G} K^2,$$

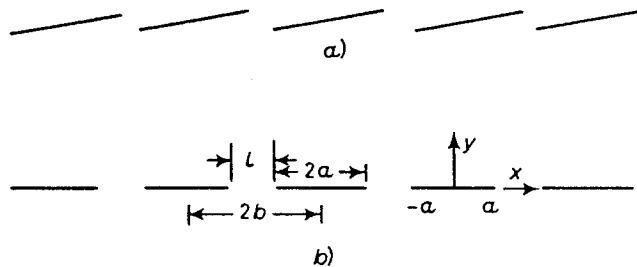


Fig. 6. - a) *En échelon* array of faults. b) Periodic array of collinear plane strain shear cracks sustaining a uniform stress drop.

and where K is the stress intensity factor, namely (e.g. [6])

$$(4.19) \quad K = \Delta\sigma \sqrt{2b \operatorname{tg}(\pi a/2b)}$$

for the periodic array. (See [6] and part II for definitions of the terms employed.) Hence, since there are 2 crack tips

$$(4.20) \quad \Delta U = 2 \int_0^a \mathcal{J} da = \frac{4(1-\nu)(\Delta\sigma)^2 b^2}{\pi G} \ln \left[\frac{1}{\sin(\pi l/4b)} \right],$$

where $l = 2b - 2a$ is the ligament size (fig. 6b)). Thus the moment, on a unit-thickness basis, for an array of n cracks is

$$(4.21) \quad M = n \int_{-a}^{+a} G \Delta u dx = \frac{8n(1-\nu) \Delta\sigma b^2}{\pi} \ln \left[\frac{1}{\sin(\pi l/4b)} \right];$$

this is asymptotically correct for large n , but will, of course, over-estimate M for small n , especially for very small ligament ratios l/b . For a single isolated crack of half-length nb , sustaining a nominal uniform stress drop $\Delta\sigma_{\text{nom}}$, the analogous calculation gives

$$(4.22) \quad M = \pi n^2 (1-\nu) \Delta\sigma_{\text{nom}} b^2.$$

Hence, for a given moment, the ratio of the actual stress drop $\Delta\sigma$ for the discontinuous array to the nominal value for a continuous rupture surface of the same overall length is

$$(4.23) \quad \Delta\sigma/\Delta\sigma_{\text{nom}} = \pi^2 n/8 \{ \ln [1/\sin(\pi l/4b)] \}$$

for sufficiently large n , with the right-hand side being a lower bound otherwise. The ratio is $1.28n$ for $l/2b = 0.25$, $0.67n$ for $l/2b = 0.1$ and $0.30n$ for $l/2b = 0.01$. There is not a strong dependence on ligament size, and, if $0.5n$ is taken as representative (which means that «large» n must mean significantly more than 2), then ruptures consisting of arrays of 10 to 20 *en échelon* cracks would have actual stress drops at least 5 to 10 times higher than the nominal drop estimated by the usual procedures. The calculation assumes that the ligaments remain elastic. Partial zones of nonelastic deformation at the tips of individual fissures are essentially equivalent to reducing $l/2b$. Since the result is not very sensitive to $l/2b$, the above calculation would seem to be essentially correct as long as the ligaments remain coherent (they are instead traversed by secondary cracks in the observations of McGarr *et al.* [41]).

MADARIAGA [40] makes other approximate estimates of $\Delta\sigma/\Delta\sigma_{nom}$, and also gives an elegant formula relating M to $\Delta\sigma$ for general arrays of rupture surfaces. This is based on the elastic reciprocal theorem. If Δu_α , $\Delta\sigma_\alpha$ are the actual slips and traction drops ($\Delta\sigma_\alpha = n_\beta \Delta\sigma_{\beta\alpha}$, where $\Delta\sigma_{\alpha\beta}$ is the tensor stress drop) on a surface or collection of surfaces S in an elastic body, and if Δu_α^* , $\Delta\sigma_\alpha^*$ are any other set of slips and associated traction drops, then

$$(4.24) \quad \int_S \Delta\sigma_\alpha^* \Delta u_\alpha \, dS = \int_S \Delta\sigma_\alpha \Delta u_\alpha^* \, dS.$$

Since the motion is slip, the normal components of $\Delta\sigma_\alpha$ can be disregarded, and $\Delta\sigma_\alpha$ can be considered as the α component of the drop in the shear stress vector along S .

Now let the $*$ field coincide with the solution to the «crack» problem for which the shear stress is dropped in value on each element of S in the same way that it would be if the coherent body sustained a uniform drop $\Delta\Sigma_{\alpha\beta}^*$ in its stress tensor (necessarily, $\Delta\Sigma_{\alpha\beta}^* = \Delta\Sigma_{\beta\alpha}^*$). In this case

$$(4.25) \quad \Delta\sigma_\alpha^* = n_\beta \Delta\Sigma_{\beta\alpha}^* - n_\alpha (n_\gamma \Delta\Sigma_{\gamma\delta}^* n_\delta),$$

and the slip displacements can be written as

$$(4.26) \quad \Delta u_\alpha^* = E_{\alpha,\beta\gamma} \Delta\Sigma_{\beta\gamma}^* / 2G,$$

where, in view of the symmetry of $\Delta\Sigma_{\alpha\beta}^*$, we set $E_{\alpha,\beta\gamma} = E_{\alpha,\gamma\beta}$. Thus, $E_{\alpha,11}$ is the slip field for the crack problem with shear stress drops generated by $\Delta\Sigma_{11} = 2G$, and all other $\Delta\Sigma_{\alpha\beta} = 0$; $E_{\alpha,12} (= E_{\alpha,21})$ is the slip field for the crack problem with stress drops generated by $\Delta\Sigma_{12} = \Delta\Sigma_{21} = G$ and all other $\Delta\Sigma_{\alpha\beta} = 0$. Hence (4.24) becomes

$$(4.27) \quad \Delta\Sigma_{\alpha\beta} \int_S n_\beta \Delta u_\alpha \, dS = \frac{1}{2} \Delta\Sigma_{\alpha\beta} \int_S (n_\beta \Delta u_\alpha + n_\alpha \Delta u_\beta) \, dS = \frac{1}{2G} \Sigma_{\alpha\beta} \int_S \Delta\sigma_\nu E_{\nu,\alpha\beta} \, dS$$

and, if we recall the definition of the moment tensor,

$$(4.28) \quad M_{\alpha\beta} = \int_S \Delta\sigma_\nu E_{\nu,\alpha\beta} dS,$$

which is a slight generalization of the result given by MADARIAGA [40]. For geometries to which solutions for crack problems with uniform stress drops are known, it leads to a simple calculation of $M_{\alpha\beta}$ for arbitrary nonuniform distributions of stress drop.

An analogous application of the reciprocal theorem chooses slip displacements for the * field as if they were the slip components of a constant vector b_α :

$$(4.29) \quad \Delta u_\alpha^* = b_\alpha - n_\alpha b_\beta n_\beta.$$

Hence, if the resulting shear traction drops are written as

$$(4.30) \quad \Delta\sigma_\beta^* = t_{\alpha,\beta} b_\alpha,$$

where, *e.g.*, $t_{\alpha,1}$ is the shear traction field associated with $b_1 = 1$, $b_2 = b_3 = 0$, then the reciprocal theorem gives the average shear traction drops of the actual field in the form

$$(4.31) \quad \int_S \Delta\sigma_\nu dS = \int_S t_{\alpha,\nu} \Delta u_\alpha dS.$$

PART II

Fundamentals of the rupture process in geological materials.

5. — Elements of elastic crack mechanics.

There is considerable evidence that much of the inelastic crustal deformation associated with earthquakes takes place, both in quasi-static processes before instability and in dynamic rupture, in the form of slip along narrow fault surfaces. Hence the mechanics of shear cracks is central to the theory of earthquake rupture, and fundamentals of elastic crack mechanics are reviewed briefly here. The presentation follows for the most part that of [6, 7, 44]. A number of recent texts on crack mechanics (concentrating on tensile fracture) are available; particularly recommended is that by LAWN and WILSHAW [45] on fracture processes in brittle solids and by BUI [46] on mathematical crack analysis.

By an elastic crack model we shall understand a model in which the material outside the crack remains ideally elastic and in which there is an abrupt drop in stress σ on the plane of the crack as the cracked region is entered (see fig. 7), *i.e.* typically to zero for tensile cracks or to an essentially uniform or slowly varying frictional stress σ^f for shear cracks. This necessarily leads to stress and strain singularities in the elastic field at the crack tip (fig. 7), and the actual flow of energy to inelastic breakdown processes near the tip is represented by the energy release \mathcal{S} per unit area of new crack surface, as the singular tip field moves through the material. More detailed models of the breakdown process, especially «slip weakening» models, which are appropriate especially when the zone of strength degradation is not confined to the immediate vicinity of the crack tip, are considered in sect. 6.

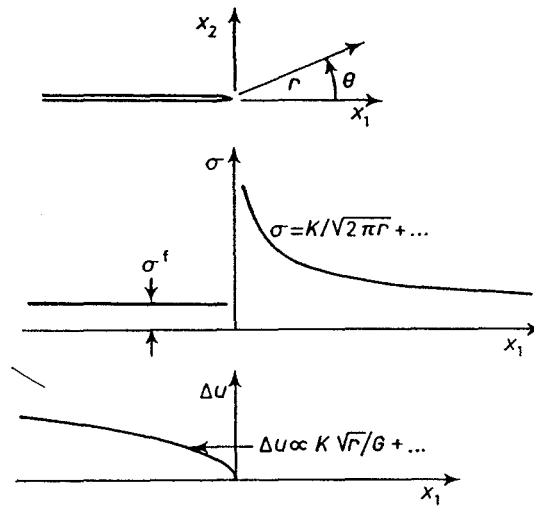


Fig. 7. — Elastic shear crack model.

However, it is well to consider that inelastic deformation prior to the emergence of well-defined macrocracks (*e.g.* continuous fields of inelastic strain, strain softening, interacting arrays of microcracks) may well be important to understanding the origin of earthquake instabilities, as well as the possible alterations of volume properties (seismic-wave speeds, electrical and fluid transport coefficients) that may lead to precursory signals. Some aspects of the theory of fracture in relation to these processes are discussed in sect. 7, whereas in sect. 8 the general group of fracture models is examined in the context of an infiltrating pore fluid (*e.g.* groundwater) interacting mechanically with the deforming rock mass.

5.1. *Crack tip stress fields (static conditions); stress intensity factors.* — Since deformations are highly concentrated at the crack tip, while the strain ϵ_{33} necessarily remains small (relative to the crack orientation in fig. 7), it suffices to

establish the structure of the near tip field for stationary (or slowly moving) cracks by seeking singular solutions to the static version of (2.3), in which u_1, u_2, u_3 are functions only of x_1 and x_2 . That is, the field reduces to one of plane strain (for u_1, u_2) and antiplane strain (for u_3). In this case eqs. (2.3) with the isotropic modulus tensor of (2.4) reduce to

$$(5.1) \quad (A + G) \left[\frac{\partial}{\partial x_1}, \frac{\partial}{\partial x_2}, 0 \right] \left(\frac{\partial u_1}{\partial x_1} + \frac{\partial u_2}{\partial x_2} \right) + G \left(\frac{\partial^2}{\partial x_1^2} + \frac{\partial^2}{\partial x_2^2} \right) [u_1, u_2, u_3] = 0.$$

Since u_3 is a plane harmonic function, it can be written as the imaginary part of an analytic function, say $\omega(\zeta)/G$, of $\zeta = x_1 + ix_2$, and u_1 and u_2 can also be represented in terms of analytic functions (e.g. [47]). The resulting representation of the displacement and stress field is

$$(5.2) \quad 2G(u_1 + iu_2) = (3 - 4\nu)\varphi(\zeta) - \zeta\overline{\varphi'(\zeta)} - \overline{\psi(\zeta)},$$

$$(5.3) \quad 2Giu_3 = \omega(\zeta) - \overline{\omega(\zeta)},$$

$$(5.4) \quad \sigma_{11} + \sigma_{22} = 2\overline{\varphi'(\zeta)} + 2\varphi'(\zeta),$$

$$(5.5) \quad \sigma_{22} - \sigma_{11} + 2i\sigma_{12} = 2\zeta\overline{\varphi''(\zeta)} + 2\psi'(\zeta),$$

$$(5.6) \quad \sigma_{32} + i\sigma_{31} = \omega'(\zeta),$$

where $\varphi(\zeta)$, $\psi(\zeta)$ and $\omega(\zeta)$ are analytic, where the superposed bar denotes complex conjugate and the prime denotes differentiation.

Following the method of Rice [6], based on analytic function theory, it can be shown that the only singular solution of these equations consistent with bounded tractions on the crack faces and giving finite displacements is

$$(5.7) \quad \begin{cases} \varphi'(\zeta) = (K_I - iK_{II})/2(2\pi\zeta)^{\frac{1}{2}}, \\ \psi'(\zeta) = (K_I + 3iK_{II})/4(2\pi\zeta)^{\frac{1}{2}}, \\ \omega'(\zeta) = K_{III}/(2\pi\zeta)^{\frac{1}{2}}, \end{cases}$$

where the K 's are coefficients chosen to correspond to standard definitions of Irwin's [48] stress intensity factors [49]. The singular stress field implied by (5.7) was first established by WILLIAMS [50] through assuming stresses in the form $\sigma_{\alpha\beta} = r^{+\lambda} f_{\alpha\beta}(\theta, \lambda)$, relative to the polar co-ordinates of fig. 7, and determining eigenvalues λ so that the resulting solution meets traction-free crack surface boundary conditions (giving $\lambda = -\frac{1}{2}, 0, \frac{1}{2}, 1$, etc.). The corresponding tractions $(\sigma_{2\alpha})_{\theta=0}$ on the plane ahead of the crack and displacement discontinuities $\Delta u_\alpha \equiv (u_\alpha)_{\theta=\pi} - (u_\alpha)_{\theta=-\pi}$ contributed by the singular terms are

$$(5.8) \quad [\sigma_{22}, \sigma_{21}, \sigma_{23}]_{\theta=0} = [K_I, K_{II}, K_{III}]/\sqrt{2\pi r},$$

$$(5.9) \quad [\Delta u_2, \Delta u_1, \Delta u_3] = [K_I, K_{II}, K_{III}]/(1 - \nu) 4(1 - \nu)\sqrt{r/2\pi}/G.$$

These features are shown in fig. 7. Evidently, mode I corresponds to tensile opening of the crack faces, mode II to in-plane shear sliding and mode III to antiplane shear sliding.

The full angular distribution of $\sigma_{\alpha\beta}$ and u_γ corresponding to the $r^{-\frac{1}{2}}$ singularity, obtained by substituting (5.7) into (5.2)-(5.6), has been given in many sources (*e.g.* eqs. (78)-(83) of [6], also [45, 46, 48-50]). The complete stress field in the vicinity of the tip consists of this singular field, plus a uniform stress field $\sigma_{\alpha\beta}^t$ (where $\sigma_{2\beta}^t$ are tractions transmitted across the crack faces at the tip), plus other terms which vanish at the tip and are of order \sqrt{r} , r , $r\sqrt{r}$, r^2 , etc.

Consider the following problems of isolated planar cracks on $x_2 = 0$, in bodies which are loaded such that, if the crack were not present, a uniform traction $\sigma_{2\alpha}^0$ would be transmitted across the crack plane, whereas when the crack is present a reduced but uniform traction (possibly zero) $\sigma_{2\alpha}^t$ is transmitted; $\Delta\sigma_\alpha = \sigma_{2\alpha}^0 - \sigma_{2\alpha}^t$ are components of stress drop. For an indefinitely long (in the x_3 -direction) « tunnel » crack with edges at $x_1 = \pm a$ (*e.g.* a crack as in fig. 6b) when $b/a \rightarrow \infty$)

$$(5.10) \quad [\Delta u_1, \Delta u_2, (1-\nu)\Delta u_3] = 2(1-\nu)[\Delta\sigma_1, \Delta\sigma_2, \Delta\sigma_3]\sqrt{a^2-x_1^2}/G$$

and by comparison with eqs. (5.9), setting $r = a - x_1$,

$$(5.11) \quad [K_I, K_{II}, K_{III}] = [\Delta\sigma_2, \Delta\sigma_1, \Delta\sigma_3]\sqrt{\pi a}.$$

Similarly, for a circular crack of radius a ,

$$(5.12) \quad \Delta u_\alpha = 8(1-\nu)(\Delta\sigma_\alpha - \nu\delta_{2\alpha}\Delta\sigma_2/2)\sqrt{a^2-\varrho^2}/(2-\nu)\pi G,$$

where ϱ is distance from the crack center, and

$$(5.13) \quad [K_I, K_{II}, K_{III}] = \\ = [(2-\nu)\Delta\sigma_2/2, \gamma_1\Delta\sigma_1 + \gamma_3\Delta\sigma_3, \gamma_1\Delta\sigma_3 - \gamma_3\Delta\sigma_1]4\sqrt{\pi a}/(2-\nu)\pi,$$

where γ_1, γ_3 are components of a unit vector directed from the crack center to the point of interest on its periphery. The above solutions can be developed from work by ESHELBY [16], although all were given earlier in references summarized, *e.g.*, by PARIS and SIH [49], who also tabulate many known crack solutions (see also [51]).

5.2. *Representation of cracks by continuously distributed dislocations.* - Two-dimensional (plane strain, antiplane strain) crack problems can also be approached by distributing continuously dislocations along the crack surfaces (*e.g.* [44]). If a discrete dislocation with Burger's vector b_α is introduced at the origin of the (x_1, x_2) -plane, the resulting stresses must (by dimensional

considerations) decay as $1/r$. Hence, seeking solutions to eqs. (5.2)-(5.6) with φ , ψ and ω given as constants times $\ln \zeta$, choosing the constants so that no net forces are produced and that the jumps in u_α are consistent with the given b_α , one obtains (e.g. [6], eqs.(111, 70))

$$(5.14) \quad [\varphi(\zeta), \psi(\zeta), \omega(\zeta)] = [b_1 + ib_2, -b_1 + ib_2, 2i(1-\nu)b_3] G(\ln \zeta)/4\pi i(1-\nu)$$

and, when $\ln \zeta$ is branch cut along the negative x_1 -axis, this is the solution for the distribution of displacement discontinuity

$$(5.15) \quad \Delta u_\alpha(x_1) = b_\alpha U(-x_1),$$

where U is the unit step function. The resulting stresses $\sigma_{2\alpha}$ on the x_1 -axis are

$$(5.16) \quad [\sigma_{21}, \sigma_{22}, \sigma_{23}] = [b_1, b_2, (1-\nu)b_3] G/2\pi(1-\nu)x_1.$$

Now consider a general distribution of discontinuity $\Delta u_\alpha(x_1)$. If we let $\sigma_{\alpha\beta}^0$ be the stress field existing before introduction of the discontinuity (the above stresses then correspond to $\sigma_{\alpha\beta} - \sigma_{\alpha\beta}^0$), the tractions $\sigma_{2\alpha}$ on the x_1 -axis are given by superposition as

$$(5.17) \quad \sigma_{2\alpha}(x_1, 0) = \sigma_{2\alpha}^0(x_1, 0) - \frac{G}{2\pi(1-\nu)} \int_{-\infty}^{+\infty} \frac{d\Delta u_\alpha(x'_1)/dx'_1}{x_1 - x'_1} dx'_1$$

for $\alpha = 1$ or 2 ; the $1-\nu$ is deleted for the antiplane mode, $\alpha = 3$. The integral is interpreted in a Cauchy principal-value sense, and $-d\Delta u_\alpha(x'_1)/dx'_1$ is the density of a continuous distribution of dislocations (i.e. $b_\alpha \rightarrow \text{density} \times dx'_1$). Hence, if the final traction $\sigma_{2\alpha}^f$ is specified as some function of x_1 along a portion L of the x_1 -axis, corresponding to a crack or group of cracks, this becomes the singular integral equation (omitting subscripts α)

$$(5.18) \quad \Delta\sigma(x_1) = \frac{G}{2\pi(1-\nu)} \int_L \frac{d\Delta u(x'_1)/dx'_1}{x_1 - x'_1} dx'_1, \quad x_1 \text{ on } L,$$

for $d\Delta u/dx_1$, where $\Delta\sigma$ is the stress drop $\sigma^0 - \sigma^f$. Such equations have unique solutions provided that n conditions of the type

$$(5.19) \quad \int_{L_k} [d\Delta u(x'_1)/dx'_1] dx'_1 = -(D)_k$$

are given (L_1, L_2, \dots, L_n are the n cracks constituting L , $(D)_k$ is the net dislocation entrapped within L_k). These conditions can be replaced, e.g., with a condition that there be no singularity at one end of a crack, with the corresponding $(D)_k$

then being determined as part of the solution. The procedure is discussed at length by MUSKHELISHVILI [47].

For a single crack lying between $-a$ and $+a$ the solution is (*e.g.* [6, 44, 47])

$$(5.20) \quad \frac{d\Delta u(x)}{dx} = -\frac{2(1-\nu)}{\pi G \sqrt{a^2-x^2}} \int_{-a}^{+a} \frac{\sqrt{a^2-s^2} \Delta\sigma(s)}{x-s} ds - \frac{D}{\pi \sqrt{a^2-x^2}},$$

and, if we compare this near $x = \pm a$ with expressions given in (5.9), the stress intensity factors at the crack tips $\pm a$ are

$$(5.21) \quad K = \frac{1}{\sqrt{\pi a}} \int_{-a}^{+a} \sqrt{\frac{a \pm x}{a \mp x}} \Delta\sigma(x) dx \pm \frac{GD}{2(1-\nu)\sqrt{\pi a}}.$$

The last two results are valid for modes I and II, and for mode III the $1-\nu$ is removed. In the case of a uniform stress drop, the terms in (5.20), (5.21) involving integrals of $\Delta\sigma$ give results for Δu and K identical to those of (5.10), (5.11), as required.

Integral equations of the kind (5.18) have been used widely in tensile crack analysis (*e.g.* [44, 52]), especially in connection with cohesive zone models, and in crystal dislocation theory to simulate the effect of large numbers of « piled up » dislocations on a slip plane (*e.g.* [53]).

For cracks that are finitely near to boundaries, the technique is modified by replacing $1/(x_1 - x'_1)$ in (5.18) by

$$1/(x_1 - x'_1) + h(x_1, x'_1),$$

where h is nonsingular within the body and arises from the solution for a discrete dislocation at x'_1 in a finite body. The resulting integral equation must then generally be solved numerically. The technique was first applied to model Earth faults by DMOWSKA and KOSTROV [54], who examined the case of a plane strain dip-slip fault near the surface of a half-space (see also [55]) and determined h by analytic function theory methods based on (5.2), (5.4), (5.5), as appropriate for the two cases of a prescribed shear stress drop and a shear stress which is related to the (deformation altered) normal stress on the fault by Coulomb friction. Recent applications based on numerical solutions of the singular integral equation for slip-weakening fault models (see sect. 6) have been made by CLEARY [56], STUART [57, 58] and STUART and MAVKO [59]. An integral equation analogous to (5.18) was developed and solved numerically for isolated three-dimensional planar cracks with uniform and nonuniform stress drops by WEAVER [60], through use of a static version of the representation of (2.12), (2.14), and BUDIANSKY and RICE [61] have recently outlined a generalization to three-dimensional cracks under dynamic loading.

5'3. *Energy release rate; J integral.* — The energy release rate \mathcal{J} is defined such that, if the crack front in fig. 7 is advanced infinitesimally by δl , $\mathcal{J} \delta l$ is the excess of the work done by external loads over the sum of the change in strain energy of the body and the work against tractions σ^f which resist motion of the crack faces (all on the basis of unit thickness in the x_3 -direction). Hence, mathematically \mathcal{J} is the rate (with respect to crack area) of energy loss through the singularity, and physically it is the energy flow to «breakdown» processes at the tip, *i.e.* the fracture energy. As IRWIN [48] observed, this quantity can be calculated as the negative of the work of removing the concentrated stresses $\sigma_{2\alpha}$ of (5.8) from δl , so that the surfaces displace by Δu_α of (5.9) with r measured from the new crack tip (in the limit $\delta l \rightarrow 0$ only the singular terms contribute). Since the material is modelled as linear elastic,

$$(5.22) \quad \mathcal{J} = \lim_{\delta l \rightarrow 0} \frac{1}{2\delta l} \int_0^{\delta l} \sigma_{2\alpha}(r, 0) \Delta u_\alpha(\delta l - r) dr = \frac{1-\nu}{2G} (K_I^2 + K_{II}^2) + \frac{1}{2G} K_{III}^2.$$

It is important to note that this expression for \mathcal{J} corresponds to coplanar crack advance or to advance with continuously turning tangent plane to the crack surface. Such is not always observed (subsect. 5'4).

A concept closely related to \mathcal{J} is that of the path-independent J integral for cracks in two-dimensional deformation fields [6,62]. If we consider first the case of traction-free crack surfaces, J is defined on contours Γ of the type shown in fig. 8a) by

$$(5.23) \quad J = \int_{\Gamma} (W n_1 - n_\alpha \sigma_{\alpha\beta} \partial u_\beta / \partial x_1) ds.$$

Here \mathbf{n} is the outer normal to Γ , ds is arc length along it, and $W = W(\boldsymbol{\epsilon})$ is the strain energy density,

$$(5.24) \quad W(\boldsymbol{\epsilon}) = \int_0^{\boldsymbol{\epsilon}} \sigma_{\alpha\beta}(\boldsymbol{\epsilon}) d\boldsymbol{\epsilon}_{\alpha\beta}.$$

In the linear elastic case $W = \frac{1}{2} \sigma_{\alpha\beta} \boldsymbol{\epsilon}_{\alpha\beta}$, but the properties of J are equally valid for nonlinear elastic materials (and, as observed by ESHELBY [63], for finitely deformed elastic materials, provided that the terms within J are properly interpreted). RICE [6, 62] showed that J is independent of the path Γ and developed several applications in which J , as evaluated on remote contours, is thereby related to parameters of nonlinear zones at crack tips. One of these is fundamental to the analysis of slip-weakening models (sect. 6). He also showed that J is equal to the energy release rate of an elastic crack, so that in the linear elastic case J is equal to \mathcal{J} as given by (5.22). This was observed independ-

ently by CHEREPANOV [64] and ATKINSON and ESHELBY [65] in the sense that they expressed \mathcal{J} as the limiting value of integrals on contours Γ shrunk onto the crack tip and reducing to J in that limit.

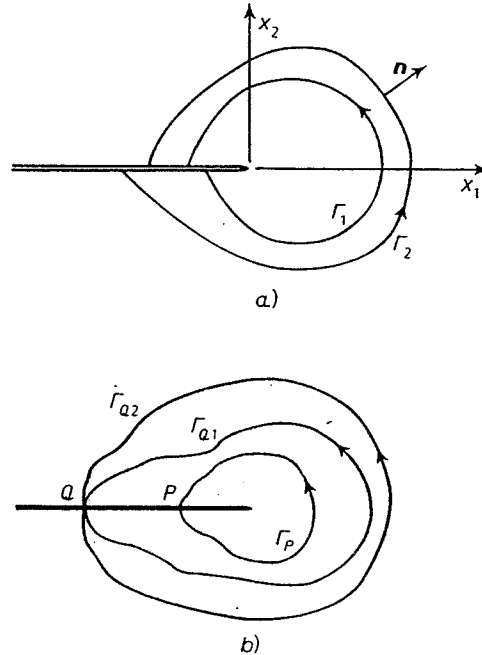


Fig. 8. - Paths for the J integral: a) traction-free crack surfaces, $(J)_{\Gamma_1} = (J)_{\Gamma_2}$; b) crack surfaces support tractions, $(J)_{\Gamma_{Q1}} = (J)_{\Gamma_{Q2}}$, $(J)_{\Gamma_Q} \neq (J)_{\Gamma_P}$.

When the crack surfaces support tractions, as will be the case for earthquake faults, J must be interpreted in a manner demonstrated by PALMER and RICE [66]. With reference to fig. 8b), J is path independent for all contours which begin and end at the same point, such as Γ_{Q1} and Γ_{Q2} , but is different for a contour such as Γ_P with a different origin point. A closed contour can be formed by traversing a path Γ_Q , following the upper crack surface to P , traversing Γ_P in the opposite sense from that shown, and following the lower crack surface to Q . The integral of the integrand of (5.23) around this closed contour is zero and hence

$$(5.25) \quad J_Q - J_P + \int_Q^P \sigma_{2\alpha}(x_1, 0) (\partial \Delta u_\alpha(x_1) / \partial x_1) dx_1 = 0.$$

Now, if Γ_P is shrunk onto the tip, $J_P = \mathcal{J}$ (i.e. the energy release rate associated with the crack tip singularity) and hence

$$(5.26) \quad \mathcal{J} = J_Q + \int_Q^{\text{tip}} \sigma_{2\alpha}(x_1, 0) (\partial \Delta u_\alpha(x_1) / \partial x_1) dx_1.$$

Thus the quantity on the right is independent of the location of Q , and for the elastic crack model of fig. 7, in which the tractions $\sigma_{2\alpha}$ take on uniform values $\sigma_{2\alpha}^f$ along the crack faces, this reduces to

$$(5.27) \quad \mathcal{J} = J_Q - \sigma_{2\alpha}^f (\Delta u_\alpha)_Q .$$

PALMER and RICE [66] give several applications of this last relation to the calculation of \mathcal{J} for shear cracks, one of which has been extended by RUDNICKI [8] to estimate \mathcal{J} for the 1857 California earthquake (subsect. 5'4), and also demonstrate directly the interpretation of the right-hand side as a crack tip energy flux.

5'4. *Cracking processes and fracture energy.* — When a brittle solid containing a crack is loaded in mode I, the crack tends to grow straight ahead as indicated in fig. 9a). Rapidly running mode-I cracks do, however, exhibit abrupt bifurcations of path (e.g. [45]), which are thought to be due to the varying angular distribution of stresses near the crack as velocity increases (subsect. 5'5). For example, YOFFE [67] showed that the hoop stress $\sigma_{\theta\theta}$ becomes maximum at $\theta \approx \pm 60^\circ$, rather than at $\theta = 0$, when the crack propagation speed reaches

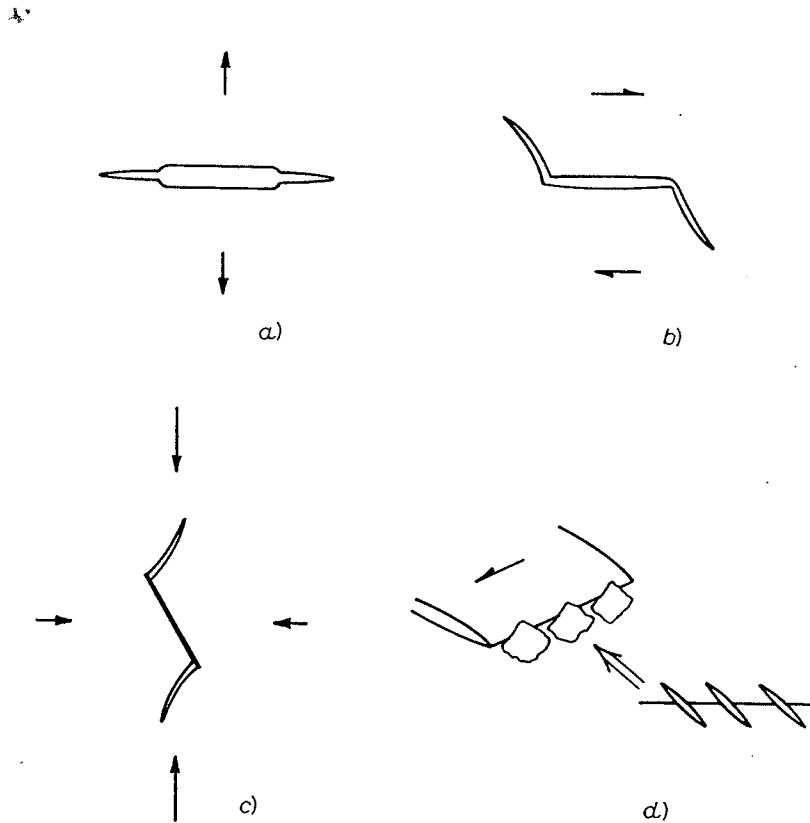


Fig. 9. — Crack paths in brittle solids: a) mode-I loading, b) mode-II loading, c) local tensile cracking from tips of a closed crack in frictional sliding, d) mode-III loading.

0.5 c_c . Also, COTTERELL and RICE [68] have recently shown that even for quasi-static crack growth the straight path will be unstable, in the sense that any small deviation of the crack surface tangent plane from straightness becomes amplified with continuing growth, whenever the nonsingular stress term σ_{11}^f at the crack tip is positive.

The testing of cracks under combined mode conditions shows decidedly nonplanar growth. For example, fig. 9b) shows brittle crack growth under mode-II loading and, as observed by ERDOGAN and SIIH [69], the crack begins to propagate at an angle coinciding closely with the maximum in $\sigma_{\theta\theta}$ (at $\theta \approx -70^\circ$) under mode-II conditions. It then follows a curved path which is, presumably, one for which pure mode-I conditions prevail locally at the tip [68]. Figure 9c) illustrates local tensile cracking from the tips of a closed crack in a compressively loaded specimen, for which the crack surfaces slide under frictional resistance [70]. The initial conditions at the tips of the closed crack are mode II in this case and hence the initial details of propagation are similar to those of fig. 9b). This mechanism at the level of grain-scale microcracks is thought to be central to the macroscopically inelastic (and dilatant) deformation of brittle rocks tested under compression, *e.g.* in the « triaxial » test [71, 72]. Finally, fig. 9d) illustrates the pattern of cracking at a mode-III crack tip in a brittle solid [45, 73]. The pattern reflects the fact that the pure shear stress state ahead of a mode-III crack has maximum principal tensile stress at 45° from the crack plane. PALANISWAMY and KNAUSS [73] and COTTERELL and RICE [68] summarize results on the stress analysis of nonplanar cracks.

In an earthquake setting, the high macroscale compressive stresses will inhibit the extent of local tensile cracking illustrated in fig. 9b) to c). But the figures suggest that the microscale cracking processes involved in macroscopic shear faulting will be complex, and will have associated with them a far greater effective fracture energy than for a single tensile crack. This seems consistent with direct observations of fault structure by MCGARR *et al.* [41], with estimates of the fracture energy of Earth faults [8, 74, 75] and with estimates of shear fracture energy from laboratory data in sect. 6.

For mode-I crack growth, the classical fracture criterion of Griffith [76] equates \mathcal{S} to the energy 2γ of forming unit area of new surfaces. Here γ is the surface energy, *i.e.* half the reversible work of separating atomic planes. RUDNICKI [8] and ATKINSON [77] summarize data on the tensile fracture of rock. Typically, the critical value of K_I is in the range 0.5 to 2.0 MN/m^{3/2} for brittle rocks. With $\nu = 0.25$ and $G = 30$ GPa (1 GPa = 10^9 N/m² = 10 kilobar) as appropriate for granite, this leads to values of \mathcal{S} in the range of 3 to 50 J/m². By comparison, 2γ is estimated to be in the range of 1 to 2 J/m², and the discrepancy is thought to be due to microcrack formation away from the main crack plane and perhaps to local plasticity.

Fracture energies estimated for slip propagation along Earth faults cover a considerable range, but the methods by which results are inferred are subject

to considerable errors. By methods discussed in subsect. 5'5, HUSSEINI *et al.* [74] estimate fracture energies (corresponding to $\mathcal{S}/2$ in their notation) associated with the arrest of earthquake rupture. They divide results into those for frictional sliding (1 to 10^4 J/m²) and for fresh fracture (10^4 to 10^6 J/m²). The latter range seems consistent with values of \mathcal{S} estimated in sect. 6 (10^4 to 10^5 J/m²) from laboratory data on rock fracture under high confining stress. The upper end of the range of Husseini *et al.* (10^6 J/m²) may reflect complex patterns of rupture propagation on a macroscale, analogous to those observed microscopically, as suggested by the barrier concept and discontinuous rupture model of Das and Aki [4]. RUDNICKI [8] applies eq. (5.27), using a far-field evaluation of the right-hand side in a manner similar to that of Palmer and Rice [66], to estimate \mathcal{S} for the onset of rupture at the locked end of a long, aseismically slipping strike slip fault. The estimate is given in terms of average plate motions and large earthquake recurrence times, and he arrives at an order-of-magnitude estimate of $4 \cdot 10^6$ J/m² for the 1857 California earthquake. He suggests that the effective \mathcal{S} during propagation could be much lower than this initiation value.

It is expected that shear fracture energies associated with the creep propagation of slip events along aseismic segments of faults would be considerably lower than for the fresh fracture of rock. Such quasi-statically propagating ruptures have been studied by KING, NASON and TOCHER [78], and one event which arrested within their instrument array had a distribution of slip offset which was very close to the pattern predicted by eq. (5.10). RICE and SIMONS [75] used this result to estimate the stress drop (0.38 bar) and calculated a value of \mathcal{S} at arrest of $2.6 \cdot 10^2$ J/m². This is probably by far the most accurate of estimates made from field data, but the result cannot be expected to be representative of seismic rupture. It does, nevertheless, fall into the broad range which HUSSEINI *et al.* [74] attributed to frictional slip.

In the presence of a corrosive environment such as water or humid air rocks exhibit time-dependent stress corrosion crack growth (*e.g.* [79]). The phenomenology of analogous behavior in glasses and technological ceramics has been reviewed by WACHTMAN [80] and LAWN and WILSHAW [45], and the modification of the Griffith criterion for elastic-brittle crack growth in a surface reactive environment is discussed by RICE [81]. This time-dependent cracking process, active at the microcrack level, can lead to brittle creep of rock [82] and RICE [11] has discussed resulting strength degradation and time dependence in the triaxial test in terms of the cracking mechanism of fig. 9c). The effect of such processes at the microcrack level could lead to analogous time-dependent but initially quasi-static propagation of macroscopic shear ruptures, but no data seem to be available on this.

5'5. *Elastodynamic crack tip fields for rapidly propagating fractures.* — To obtain the structure of near-tip elastodynamic fields, analogous to that of

eqs. (5.7)-(5.9) of the quasi-static case, observe that the right-hand side of (5.1) is then given by

$$\rho \partial^2 / \partial t^2 [u_1, u_2, u_3].$$

For purposes of analyzing the structure of the singularity at a crack tip moving with speed v , this can be written as

$$\rho v^2 \partial^2 / \partial x_1^2 [u_1, u_2, u_3],$$

since the difference between $\partial^2 / \partial t^2$ and $v^2 \partial^2 / \partial x_1^2$ involves only terms with lower-order derivatives on spatial variables that do not contribute to determining the form of the singularity. Note also that this replacement is exact everywhere (*i.e.* not just asymptotically) for « steady state » crack motion problems as considered by YOFFE [67] and CRAGGS [83], in which v is constant and the field depends only on $x_1 - vt$ and x_2 .

The form of the near-tip field can then be extracted from the special solutions of Craggs [83], and RICE [6] gave an analysis, paralleling the Williams [50] eigenfunction expansion, for mode I. A general analysis of all three modes was given subsequently by KOSTROV and NIKITIN [84] and is followed here. They observe that the governing equations (5.1), with the right-hand side as above, take the form (with $u_\beta = u_\beta^d + u_\beta^s$)

$$(5.28) \quad \begin{cases} \alpha_d^2 \partial^2 u_\beta^d / \partial x_1^2 + \partial^2 u_\beta^d / \partial x_2^2 = 0, & \beta = 1, 2, \\ \alpha_s^2 \partial^2 u_\beta^s / \partial x_1^2 + \partial^2 u_\beta^s / \partial x_2^2 = 0, & \beta = 1, 2, 3, \end{cases}$$

where $\partial u_1^d / \partial x_2 - \partial u_2^d / \partial x_1 = \partial u_1^s / \partial x_1 + \partial u_2^s / \partial x_2 = 0$, $u_3^d = 0$, and

$$(5.29) \quad \alpha_d^2 = 1 - v^2 / c_d^2, \quad \alpha_s^2 = 1 - v^2 / c_s^2.$$

These equations have subsonic solutions in the form

$$(5.30) \quad \begin{cases} u_\beta^d = \text{Re} [U_\beta^d(\zeta_d)] & \text{with } U_2^d = i\alpha_d U_1^d, \\ u_\beta^s = \text{Re} [U_\beta^s(\zeta_s)] & \text{with } \alpha_s U_2^s = iU_1^s, \end{cases}$$

where the U_β^d , U_β^s are analytic functions of

$$(5.31) \quad \zeta_d = x_1 + i\alpha_d x_2, \quad \zeta_s = x_1 + i\alpha_s x_2$$

and Re means « real part ». KOSTROV and NIKITIN [84] show that singular solutions leaving the crack surfaces stress free are given by (with notation for stress intensity factors consistent with subsect. 5.1)

$$(5.32) \quad \begin{cases} -G[(1 + \alpha_s^2) U_1^d(\zeta) + 2U_1^s(\zeta)] = K_I \zeta^{\frac{1}{2}} / 2\sqrt{2\pi}, \\ (iG/\alpha_s)[2\alpha_s \alpha_d U_1^d(\zeta) + (1 + \alpha_s^2) U_1^s(\zeta)] = K_{II} \zeta^{\frac{1}{2}} / 2\sqrt{2\pi}, \\ iG\alpha_s U_3^s(\zeta) = K_{III} \zeta^{\frac{1}{2}} / 2\sqrt{2\pi}, \end{cases}$$

and $U_2^d(\zeta)$, $U_2^s(\zeta)$ are defined in (5.30). Here the K 's, which will in general be time dependent, are chosen so that the tractions on the line ahead of the crack are of the same form as in (5.8), namely

$$(5.33) \quad [\sigma_{22}, \sigma_{21}, \sigma_{23}]_{\theta=0} = [K_I, K_{II}, K_{III}]/\sqrt{2\pi r}.$$

The resulting displacement discontinuities along the crack take the form (compare eq. (5.9))

$$(5.34) \quad [\Delta u_2, \Delta u_1, \Delta u_3] = [f_I K_I, f_{II} K_{II}, f_{III} K_{III}/(1-\nu)]4(1-\nu)\sqrt{r/2\pi}/G,$$

where the f 's are monotonically increasing functions of velocity, normalized so that $f(0) = 1$, given by

$$(5.35) \quad f_I = \alpha_d v^2/(1-\nu)Rc_s^2, \quad f_{II} = \alpha_s v^2/(1-\nu)Rc_s^2, \quad f_{III} = 1/\alpha_s,$$

where

$$(5.36) \quad R = 4\alpha_s\alpha_d - (1 + \alpha_s^2)^2$$

is a function which behaves as $2v^2(1/c_s^2 - 1/c_d^2) = v^2/(1-\nu)c_s^2$ for small v and which vanishes at the Rayleigh speed c_R . Hence f_I and $f_{II} \rightarrow \infty$ as $v \rightarrow c_R$, $f_{III} \rightarrow \infty$ as $v \rightarrow c_s$.

The complete angular distributions of stress are given by RICE [6] for mode I. He shows that in addition to the shifting of the maximum for $\sigma_{\theta\theta}$ away from the crack plane, observed by YOFFE [67] (see also [85]), the ratio σ_{11}/σ_{22} ahead of the crack increases continuously from unity at $v = 0$ to infinity at the Rayleigh speed. Both of these observations seem consistent with extensive microfracturing in directions noncoincident with the crack plane at rapid crack speeds.

Indeed, this intensification of stress off the crack plane seems to be a general feature of stress fields at the tips of rapidly moving cracks. For example, ERDOGAN [85] plots the shearing stress σ_{θ_3} at a mode-III crack tip and observes that the maximum shifts away from the crack plane at $v \approx 0.6c_s$. Also, KOSTROV [86] has examined the ratio of σ_{11} at $\theta = -90^\circ$ to σ_{21} at $\theta = 0$ (for the same value of r) for the mode-II crack tip field, and reports that this ratio increases rapidly toward infinity as the Rayleigh speed is approached. Kostrov's observation suggests that near the Rayleigh speed local tensile stresses at the tips of earthquake shear ruptures may become large enough to exceed the ambient compressive stress field and lead to extensive local tensile cracking at high angles with the fracture plane (see sect. 6 for a quantitative estimate). Thus the possibility arises that rapidly propagating earthquake shear ruptures are self-destabilizing near the limiting speed, and subject to arrest or discontinuous propagation paths due to massive fracturing off the plane of the main rupture, much as for shear cracks studied experimentally in brittle solids (fig. 9).

This may be a significant factor leading to the discontinuous, segmented appearance of fracture surfaces cited by MCGARR *et al.* [41] and DAS and AKI [4], and to some of the abnormally large values of fracture energy inferred by HUSSEINI *et al.* [74]. It may also be related to observations of Lindh *et al.* [87] that foreshocks preceding three California earthquakes that they studied had fault plane orientations that differed by 5° to 10° from the orientation inferred for the main shock. Each foreshock could possibly represent a self-arresting shear crack, with an array similar to that in fig. 6 being formed before the final rupture.

As KOSTROV and NIKITIN [84] show (see also [7, 39, 65]), the energy release rate \mathcal{S} may be calculated from the J integral, eq. (5.23), with W replaced by $W + \frac{1}{2}\rho v^2(\partial u_\alpha/\partial x_1)(\partial u_\alpha/\partial x_1)$ and Γ shrunk onto the tip. (For steady-state problems the integral is then independent of path Γ and hence $J = \mathcal{S}$ for all contours.) The result is

$$(5.37) \quad \mathcal{S} = \frac{1-\nu}{2G} (f_I K_I^2 + f_{II} K_{II}^2) + \frac{1}{2G} f_{III} K_{III}^2$$

with the f 's defined by (5.35).

Solutions are known for the stress intensity factors only for a limited number of dynamic-crack problems. For cracks which originate from zero length and spread at a uniform speed v (*e.g.* [38, 88, 89]), K is proportional to $\Delta\sigma\sqrt{vt}$ and goes to zero as the limiting speed is approached for the mode considered, but in such a way that fK (*i.e.* the intensity coefficient governing Δu) remains finite. It is then clear from (5.37) that $\mathcal{S} \rightarrow 0$ at the limiting speed. This suggests that, as cracks grow and $\Delta\sigma\sqrt{a}$ becomes large, v will be driven towards the limiting speed, unless secondary processes relating to high stresses off the fracture plane intervene, perhaps necessitating a sequential reinitiation of rupture and acceleration again toward the limiting speed.

An important class of solutions developed by KOSTROV [90] and ESHELBY [91] for mode III, by FREUND [92] for mode I and by FOSSUM and FREUND [93] for mode II relates to short-time nonuniform crack extension into an initially static stress field, before reflected waves from the other crack tip or boundaries intervene. In such cases K has the form, when the crack has advanced distance a and has current speed $v = \dot{a}$,

$$(5.38) \quad K = k(v) K_0(a).$$

Here $k(v)$ is a function which decreases from unity at $v = 0$ to zero at the limiting speed, and $K_0(a)$ is the stress intensity factor that would result at the tip of a semi-infinite static crack which had advanced by distance a into the same initial stress field. For example,

$$(5.39) \quad k(v) = (1 - v/c_s)^{\frac{1}{2}}$$

for mode III. These developments allow short-time equations of motion to be written for cracks if, for example, the requisite fracture energy \mathcal{S} of (5.37) is specified as a function of position along the fracture path and perhaps of v , and the techniques can be extended to the impingement of stress wave loadings on cracks [39]. The structure of eqs. (5.38) and (5.37) implies that an elastic crack tip has no «inertia», in the sense that a discontinuous change of the requisite \mathcal{S} along the fracture path implies a discontinuous change in v . Hence crack propagation can be arrested instantaneously by a sufficiently large increase in \mathcal{S} or by impingement of an unloading stress wave of sufficient magnitude.

HUSSEINI *et al.* [74] applied these concepts to the arrest of a propagating earthquake rupture (see also the discussion by AKI and RICHARDS [1]), and thereby obtained the estimates of the fracture energy of earthquakes discussed in subsect. 5'4. They consider two mechanisms for arrest, within the content of a simple model in which the fault is considered as a semi-infinite mode-III crack that suddenly appears and begins to propagate at $t=0$ under the action of a stress drop distribution that extends back only over a finite portion of crack (to simulate a finite fault). The first mechanism envisions a uniform stress drop as the crack propagates, and considers the required fracture energy to increase either continuously or abruptly along the fracture path. The second, which they call the seismic-gap mechanism, envisions that the fracture energy is uniform but that the region of significant stress drop is finite, with $\Delta\sigma$ falling to zero after some distance of propagation. The model is a severe idealization and the seismic-gap analysis assumes that the seismic moment and the area-average stress drop are related in the same manner as for a uniform stress drop on a circular rupture (eq. (4.16)), which is not rigorously true even for a circular rupture (subsect. 4'3). Further, the area of rupture is estimated from the corner frequency analysis. Hence there are significant uncertainties in the estimated fracture energies and these should be regarded only as very rough order-of-magnitude estimates. Further, it must be realized that faults subject to highly nonuniform, concentrated stressing may experience negative stress drops over portions of the fracture that extend outside of the high-stress epicentral region. Such fractures will ultimately arrest even with zero fracture energy, as in the model of shear crack arrest by BURRIDGE and HALLIDAY [94].

Finally, it is noted that the functions $f(v)$ of (5.35) have a fundamental role in problems of steady-state crack motion as considered by YOFFE [67] and CRAGGS [83]. In particular, the structure of the solution developed through eqs. (5.28)-(5.34) implies that, if a discrete dislocation with Burger's vector b_α moves at uniform speed v in the x_1 -direction, and is currently at the origin of the x_1, x_2 co-ordinate system, the stresses $\sigma_{2\alpha}$ on the x_1 -axis are (compare eq. (5.16))

$$(5.40) \quad [\sigma_{21}, \sigma_{22}, \sigma_{23}] = [b_1/f_{II}, b_2/f_I, (1-\nu)b_3/f_{III}]G/2\pi(1-\nu)x_1.$$

Thus for the steady-state problem of a crack of fixed length $2a$ moving at uniform speed v (growing at $x_1 = a$, healing at $x_1 = -a$), eq. (5.20) for Δu applies if $\Delta\sigma$ is replaced by $f\Delta\sigma$, where f pertains to the particular mode considered. Also, eq. (5.21) applies for K if D is replaced by D/f . These results are used (with $a \rightarrow \infty$) in subsect. 6.3 for an asymptotic analysis of dynamic crack growth with a small slip-weakening zone.

6. - Slip-weakening instability models.

In order to deal with fault motion in cases for which the zone of strength degradation is not confined to the immediate vicinity of the crack tip, as well as to obtain an interpretation of the fracture energy \mathcal{F} of elastic crack mechanics, slip-weakening models as illustrated in fig. 10 are considered here.

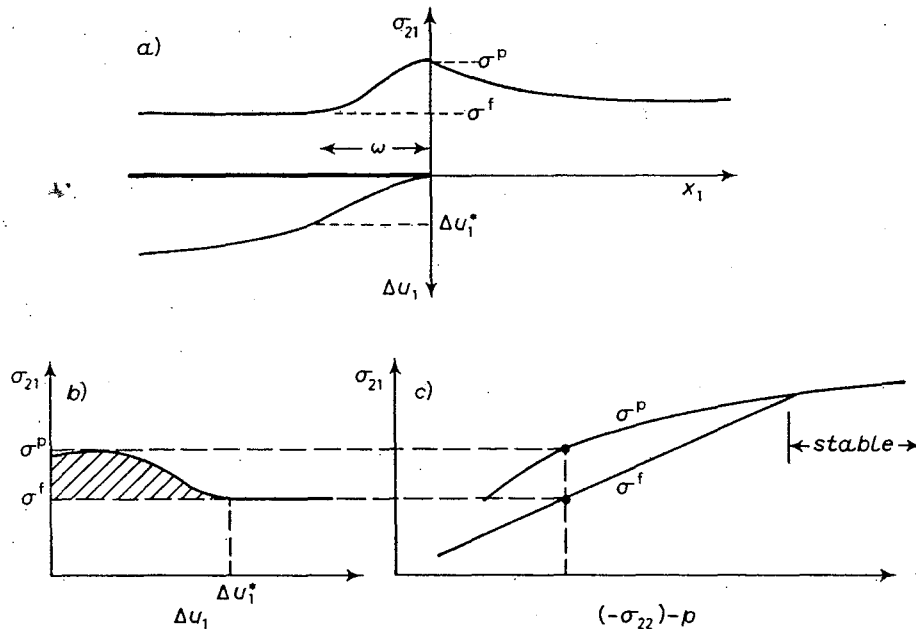


Fig. 10. - Slip-weakening model: a) Fault and distribution of shear stress σ_{21} and slip displacement Δu_1 . b) Shear stress vs. slip relation; cross-hatched area corresponds to fracture energy $\mathcal{F} = (\sigma^p - \sigma^f)\Delta u_1^*$. c) Dependence of peak strength σ^p and residual frictional strength σ^f on the effective normal stress.

The mode-II case is shown and (fig. 10b)) the strength σ_{21} of the material in resisting slip is assumed to vary with the amount of slip, Δu_1 . In the simplest case the response is modelled as rate insensitive and σ_{21} exhibits a peak strength σ^p (corresponding to the onset of slip for fresh fracture, but perhaps preceded by slip at lower stress levels for a pre-existing fault), and degrades to a constant residual friction level, σ^f , when Δu_1 exceeds an amount Δu_1^* . This is a more detailed model of the drop from static to sliding friction, which is often regarded

as occurring abruptly in classical friction studies. The corresponding distributions of σ_{21} and Δu_1 are shown in fig. 10a). Since the strength of the material is finite, there is no singularity but rather a continuous stress distribution at the crack tip. The notation ω denotes the size of the slip-weakening zone, *i.e.* the zone in which $0 < \Delta u_1 < \Delta u^*$ and $\sigma_{21} > \sigma^f$.

Such slip-weakening models are an extension to shear faults of « cohesive zone » models for tensile cracks, as introduced by BARENBLATT [95] to represent molecular cohesion in brittle fracture and by DUGDALE [96] and BILBY *et al.* [52] to represent approximately effects of plastic yielding in ductile materials. WILLIS [97], by direct calculations based on linear elasticity, and RICE [6, 62], by application of the J integral, showed that these models lead to fracture criteria that are equivalent to the critical \mathcal{J} criterion of elastic crack mechanics when the cohesive zone is small compared to overall crack size, and showed that the critical \mathcal{J} is equal to the area under the curve of cohesive stress (σ_{22}) *vs.* opening displacement (Δu_2). (On the other hand, significant differences from elastic fracture mechanics predictions arise when the applied stress is comparable to the cohesive stress [6, 52].) IDA [98] observed that the same results follow for shear cracks in which the shear stress σ_{21} falls to zero with increasing slip Δu_1 , and PALMER and RICE [66] give the more general interpretation for shear failure illustrated in fig. 10 (see also [11, 99]).

As shown by the connections between fig. 10b) and c), the parameters σ^p and σ^f are not constants but depend on the compressive stress ($-\sigma_{22}$ or, when fluid pore pressure p is present, sect. 3, on the « effective » compressive stress $-\sigma_{22} - p$) acting on the fault. The form of the σ^p and σ^f variations with compressive stress is suggested by experimentation on fault sliding, *e.g.*, as summarized by BARTON [100] and RUMMEL *et al.* [72]. At high compressive stress, and perhaps also at very low stress, the sliding process is stable and does not lead to (potentially) earthquake-generating drops in strength associated with stick slip. Increasing compressive stress corresponds generally to increasing depth in the crust and increasing temperature; the latter tends also to increase the stability of sliding at high compression [101].

PALMER and RICE [66] applied eq. (5.25) for $J_Q - J_P$ (based on the contours of fig. 8b)) to analysis of the model in fig. 10. We consider a pure mode-II slip event (the analysis is identical for pure mode III) so that the subscripts α in (5.25) can be dropped; $\sigma_{21}(x_1, 0)$ is denoted by $\sigma(x_1)$, $\Delta u_1(x_1)$ by $\Delta u(x_1)$. Since there is no singularity at the tip, $J_P = 0$ when the contour Γ_P is shrunk onto the tip and hence

$$(6.1) \quad J_Q + \int_0^{\text{tip}} \sigma(x_1) (\partial \Delta u(x_1) / \partial x_1) dx_1 = 0.$$

If we assume that compressive stress $-\sigma_{22}$ (or $-\sigma_{22} - p$) is uniform over the fault and that slippage is imminent, σ is a function of Δu only as in fig. 10b).

If the end region ω is confined to a finite segment of the fault as in fig. 10a), and point Q lies outside the end region,

$$(6.2) \quad \int_Q^{\text{tip}} \sigma(\partial \Delta u / \partial x_1) dx_1 = -\sigma^t(\Delta u)_Q + \int_Q^{\text{tip}} \{\sigma - \sigma^t\} (\partial \Delta u / \partial x_1) dx_1 = \\ = -\sigma^t(\Delta u)_Q + \int_{\Delta u^*}^0 \{\sigma[\Delta u] - \sigma^t\} d(\Delta u),$$

where the notation $\sigma[\Delta u]$ denotes the slip-weakening relation of fig. 10b). Hence from (6.1) the condition for incipient fault extension is that [66]

$$(6.3) \quad J_Q - \sigma^t(\Delta u)_Q = \int_0^{\Delta u^*} \{\sigma[\Delta u] - \sigma^t\} d(\Delta u).$$

The right-hand side of this expression corresponds to the cross-hatched area of fig. 10b); the left-hand side is independent of the location of point Q (so long as it lies outside the end region) and of the path Γ_Q for the J integral. PALMER and RICE [66] gave several evaluations of the left-hand side, and hence derived criteria for the onset of shear crack extension, for slip surfaces in clay soils. Following their work, we examine the limiting case in which the slip-weakening model and elastic-crack models can be compared. This occurs when the zone ω of strength degradation is small compared to overall crack size. In this case Rice's [6, 62] boundary layer formulation for small-scale yielding can be applied, with the slip surface regarded as semi-infinite, the body as infinite, and the remote stress field given by the characteristic elastic singular field

$$(6.4) \quad \sigma_{\alpha\beta} \rightarrow (K/\sqrt{r}) f_{\alpha\beta}(\theta) \quad \text{as } r \rightarrow \infty,$$

where K is the stress intensity factor for the analogous elastic-crack problem with $\sigma_{21} = \sigma^t$ everywhere along the crack surface. The point Q and contour Γ_Q may be chosen arbitrarily. By moving these to infinity and observing that perturbations of the stress field due to the near-tip cohesive zone decay sufficiently rapidly so as not to contribute to J_Q or $(\Delta u)_Q$ in this limit, it is seen that $J_Q - \sigma^t(\Delta u)_Q$ is given (for all choices of Q lying beyond the strength degradation zone) by the same expression as for the elastic-crack model. From eq. (5.26), this value is just \mathcal{J} , and hence the critical \mathcal{J} of elastic-crack mechanics is defined in terms of the slip-weakening model by [66]

$$(6.5) \quad \mathcal{J} = \int_0^{\Delta u^*} \{\sigma[\Delta u] - \sigma^t\} d(\Delta u),$$

i.e. by the cross-hatched area in fig. 10*b*). Hence \mathcal{J} is the excess of the actual work of the breakdown process over the work of frictional sliding against the residual stress σ^f . It is convenient to define a characteristic breakdown slip $\overline{\Delta u}$ by

$$(6.6) \quad (\sigma^p - \sigma^f) \overline{\Delta u} = \int_0^{\Delta u^*} \{\sigma[\Delta u] - \sigma^f\} d(\Delta u)$$

so that $\mathcal{J} = (\sigma^p - \sigma^f) \overline{\Delta u}$.

Proceeding with the same boundary layer analysis, it is also possible to estimate the size of the end region ω , although it is important to realize that such estimates will only be approximate, and generally somewhat smaller than actual, when the crack size is not large compared to ω . For this purpose Δu is given by the sum of the expression in (5.9) plus another contribution due to the excess of σ over σ^f within the cohesive zone. The latter contribution is calculated from (5.20) by first moving the co-ordinate origin to the right crack tip and letting $a \rightarrow \infty$, replacing $\Delta\sigma$ by $-(\sigma - \sigma^f)$, since for the superposition procedure $\Delta\sigma$ is measured relative to σ^f . Hence

$$(6.7) \quad \frac{d\Delta u(x_1)}{dx_1} = -\frac{2(1-\nu)K}{G\sqrt{-2\pi x_1}} + \frac{2(1-\nu)}{\pi G\sqrt{-x_1}} \int_{-\omega}^0 \frac{\sqrt{-x'_1}[\sigma(x'_1) - \sigma^f]}{x_1 - x'_1} dx'_1.$$

Since there must be no singularity at the crack tip, K and the stress distribution must be related by

$$(6.8) \quad K = \sqrt{\frac{2}{\pi}} \int_{-\omega}^0 \frac{\sigma(x'_1) - \sigma^f}{\sqrt{-x'_1}} dx'_1,$$

and thus (6.7) becomes

$$(6.9) \quad \frac{d\Delta u(x_1)}{dx_1} = \frac{2(1-\nu)\sqrt{-x_1}}{\pi G} \int_{-\omega}^0 \frac{\sigma(x'_1) - \sigma^f}{\sqrt{-x'_1}(x_1 - x'_1)} dx'_1.$$

The full procedure of solution is to solve this last equation as a nonlinear integral equation (since $\sigma(x_1)$ and $\Delta u(x_1)$ are related as in fig. 10*b*) and to use (6.8) to determine the associated K at the onset of growth; this K value is such that $(1-\nu)K^2/2G$ ($= \mathcal{J}$) necessarily meets (6.5). The details can be carried out without numerical methods only when $\sigma - \sigma^f$ is constant out to a critical slip ($= \overline{\Delta u}$), as shown by the dashed curves in fig. 11. If we call the size of the end region ω_1 in this case, eq. (6.8) requires that

$$(6.10) \quad \omega_1 = \pi K^2/8(\sigma^p - \sigma^f)^2,$$

which, with eqs. (6.5), (6.6) and the relation of \mathcal{J} to K , can be written as

$$(6.11) \quad \omega_1 = [\pi/4(1 - \nu)] \overline{\Delta u} [G/(\sigma^p - \sigma^f)].$$

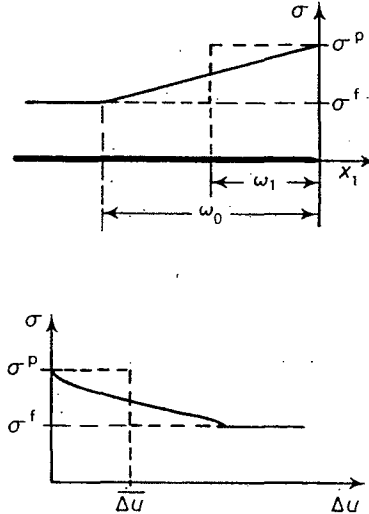


Fig. 11. - Two shear stress vs. slip relations, both with same strength drop and \mathcal{J} (or $\overline{\Delta u}$) values, and corresponding distributions of shear stress in weakening zone (for case when weakening zone is small compared to overall fault dimensions).

PALMER and RICE [66] used an inverse procedure to solve another case, in which σ is assumed to vary linearly with x_1 within the end zone (solid line in fig. 11), and in this case eqs. (6.5), (6.6), (6.8) lead to the end zone size

$$(6.12) \quad \omega_0 = [9\pi/16(1 - \nu)] \overline{\Delta u} [G/(\sigma^p - \sigma^f)],$$

which is 9/4 times the estimate of (6.11). The associated σ vs. Δu relation is obtained from (6.9) and has been plotted as the solid line in fig. 11; the parameter Δu^* is found to equal $9\overline{\Delta u}/4$. The latter result for ω_0 is probably more realistic and will be used for subsequent estimates. All of the equations derived here apply also to mode-III slip-weakening models if $1 - \nu$ is deleted, e.g., in (6.7), (6.9), (6.11) and (6.12).

6.1. *Large-scale instability models.* - STUART [57] and STUART and MAVKO [59] have obtained numerical solutions for slip-weakening models corresponding to through-crust strike-slip faults (mode-III slip). In these cases the end zone spreads over substantial distances and the elastic-crack model cannot be used. They specify the rate of crustal displacement at some distance from the fault and assume that the resisting shear stress has the form

$$(6.13) \quad \sigma - \sigma^f = S \exp [- (\Delta u)^2/a^2] \exp [- (z - z_0)^2/b^2],$$

and that the stress is everywhere equal to σ^f at the onset of a given loading episode. Here z is depth into the crust and S , a , z_0 and b are taken as constants. Thus $\sigma^p - \sigma^f$ and the effective fracture energy \mathcal{F} vary in proportion to $\exp[-(z-z_0)^2/b^2]$; z_0 can be identified as the depth at which compressive-stress levels on the fault correspond to the maximum difference between σ^p and σ^f in fig. 10*c*), and b is a measure of the extent of the brittle zone of the Earth's crust. Their σ vs. Δu and z (or compressive stress) relation is, however, chosen arbitrarily rather than fitted to experimental results.

They find in all cases that the model predicts extensive stable slip on the fault. Sometimes this is terminated by an instability (earthquake), preceded by a rapidly accelerating but still quasi-static rate of slip. Sometimes the entire fault can be slipped to the residual friction level without instability. The conditions for instability are not fully established by the particular numerical results that they report, but an important parameter is $(G/z_0)/(S/a)$, which can be interpreted as the ratio of an elastic-plate stiffness G/z_0 to a slip-weakening stiffness S/a . Small values of the parameter lead to instability, large values to completely aseismic accommodation of the imposed plate motion.

STUART [58] has recently reported a similar analysis of mode-II slip along a thrust fault dipping at 30° , intended to model preseismic slip before the 1971 San Fernando earthquake. He uses (6.13) with z measured along the fault dip and z_0 , the point of maximum resistance, is taken as 15 km. In this way he is able to reproduce some features of observed surface uplift, and migration of the location of maximum uplift, over a 7-year period before the instability. The model suggests that the uplift is due to the updip migration of slip toward the point of maximum strength, as slip weakening of the fault takes place at greater depths, and instability occurred as the extensively slipped zone penetrated towards the maximum-strength location.

6.2. *Some estimates of fracture parameters in the slip-weakening model.* — Fig. 12 describes results by RUMMEL *et al.* [72] for a 54° sawcut fault with polished surfaces in a granite specimen that is loaded to instability in the triaxial apparatus with 0.47 GPa (4.7 kilobar) confining pressure. The slip event was an unstable stick slip, but a computer playback of a high-speed tape recording gave the stress difference ($\sigma_1 - \sigma_3$) vs. axial shortening (ΔL) relation shown in fig. 12*b*). By referring to the calculations indicated in fig. 12*c*), and determining the part of the shortening ΔL_s due to slip as in fig. 12*b*), the corresponding relation between shear stress and slip on the fault plane has been determined and is shown in fig. 12*d*). The first column of table I shows the resulting values of \mathcal{F} , $\sigma^p - \sigma^f$, $\overline{\Delta u}$ and the end zone size ω_0 . The latter would pertain if this same σ vs. Δu relation applied near the tip of a long fault, but the experiments were done with a 2 cm diameter specimen (about 5% of ω_0), so that slip occurred in an essentially simultaneous manner everywhere on the fault surface, rather than in a cracklike mode as illustrated in fig. 10*a*). A further difference between

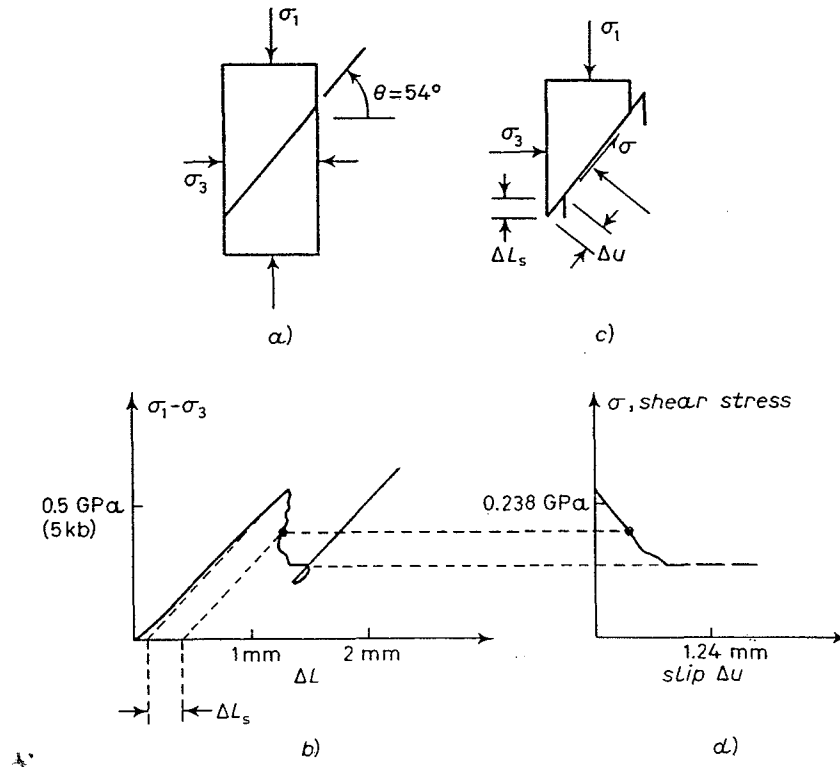


Fig. 12. - *a, b*) Results of Rummel *et al.* [72] from computer playback of stress vs. specimen shortening for stick slip event on a polished sawcut surface in granite, tested in a triaxial apparatus ($\sigma_3 = 0.47$ GPa). *c, d*) Procedure for inferring the shear stress vs. slip relation ($\sigma = (\sigma_1 - \sigma_3) \sin 2\theta/2$, $\Delta u = \Delta L_s/\sin \theta$). See first column of table I for results.

TABLE I. - *Shear fracture energy of granite from σ vs. Δu relations in triaxial test of Rummel *et al.* [72].*

| | Polished sawcut | Intact specimens | | |
|-----------------------------------|------------------|------------------|------------------|------------------|
| σ_3 (GPa) | 0.470 | 0.300 | 0.157 | 0.055 |
| \mathcal{F} (J/m ²) | $4.5 \cdot 10^4$ | $7.3 \cdot 10^4$ | $7.1 \cdot 10^4$ | $4.7 \cdot 10^4$ |
| $\sigma^p - \sigma^t$ (GPa) | 0.131 | 0.147 | 0.142 | 0.107 |
| $\overline{\Delta u}$ (mm) | 0.34 | 0.49 | 0.50 | 0.44 |
| ω_0 (m) (*) | 0.36 | 0.48 | 0.50 | 0.58 |

(*) Computed from eq. (6.12) with $\nu = 0.25$, $G = 30$ GPa; 0.1 GPa = 1 kilobar.

the experiment and a large-scale slip event is that the compressive stress on the fault surface decreases during slip in the experiment. From fig. 10c), this can be assumed to increase the strength drop, $\sigma^p - \sigma^t$, and estimated \mathcal{F} value over what would result for a large fault. This may be an important factor in discrepancies between laboratory and inferred earthquake stress drops.

Figure 13a) shows the results of tests to failure by RUMMEL *et al.* [72] of initially intact granite specimens at various confining pressures in a stiff, servo-controlled triaxial apparatus. Deformation concentrates into a fault (with $\theta \approx 54^\circ$) near peak load, but the effective stiffness of the apparatus is such that failure occurs stably in these tests. The resulting σ vs. Δu relations for the fault surface are calculated in a manner analogous to that of fig. 12, and are shown in fig. 13b). Inferred fracture parameters are shown in the last three columns of table I.

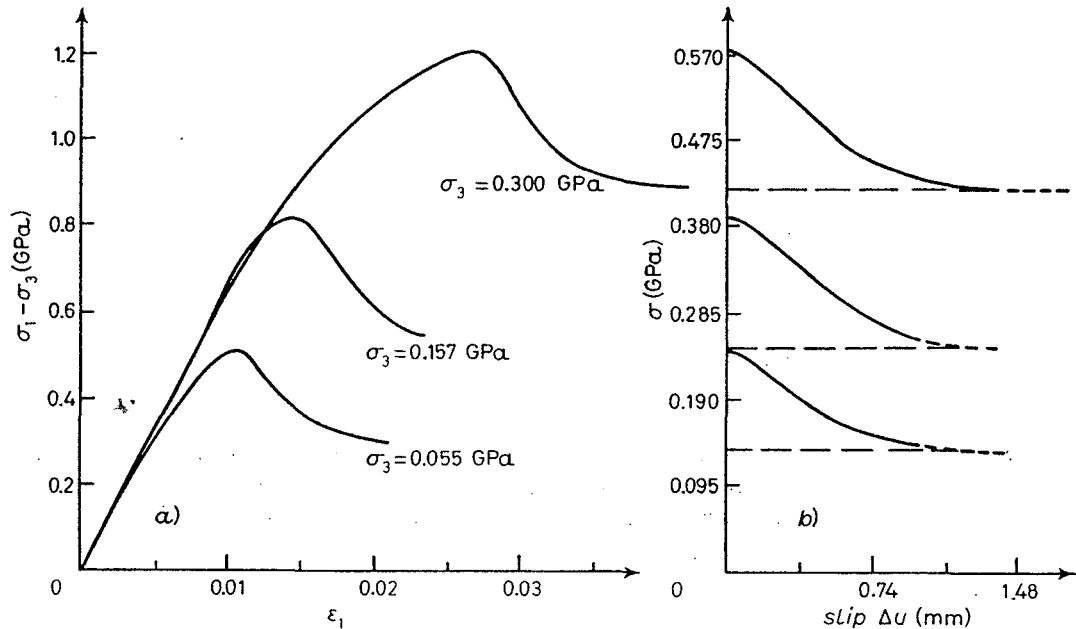


Fig. 13. — a) Results of Rummel *et al.* [72] on servo-controlled triaxial test of intact granite specimens to failure. A shear fracture forms near peak load with $\theta \approx 54^\circ$. b) Shear stress vs. slip relations, inferred as in previous figure. See table I for results.

The estimates of \mathcal{J} are found to lie in the range of 10^4 to 10^5 J/m², which is toward the lower end of the 10^4 to 10^6 J/m² inferred by HUSSEINI *et al.* (subsect. 5'4, 5'5) for the arrest of earthquakes involving fresh fracture. It should also be noted that the fracture parameters of the polished sawcut at 0.47 GPa confining pressure and intact specimen at 0.055 GPa are comparable, and both would, therefore, be expected to show similar response to the stress concentration of a crack with overall length that is large compared to ω_0 . But the σ vs. Δu relations are different (compare fig. 12d), 13b)) in that the sawcut exhibits a much more rapid initial decrease of strength with slip. This feature apparently dominates response in small specimens, with the sawcut exhibiting stick slip and the intact-specimen stable failure.

The characteristic slip-weakening displacement $\overline{\Delta u}$ reported in table I is in the range of 0.5 mm, which might be expected to coincide approximately

with grain size. However, a review of data by RICE [11] suggests that this parameter may vary over a very large range in different cases, with there being a corresponding variation in the strength degradation zone size ω_0 . Variations in the later are further accentuated by variations in strength drop, as shown by (6.12). DIETERICH [43] has recently reported results on strength degradation with slip for granodiorite surfaces lapped with either #60, #240 or #600 abrasive. These give a progressively finer surface appearance with reported center-line average surface roughnesses of 6, 0.7 and 0.5 μm , respectively. The characteristic slip-weakening displacements $\overline{\Delta u}$ (taken as a half of his weakening displacement d_c) vary accordingly and are 5 to 12 μm , 2.5 to 7.5 μm and 0.5 to 1.5 μm , respectively. These values are much smaller than the 0.34 mm inferred in table I from the polished sawcut experiment of Rummel *et al.* [72]. However, the latter involved compressive stresses of the order 500 MPa (5 kb) and slip was preceded by overall inelastic, dilatant deformation of the sample, whereas Dieterich's [43] experiments involved a much lower compressive stress (approximately 6 MPa).

A significant but little addressed question involves the scaling of results to field conditions. BARTON [100] has addressed this for the sliding of rock joints and shows that frictional results are dependent on roughness over much larger size scales than those noted above. A $\overline{\Delta u}$ value of 2 to 3 mm may be inferred from results of Coulson [102] on the sliding of a natural joint in coarse-grained granite. But, by studies of model materials with various degrees of roughness, BARTON [103] shows that the slip displacement necessary to reach peak strength (and, presumably, the continuing displacements to reach residual friction) scales approximately with the size of the contacting area, up to a size that is presumably sufficient for a given friction surface to fully sample the statistics of the roughness distribution. He also shows [100, 103] that the peak strength degrades with size over this same range. There is little that can be said of the scaling to natural earthquake faults. It is possible that roughness over much larger size scales than those of laboratory experiments would lead to large values of $\overline{\Delta u}$, associated with average strength drops that do not greatly exceed the nominal stress drops inferred for earthquakes. The numbers are merely speculative, but a $\overline{\Delta u}$ of 0.1 m and strength drop $\sigma^p - \sigma^f$ of 100 bar would be consistent with a fracture energy of 10^6 J/m^2 and would lead to a strength degradation zone $\omega_0 \approx 1 \text{ km}$. It is likely that local heterogeneities within a zone of this size, as remnants of discontinuities in prior rupture events, could lead to yet larger but localized strength drops, corresponding to small earthquakes that extend only over limited portions of ω_0 , and that are perhaps analogous to microscale instabilities revealed as acoustic emissions during the nominally stable slippage of laboratory samples.

6.3. *Some dynamical aspects of slip-weakening models and tendencies for discontinuous rupture.* — The tendency for discontinuous rupture at high crack

speeds has been noted in subsect. 5'5. Implications of the slip-weakening model for such phenomena are studied here. As noted at the close of subsect. 5'5, the solution for steady-state dynamic crack problems parallels that for static problems, but with $\Delta\sigma$ replaced by $f(v)\Delta\sigma$. The steady-state model is appropriate for describing the slip distribution within a slip-weakening zone that occupies a small fraction of the overall size of a rupture that propagates without changes in speed over distances that are several times the weakening-zone size. Accordingly, if K is the dynamic stress intensity factor for the associated elastic-crack model with uniform friction stress on the crack surface, then eqs. (6.7) and (6.9) for the slip-weakening model are valid with Δu replaced by $\Delta u/f(v)$, whereas (6.5) and (6.8) are valid as stated, provided that the dynamic expression of (5.37) for \mathcal{S} is used in the former. These observations suffice to show that, if the solution to the quasi-static slip-weakening model is written as

$$(6.14) \quad \sigma(x_1) - \sigma^f = F(x_1/\omega_0), \quad \Delta u(x_1) = \omega_0 H(x_1/\omega_0),$$

where ω_0 is the end zone size at $v = 0^+$, estimated approximately by (6.12), then the solution meeting the same slip-weakening relation in the dynamic case is

$$(6.15) \quad \sigma(x_1) - \sigma^f = F(x_1/\omega), \quad \Delta u(x_1) = f(v)\omega H(x_1/\omega),$$

where the (contracted) size of the strength degradation zone is

$$(6.16) \quad \omega = \omega_0/f(v).$$

As cracks grow in size so that the value of \mathcal{S} as estimated statically greatly exceeds the fracture energy, the speed v is driven toward the limiting speed at which $f(v) \rightarrow \infty$ (and $K \rightarrow 0$). Hence the zone of strength degradation diminishes in size and, since $\Delta u = \Delta u^* \approx 9\bar{\Delta u}/4$ (presumed independent of v) must result at $x_1 = -\omega$, the strains ε_{11} along the surface of a mode-II slip-weakening zone increase in magnitude. The average values of these strains are $\pm \frac{1}{2}\Delta u^*/\omega$ on the upper and lower slip-weakening zone surfaces, so that the average alteration in tensile stress $\Delta\sigma_{11}$ along the stretched side of a mode-II weakening zone is

$$(6.17) \quad \langle \Delta\sigma_{11} \rangle = \frac{2G}{1-\nu} \langle \varepsilon_{11} \rangle = \frac{2G}{1-\nu} \frac{\Delta u^*}{2\omega} = \frac{4}{\pi} f_{II}(v)(\sigma^p - \sigma^f),$$

by using eqs. (6.12), (6.16). Thus $\langle \Delta\sigma_{11} \rangle$ becomes (formally) infinite at the limiting speed $v = c_R$.

Clearly, if $\langle \sigma_{11} \rangle$ becomes large enough to exceed the initial compressive stress $-\sigma_{11}^0$ acting before fault introduction, local tensile fracturing is to be expected and the shear crack configuration may become unstable in a manner

analogous to that for shear cracks in brittle solids (fig. 9). But even before such conditions are reached, the shear stresses induced on planes making nonzero angles with the rupture plane may exceed significantly the shear stress on the main rupture plane (*e.g.* $\Delta\sigma_{11}/2$ is the shear stress change on a 45° plane). This may induce discontinuities in the direction of rupture propagation, depending on the relative shear strength of the main rupture plane and of the adjacent material. Since the shear strength of brittle geological materials is dependent strongly on the normal compressive stresses, the effect should be aggravated by the simultaneous reductions of the compressive stress — σ_{11} . These considerations merit more detailed analysis in relation to the overall stress distribution near the rupture zone and to the shear and tensile fracture strength of rock.

The effects for mode-II cracks become most pronounced only very near c_R . For example, if $\nu = 0.25$, $f_{II}(v) < 2.5$ for $v < 0.85c_s$ ($0.925 c_R$), whereas $f_{II}(v) = 6.4$ at $v = 0.9c_s$ ($0.98 c_R$) and $f_{II}(v) = 12.1$ at $v = 0.91c_s$ ($0.99 c_R$). The latter two figures make $\langle\Delta\sigma_{11}\rangle$ 8 and 15 times, respectively, $\sigma^p - \sigma^t$.

Similar effects exist at mode-III slip zones, for which

$$(6.18) \quad \langle\Delta\sigma_{13}\rangle = 2G\langle\Delta\varepsilon_{13}\rangle = G \frac{\Delta u^*}{2\omega} = \frac{2}{\pi} f_{III}(v)(\sigma^p - \sigma^t),$$

so that the shear stress changes on planes at 90° with the rupture plane become very large when v is near to c_s .

Another type of rupture discontinuity in slip-weakening models has been demonstrated by ANDREWS [36] and further analyzed by BURRIDGE *et al.* [37]. This applies to mode-II cracks and it is found that at a speed near to c_R the shear stresses on the x_1 -axis at some distance ahead of the slip-weakening zone exceed σ^p . This has been interpreted as allowing two disconnected zones of slip over a narrow range of speeds. These are suggested to coalesce in a nonsteady manner and to allow, ultimately, the steady spread of rupture at speeds exceeding, approximately, $1.5c_s$. Whether this will actually be observed, or whether the off-plane effects discussed earlier will first intervene remains an open question. Further, it would again seem advisable to examine the full stress field near the crack because more critical stress conditions may well be achieved at points removed from the end zone but off rather than on the main rupture plane.

6.4. Time-dependent constitutive models for frictional slip. — Studies by DIETERICH [43, 104, 105] suggest pronounced time dependences of the frictional strength of smooth rock surfaces. His first experiments [104] suggested that the coefficient of static friction, μ , increases with the time of stationary contact; the effect is sensitive to normal stresses (over the range from 20 to 480 bar studied) and is described approximately by [105]

$$(6.19) \quad \mu \approx \mu_0 + A \log(1 + Bt),$$

where t is the time of contact, $\mu_0 \approx 0.6$ to 0.8 , $A \approx 0.01$ to 0.02 , and $B \approx 1$ to $2/s$ for surfaces of sandstone, granite, quartzite and graywacke. DIETERICH attributes the results to the time-dependent enlargement of asperity contacts, and suggests that this time dependence is closely associated with the presence of moisture [105]. Evidence for this time-dependent enlargement is provided by TEUFEL and LOGAN [106], who used thermo-dyes, which change color from heating during slip, to estimate the size of contacts.

In later experiments in which μ for steady slip was measured, it was found that abrupt increases in the slip rate caused a displacement-dependent weakening of μ over slip distances d_c of the order 1 to $25 \mu\text{m}$ (depending on surface preparation [43, 105]) before a steady slip rate was established. DIETERICH interprets d_c as the slip distance necessary to establish a new population of asperity contacts, and, by assuming, therefore, that $d_c/\dot{\delta}$ (where $\dot{\delta}$ = slip velocity) is an average asperity contact lifetime, he proposes that the value of μ for steady slip is a decreasing function of $\dot{\delta}$ given by replacing t with $d_c/\dot{\delta}$ in (6.19),

$$(6.20) \quad \mu \approx \mu_0 + A \log(1 + Bd_c/\dot{\delta}).$$

This equation describes reasonably his results for Westerly granite [105] over the range of $\dot{\delta}$ from 10^{-4} to 10^{-1} mm/s. DIETERICH also shows that the presence or absence of unstable stick slip following imposed velocity changes can be explained by comparing the strength drop, divided by d_c , to the stiffness of the loading apparatus.

DIETERICH [43] and RUINA [107] have attempted to develop constitutive descriptions for general slip histories, for analysis of slip-weakening instability models. RUINA [107] examines an expression for μ in the internal variable form (leaving open possible dependence on normal stress)

$$(6.21) \quad \mu = \bar{\mu}(\theta) + \eta(\dot{\delta}).$$

Here θ is a variable that characterizes the state of the surface, and is conveniently identified as the average time of asperity contact so that $\bar{\mu}(\theta)$ is given by (6.19) with t replaced by θ . The function $\eta(\dot{\delta})$ represents an inherent viscosity effect, $d\eta/d\dot{\delta} > 0$. Its presence is suggested by experiments of Dieterich [43] on granodiorite, which showed an increase in frictional resistance following a change in imposed velocity, before the slip weakening reduced the resistance to a level appropriate to the newly imposed velocity. The effect was less pronounced in the results for Westerly granite [105] leading to (6.20). Factors of 10 increase in $\dot{\delta}$ seem to lead to approximately comparable sudden changes in μ , of the order of 0.01, for granodiorite, so that $\eta(\dot{\delta})$ is a slowly changing function, perhaps logarithmically dependent on $\dot{\delta}$. Nevertheless, its inclusion influences the stability of the friction process [107]. DIETERICH [43] incorporates the $\dot{\delta}$ effect by writing $\mu = \bar{\mu}(\theta)h(\dot{\delta})$.

The constitutive description is completed by specifying the evolution equation for θ , which must reduce to $\dot{\theta} = 1$ when $\dot{\delta} = 0$. The simplest of several forms considered by RUINA [107] is

$$(6.22) \quad \dot{\theta} = 1 - \theta \dot{\delta} / d_c$$

and this reduces to the Dieterich relation $\theta = d_c / \dot{\delta}$ at steady slip (*i.e.* $\dot{\delta}$ constant and $\dot{\theta} = 0$). As an illustration, if the slip rate is suddenly increased from $\dot{\delta}_1$ to $\dot{\delta}_2$ at $t = 0$, and a steady slip state prevailed (with $\theta_1 = d_c / \dot{\delta}_1$) before the increase, then integration of (6.22) leads to

$$(6.23) \quad \theta = \theta_2 + (\theta_1 - \theta_2) \exp[-\delta / d_c],$$

where $\delta = \dot{\delta}_2 t$, $\theta_2 = d_c / \dot{\delta}_2$, and thus

$$(6.24) \quad \mu - \mu_1 = A \log [(1 + B\theta) / (1 + B\theta_1)] + \eta(\dot{\delta}_2) - \eta(\dot{\delta}_1).$$

The terms involving η represent an instantaneous increase in resistance at $\delta = 0^+$, whereas the logarithmic terms represents a gradual slip weakening with ongoing δ , according to (6.23).

Limited applications of a similar constitutive framework to predictions of slip propagation in fault models have been made by DIETERICH [43], although a comprehensive understanding of instability predictions is not yet available. Also, the characteristic slip-weakening displacements d_c are far smaller than anticipated for natural faults, although the model and related experiments on rock specimens that are large enough to fully contain slip events may serve as a valuable analog to similar events under field conditions. Indeed, one feature of the smooth rock surfaces is that the strength degradation zone (which should scale with $\overline{\Delta u}$ or d_c for similar strength drops) is sufficiently small that confined slip events can be studied on the laboratory scale [43].

Other processes may lead also to time dependence in slip-weakening constitutive relationships. For example, BARTON [100] observes that frictional slip on nonsmooth rock surfaces will require deformation of adjoining material, and is able to correlate roughness effects with rock strength in unfaulted specimens. Hence, to the extent that this strength is influenced by moisture-assisted time-dependent microcracking [79, 82], related time effects are expected in the σ vs. Δu relation. Additional effects may arise from creep and time-dependent restrengthening of finely pulverized fault gouge materials. Finally, RUTTER and MAINPRICE [108] suggest that their results, at low stress levels, from relaxation tests on stress vs. slipping rate on faults in Tennessee sandstone can be explained in terms of a pressure solution process. Their analysis of the mechanism appeals to the presence of fluid films along faults and considers that material dissolved into the fluid at points of high chemical

potential, such as asperity contacts, is transported by ionic diffusion in the film and redeposited. They suggest that the mechanism could produce slip rates on the order of a few mm/y under 100 bar level shear stresses at 300°C (approximately 10 km depth), although the estimate is based on a number of parameters which are not accurately known.

7. – Instabilities in nonelastically deforming rock masses.

In this section some analyses of instabilities in rock masses undergoing distributed inelastic deformation (as opposed to slip on macroscale faults) are reviewed. The first topic relates to the onset of shear localizations that ultimately develop into faults, the second to the deformation to instability of a rock mass containing an inclusionlike zone of material that is deformed into the strain-softening regime. Both topics rely on inelastic constitutive relations for rock deformation. These relations cannot be stated in a precise, generally valid form, but a simple constitutive model due to RUDNICKI and RICE [109] which incorporates frictional and dilatant effects in brittle rock deformation is outlined here. The model neglects strain rate effects. To motivate the development, consider an element of material subjected to a shear stress τ and a hydrostatic stress σ , positive in compression. Increments of shear and volumetric strain are written as

$$(7.1) \quad d\gamma = d\tau/G + d^p\gamma, \quad d\varepsilon = -d\sigma/K + d^p\varepsilon.$$

Here $d^p\gamma$, $d^p\varepsilon$ are the inelastic, or « plastic » increments of strain, which vanish when the stress increments considered induce only elastic response; G and K are the incremental elastic shear and bulk moduli. Since inelastic strain results mainly from frictional processes and associated microcrack growth (e.g. as in fig. 9c)), and these are driven by shear stress but inhibited by hydrostatic stress, the inelastic strain increments are written as

$$(7.2) \quad d^p\gamma = (d\tau - \mu d\sigma)/h, \quad d^p\varepsilon = \beta(d\tau - \mu d\sigma)/h.$$

Here h is the modulus for inelastic shear strain and $h > 0$ describes strain hardening, $h < 0$ strain softening; μ is a frictional factor, and β is a dilational factor (e.g. $d^p\varepsilon = \beta d^p\gamma$).

RUDNICKI and RICE [109] generalize these relations to arbitrary deformation states by assuming that inelastic dilation is isotropic, that $\sigma = -\sigma_{\alpha\alpha}/3$, that τ can be identified with the second invariant of deviatoric stress, and that components of inelastic deviatoric strain increments are in proportion to one another as corresponding components of deviatoric stress. Hence, if one considers small strains so that $\varepsilon_{\alpha\beta}$ is defined by (2.2) and neglects the distinction

which they make between ordinary and corotational stress rates,

$$(7.3) \quad \dot{\varepsilon}_{\alpha\beta} = \frac{1}{2G} \dot{\sigma}'_{\alpha\beta} + \frac{1}{9K} \delta_{\alpha\beta} \dot{\sigma}_{\gamma\gamma} + \frac{1}{h} \left(\frac{\sigma'_{\alpha\beta}}{2\tau} + \frac{\beta}{3} \delta_{\alpha\beta} \right) \left(\frac{\sigma'_{\gamma\delta}}{2\tau} + \frac{\mu}{3} \delta_{\gamma\delta} \right) \dot{\sigma}_{\gamma\delta},$$

where

$$(7.4) \quad \sigma'_{\alpha\beta} = \sigma_{\alpha\beta} - \frac{1}{3} \delta_{\alpha\beta} \sigma_{\gamma\gamma}, \quad \tau = \sqrt{\frac{1}{2} \sigma'_{\alpha\beta} \sigma'_{\alpha\beta}}.$$

Estimates of the parameters μ and β from fitting the model to triaxial test results for rock in the brittle range (e.g. [71]) give [109, 110] $\beta = 0.2$ to 0.4 (typically increasing during inelastic straining toward peak, but diminished by increasing confining pressure) and $\mu = 0.4$ to 0.9 .

7.1. *Theory of shear localization of deformation.* – It is possible that the processes which lead to macroscopic-fault formation can be understood only by appeal to some strong initial nonuniformity in material properties, which locally concentrates deformations that finally traverse large regions of the material in a cracklike mode. This is analogous to the role of a Griffith crack in the tensile fracture of an otherwise perfect solid. An alternative approach, which can be regarded as setting an upper limit to stability against fault formation, is to seek conditions under which uniform (or smoothly varying) patterns of deformation become unstable in the sense that a bifurcation of continuing deformation into a localized « shear band » becomes possible. This approach to shear localization is reviewed here. It has been developed by HILL [111], MANDEL [112] and THOMAS [113] for elastic-plastic solids with rate-insensitive constitutive relations, and has been reviewed recently by RICE [114], who gave results for a wide variety of constitutive models; RUDNICKI and RICE [109] derived localization conditions for the constitutive model of (7.1)-(7.4) and for an improvement of it which will be considered shortly.

With reference to fig. 14, a homogeneously deformed, uniformly stressed solid is considered, and it is assumed that increments of stress and deformation gradient are related by a constitutive relation of the form

$$(7.5) \quad \dot{\sigma}_{\alpha\beta} = L_{\alpha\beta\gamma\delta} \partial \dot{u}_{\gamma} / \partial x_{\delta}.$$

The incremental moduli L may have different branches, say for elastic unloading vs. continued elastic-plastic deformation. Conditions are sought under which continuing increments of deformation may be nonunique and exhibit a local bifurcation into a shear band mode, such that $\dot{\sigma}_{\alpha\beta}$ and $\partial \dot{u}_{\gamma} / \partial x_{\delta}$ vary with position in the direction normal to the incipient shear band. If superscripts o represent the continuing homogeneous field outside the band, the bifurcation occurs when [109, 114] the kinematical condition

$$(7.6) \quad \partial \dot{u}_{\gamma} / \partial x_{\delta} = (\partial \dot{u}_{\gamma} / \partial x_{\delta})^o + g_{\gamma} n_{\delta}$$

and the continuing equilibrium condition

$$(7.7) \quad n_\alpha \dot{\sigma}_{\alpha\beta} = n_\alpha \dot{\sigma}_{\alpha\beta}^o$$

can be met for some nonzero nonuniformity vector \mathbf{g} of velocity gradients.

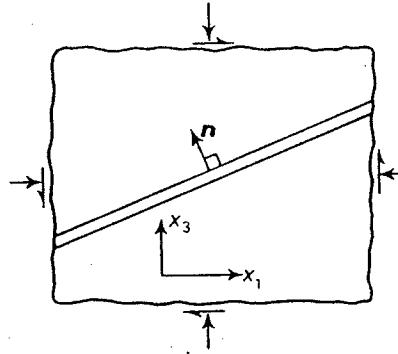


Fig. 14. — Analysis of bifurcation of uniform deformation into a localized shear band.

If we assume that the same incremental modulus tensor \mathbf{L} applies both inside and outside the band at inception of bifurcation (RICE and RUDNICKI [115] show that the bifurcation state so predicted will generally precede, and serve as the lower limit to, the range of bifurcations associated with elastic unloading outside the band), the conditions (7.6) and (7.7) are equivalent to requiring that

$$(7.8) \quad (n_\alpha L_{\alpha\beta\gamma\delta} n_\delta) g_\gamma = 0$$

have a nonzero solution for \mathbf{g} . This is first possible when a deformation state is reached for which

$$(7.9) \quad \text{determinant of } (n_\alpha L_{\alpha\beta\gamma\delta} n_\delta) = 0.$$

This equation determines the critical state associated with a plane of normal \mathbf{n} ; the critical condition must then be optimized over all orientations \mathbf{n} by procedures described in [109, 114] to determine the critical deformation state and the plane of incipient localization.

RUDNICKI and RICE [109] applied this procedure to the constitutive model of (7.3) and showed that over a wide range of the parameters μ, β the critical orientation \mathbf{n} is such that it lies in the plane of the greatest and least principal stresses, and that the corresponding value of the plastic-hardening modulus h at bifurcation is

$$(7.10) \quad h = \frac{1+\nu}{9(1-\nu)} (\mu - \beta)^2 G - \frac{1+\nu}{2} \left(2P + \frac{\mu - \beta}{3} \right)^2 G,$$

where ν is the incremental elastic Poisson ratio and

$$(7.11) \quad P = \sigma'_2/2\tau + \beta/3$$

(where σ'_2 is the intermediate principal deviatoric stress) is a normalized value of the intermediate principal plastic strain rate consistent with the current state of stress.

Equation (7.10) is not fully adequate to describe bifurcations (*e.g.* it predicts unrealistically large negative values of h for the axisymmetric compression test, *i.e.* the « triaxial » test [109]) because of inadequacies of the constitutive model on which it is based, but it shows important trends that are reflected in results for more elaborate constitutive models [109, 114, 116]. First, the value of h at localization varies strongly with the nature of the deformation state prior to localization, as reflected in the dependence on P . For example, if $P=0$, which means that the plastic state corresponds to plane strain (which may be rather typical of the geological setting for strike-slip and thrust faulting), the critical h is positive (if $\mu \neq \beta$) and is given by

$$(7.12) \quad h = [(1 + \nu)^2/18(1 - \nu)](\mu - \beta)^2 G.$$

On the other hand, very different deformation states such as axisymmetric compression or extension [$P = (1 \pm \beta/\sqrt{3})/2\sqrt{3}$] are much more resistant to localization, and the predicted h for this model will generally be negative (strain softening). The gravest state is slightly removed from plane strain, and occurs for $P = -(\mu - \beta)/6$; the corresponding critical h is larger than that for plane strain by a factor of $2/(1 + \nu)$. Second, the tendency for localization is accentuated by a high frictional component of the plastic strength. This is reflected in the dependence on the frictional parameter μ in (7.12). The difference between μ and β corresponds to a deviation from « plastic normality » [109], and such deviations are found to promote localization in several other cases examined [114, 116].

As RUDNICKI and RICE [109] noted, predictions of localization, especially for deformation states well removed from plane strain, are strongly sensitive to the stiffness of constitutive response for abrupt changes in the direction of stressing. They showed that, for rock « plasticity » arising from frictional slip processes as in fig. 9c), a vertex structure must develop on the yield locus in σ space at the current stress state, and suggested that the effect could be modelled in a simple manner by appending a term

$$\frac{1}{2h_1} \left(\dot{\sigma}'_{\alpha\beta} - \frac{\sigma'_{\alpha\beta} \sigma'_{\gamma\delta}}{2\tau^2} \dot{\sigma}'_{\gamma\delta} \right)$$

to the right-hand side of (7.3). This term vanishes when $\dot{\sigma}'$ has the direction of σ' , so that the original constitutive model then applies, and h_1 is a « vertex »

modulus. This is expected to be of the same order as G , and much greater than $|h|$, for brittle rock. Its inclusion brings the predicted critical point much closer to the nonhardening state ($h = 0$), although states such as plane strain remain less resistant to localization than axisymmetric compression, in which somewhat negative values of h are still predicted. Some indications of a slightly negative h at localization in the triaxial test are found, for example, in the tests in a stiff apparatus (so that instability does not occur by machine interaction shortly after the onset of softening) by WAWERSIK and FAIRHURST [117] and WAWERSIK and BRACE [118]. This testing state is also strongly sensitive to imperfections of material or loading system. For example, shear constraints of the end loading plates in a triaxial apparatus induce a locally concentrated strain state that is closer to plane strain than to axially symmetric compression at the outer rims of the specimen ends. Thus end constraint may allow localization to initiate there and spread by self-strain concentration through the specimen before bifurcation conditions for a state of homogeneous axisymmetric compression are met.

For $\mu = 0.6$ and $\beta = 0.3$, which are thought to be typical of granite in the brittle range, RUDNICKI and RICE [109] show that over a wide range of values of the vertex modulus h_1 (0.1 to 1.0 G) the predicted angle θ (consistent with the notation in fig. 12a) for localization in the axisymmetric test varies from 55° to 54.6° . This is, for example, rather close to the value $\theta \approx 54^\circ$ reported by RUMMEL *et al.* [72] for their tests of intact granite specimens shown in fig. 13a).

7.2. *Structure of shear zones.* — The motivation for studies of shear localization is that they might contribute to understanding the structure of tectonic shear zones. Direct observations of such zones in the field and in laboratory simulations [119, 120] based on the Riedel shear of clay samples, as well as studies of artificial fault gouge between rock faces in the triaxial test [121] and of various granular materials in the ring-shear apparatus [122], suggest a complex sequence of localizations before a well-defined macroscale fault zone is formed. The localization bifurcations just addressed would seem to correspond to the first localizations observed (Riedel shears [119]) but do not necessarily coincide with the ultimate direction of macroscale motion.

Figure 15 is based on Skempton's [119] idealization of field and laboratory observations. Under imposed deformations that ultimately result in displacements along D , the first features observed are the *en échelon* Riedel shears R , often accompanied by less dominant conjugate Riedel shears (R'). Thrust shears (P) are sometimes observed at late stages in the shear process, and tensile cracks (T) may form if the confining pressure is small. The important point is that the final displacement shears D , which accommodate large imposed motions, are accompanied by a highly complex structure of prior ruptures. BYERLEE *et al.* [121] report early deformation features similar to the Riedel shears (R) in their simulated fault gouge experiments, while final motion takes

place at the boundary (D) between the gouge and coherent rock. They report an angle $\psi \approx 20^\circ$ for the R features; SKEMPTON reports values ranging from 10° to 30° , but possibly altered by continuing deformation.

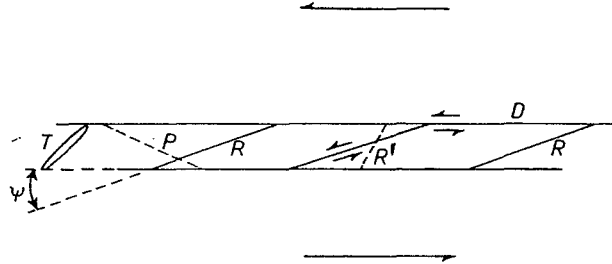


Fig. 15. — Localized shear structures within a macroscale fault which ultimately displaces along D , based on [119]. Riedel shears R form as an early feature; conjugate Riedel shears (R') and thrust shears (P) are sometimes observed, as well as tensile cracks (T) at low confining pressure.

SKEMPTON associates R and R' with Rankine's rupture lines of the Mohr-Coulomb failure theory, in which case $\psi = \varphi/2$ (assuming the deviatoric stress state is pure shear relative to D at the time of formation), and $90^\circ - \varphi$ is the angle between R and R' , where φ is the angle of internal friction. Alternatively, they may be an example of the localization instability studied by RUDNICKI and RICE, subsect. 7'1, and their predictions of ψ for $\mu = 0.6$ range from approximately 9° (for $\beta = 0$, no dilatancy) to 18° (for $\beta = 0.6$) and are little affected (say, $\pm 1^\circ$) by the vertex modulus h_1 over the range studied. Both estimates of ψ assume that the deviatoric stress state is pure shear, and this is unlikely to be precisely the case in the fault gouge experiments.

These observations seem relevant to earthquakes in three major respects. First, the different orientations of seismically inferred fault planes reported by LINDH *et al.* [87] for foreshocks *vs.* those for the main rupture (identified with the aftershock plane) may be an example of the formation of features analogous to the Riedel shears, and may have potential for the prediction of impending rupture. (It remains an open question as to why the initial shear failures do not extend over great distances, but rather form an *en échelon* array.) Second, the tendency of stress fields associated with rapidly propagating ruptures to favor off-plane orientations has been noted in subsect. 5'5 and 6'3. If natural fault zones at depth in the Earth have a complexity of structure analogous to that in fig. 15, there may be an ample distribution of weakened surfaces to allow the types of discontinuous rupture propagation suggested by the stress fields. Third, each individual feature of the shear zone of fig. 15 may correspond to the types of slip motion, and exhibit the levels of strength, suggested by laboratory fault slip experiments, but the effective slip-weakening relations between σ and Δu on a tectonic scale should perhaps be identified with the overall shear behavior of a finite-width, complexly faceted fault zone.

7.3. *Strain-weakening inclusion model for earthquake instability.* — RUDNICKI [110] developed a model for analyzing earthquake instabilities in which a limited zone of rock is assumed to be stressed into the inelastic and, ultimately, strain-weakening regime, while the surroundings remain elastic and are subjected to steadily increasing remote stress. For simplicity of analysis he took the inelastic zone to have the form of an ellipsoidal inclusion, with local properties being uniform within the inclusion. In this case it is a consequence of Eshelby's [16] general solutions that, independently of the stress-strain relations of the inclusion material, the stress and strain ($\sigma^{\text{inc}}, \epsilon^{\text{inc}}$) are uniform within it and are related to the far-field stress and strain ($\sigma^\infty, \epsilon^\infty$) by

$$(7.13) \quad \epsilon_{\alpha\beta}^{\text{inc}} - \epsilon_{\alpha\beta}^\infty = Q_{\alpha\beta\gamma\delta}(\sigma_{\gamma\delta}^\infty - \sigma_{\gamma\delta}^{\text{inc}}).$$

Here Q is a constant tensor, dependent only on the orientation and ratios of principal axes of the ellipsoid and on the elastic constants of the material outside it. Components of Q are given for several cases by RUDNICKI [110], although his results for narrow inclusions are subject to corrections noted in [11, 123]. Thus, since ϵ^∞ is a known function of σ^∞ (*i.e.* the linear elastic stress-strain relations), and since it is assumed that some constitutive relation, *e.g.* (7.3), has been specified relating ϵ^{inc} to σ^{inc} , (7.13) enables the state within the inclusion to be calculated as a function of σ^∞ . At least this is the case when the inclusion is strain hardening or only slightly strain softening, but, if the inclusion is driven to a sufficiently softened state, it is found that $\dot{\epsilon}^{\text{inc}} \rightarrow \infty$ for a fixed $\dot{\sigma}^\infty$ and no further static solution exists. This corresponds to a rate of softening that falls below the effective elastic unloading stiffness of the surroundings, and is taken as the onset of a seismic earthquake instability. For the case shown in fig. 16a), the remotely applied stress is a pure shear τ_∞ relative to principal axes of the ellipsoid, and $\gamma_\infty (= \tau_\infty/G)$ is the remote shear strain. If τ_{inc} and γ_{inc} are the corresponding quantities in the inclusion, then (7.13) reduces to

$$(7.14) \quad \gamma_{\text{inc}} - \gamma_\infty = (\xi/G)(\tau_\infty - \tau_{\text{inc}}),$$

where

$$(7.15) \quad \xi = 2(4 - 5\nu)/(7 - 5\nu)$$

for a spherical inclusion, and

$$(7.16) \quad \xi = 4(1 - \nu)a/\pi(2 - \nu)b$$

for a narrow ($b \ll a$) axisymmetric ellipsoid.

Figure 16b) illustrates an interpretation of the model and a graphical procedure for its solution due to RICE [11]. The stress-strain relation for the inclu-

sion is displaced from the origin. This allows the model to represent a seismic-gap zone which has not accommodated as much as its surroundings to overall tectonic motions, and thus sustains higher stress. If one considers a level of remote stress τ_∞ , and associated γ_∞ , corresponding to point *A* in fig. 16*b*), then eq. (7.14) requires that the state τ_{inc} , γ_{inc} within the inclusion lie on a line through *A* with slope $-G/\xi$. This determines the inclusion state at *A'* as shown.

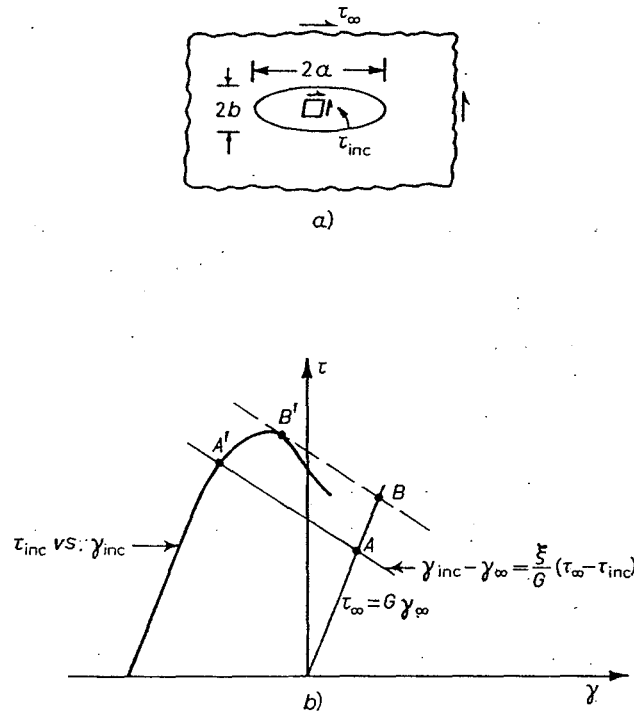


Fig. 16. - Description of instability of a strain-weakening ellipsoidal inclusion under remote shear loading. The displaced origin for the inclusion stress-strain relation means that the inclusion represents a seismic gap zone. Instability occurs at state *B'*.

The same procedure determines the history of inclusion states as τ_∞ is increased, and finally a set of states *B*, *B'* is reached as shown, beyond which no further static solution exists, and a seismic instability ensues.

The geometry of the construction shows that, if the remote tectonic stress τ_∞ increases at a uniform rate $\dot{\tau}_\infty$, the strain rate within the inclusion will accelerate in time with $\dot{\gamma}_{inc} \rightarrow \infty$ as the instability point is neared.

The model assumes a uniform state of material within the inclusion, and this is clearly a strong idealization. However, it illustrates in a simple way the interaction between a nonelastic strain-weakening zone and the surroundings, and shows the role of the elastic stiffness of the surroundings (G/ξ in this case) in dictating instability conditions.

8. – Mechanical effects of an infiltrating pore fluid.

In this section the possibility is considered that rock masses at the sites of crustal earthquakes are infiltrated with ground water. The mechanical interactions that result have been suggested as controlling the time dependence of stress redistribution shortly after faulting, thus contributing to the time scale of after-shocks [124, 125]. They act also to partially stabilize the rupture process, whether in the form of slow shear crack propagation [11, 75, 99], or of deformation to instability of a strain-weakening region or faulted zone [11, 123, 126, 127]. This stabilization is such that the rupturing system does not become dynamically unstable at the critical conditions inferred from models that neglect pore fluid effects. Instead time-dependent but, at least initially, quasi-static processes of deformation occur within the rupturing zones, which may in some cases allow the completely aseismic completion of the rupture event, and in others lead to an accelerating creeplike progression towards seismic instability on a time scale controlled by fluid transport, tectonic loading rate and constitutive properties of the failing region.

The effects divide into those which can be understood on the basis of coupling between pore fluids and Biot [128] elastic deformation of the host rock and those which rely on inelastic dilatant deformation. Accordingly, the next subsection reviews Biot's theory of elasticity for fluid-infiltrated solids, and this is followed by a description of various applications of the theory to rupture models. Next, the formulation of constitutive relations that incorporate inelastic dilatancy is reviewed, followed by a discussion of further applications.

8.1. Biot theory of coupled deformation/diffusion processes in fluid-infiltrated elastic solids. – The basic theory of fluid-infiltrated elastic solids has been established in a series of papers by BIOT [128, 129] and reviewed recently by RICE and CLEARY [99]. Here we consider the linear quasi-static theory, and regard the material as isotropic and homogeneous. In addition to stress and strain as fundamental state variables, one now introduces the pore pressure p and the fluid mass content m per unit volume. Pore pressure is defined as the pressure on an imagined fluid reservoir which would just equilibrate an element of material to which it is connected from either giving off or receiving fluid from the reservoir. Fluid mass density ρ is defined locally as the mass density of fluid in the equilibrating reservoir; thus $\rho = \rho(p)$, neglecting temperature effects. Stress is defined as the measure of total forces per unit areas of an element; there is no need to distinguish one part as being carried by the solid and another by the fluid. Strain refers to the relative displacement of solid points in the host phase. Stress, strain and pore pressure will all be interpreted as alterations from some ambient equilibrium state, and thus body forces are neglected.

The following terminology is introduced: « drained » deformation refers to alterations of state at constant fluid pore pressure p ; « undrained » deformation to alterations of state at constant fluid mass content m . Clearly, material response will be stiffer under undrained than drained conditions.

Stress-strain relations are

$$(8.1) \quad \sigma_{\alpha\beta} = (K - 2G/3)\delta_{\alpha\beta}\varepsilon_{\gamma\gamma} + 2G\varepsilon_{\alpha\beta} - \zeta p\delta_{\alpha\beta},$$

where K is the elastic bulk modulus for drained conditions, G is the shear modulus, and ζ is a new material constant. It can be written as $\zeta = 1 - K/K'_s$, where K'_s is an alternate new constant which can, in certain simple cases [99, 130, 131], be identified as the bulk modulus K_s of the solid material. These cases are such that all pore space is continuous and fluid filled, the fluid is chemically inert, and all points of the solid respond to isotropic stress with an isotropic dilation governed by the same bulk modulus K_s .

For undrained deformation the stress-strain relation must have the form

$$(8.2) \quad \sigma_{\alpha\beta} = (K_u - 2G/3)\delta_{\alpha\beta}\varepsilon_{\gamma\gamma} + 2G\varepsilon_{\alpha\beta},$$

where K_u is the undrained bulk modulus, and this together with (8.1) suffices to show that under undrained conditions

$$(8.3) \quad p = - (K_u - K)\varepsilon_{\gamma\gamma}/\zeta.$$

But thermodynamics requires [128, 129] that $\sigma_{\alpha\beta}d\varepsilon_{\alpha\beta} + p d(m/\rho)$ be an exact differential, which in turn implies that

$$(8.4) \quad \partial m(\boldsymbol{\varepsilon}, p)/\partial\varepsilon_{\alpha\beta} = - \rho \partial\sigma_{\alpha\beta}(\boldsymbol{\varepsilon}, p)/\partial p = \rho\zeta\delta_{\alpha\beta}.$$

This relation, together with the fact that m is unaffected by variations of $\varepsilon_{\gamma\gamma}$ and p meeting (8.3), requires that

$$(8.5) \quad m = m_0 + \rho\zeta[\varepsilon_{\gamma\gamma} + \zeta p/(K_u - K)].$$

Here m_0 is the value of m in the reference state and, within the linear theory, ρ in this expression can be regarded as constant and equal to its value in the reference state.

The final constitutive relation is Darcy's linear pore fluid diffusion equation

$$(8.6) \quad q_\alpha = - \rho\kappa\partial p/\partial x_\alpha,$$

where q_α is the fluid mass flux per unit area in the α -direction and κ is a permeability coefficient, sometimes written as k/μ , where μ is fluid viscosity and k has units of length squared. Again ρ in this expression can be regarded as constant in the linear theory.

Equations (8.1), (8.5) and (8.6) provide the full set of constitutive relations, and introduce three new material constants: ζ , K_u and κ . The full field equations are given by observing that $\boldsymbol{\varepsilon}$ can be expressed in terms of \mathbf{u} by (2.2), and that the stress equilibrium equations

$$(8.7) \quad \partial\sigma_{\alpha\beta}/\partial x_\alpha = 0$$

and fluid mass conservation equation

$$(8.8) \quad \partial q_\alpha/\partial x_\alpha + \partial m/\partial t = 0$$

must be met. By using (8.1), equilibrium requires that

$$(8.9) \quad (K + G/3)\partial(\partial u_\beta/\partial x_\beta)/\partial x_\alpha + G\nabla^2 u_\alpha - \zeta\partial p/\partial x_\alpha = 0,$$

and, by (8.5), (8.6), mass conservation requires, after using (8.9), that

$$(8.10) \quad (c\nabla^2 - \partial/\partial t)[\zeta p + (K_u - K)\partial u_\beta/\partial x_\beta] = 0,$$

where now c represents a diffusivity, given by

$$(8.11) \quad c = \kappa(K_u - K)(K + 4G/3)/\zeta^2(K_u + 4G/3).$$

Note that the bracketed terms in (8.10) are proportional to $m - m_0$, and hence that this quantity (and not p in general) satisfies the homogeneous diffusion equation.

Equations (8.9), (8.10) complete the theory, but it proves convenient in discussing solutions to use alternative quantities to ζ and K_u . Particularly, RICE and CLEARY [99] used the undrained Poisson ratio ν_u and an undrained pore pressure coefficient B (defined so that $p = -B\sigma_{\gamma\gamma}/3$ for undrained stress application), and tabulated experimental values of these. In general $\nu < \nu_u < \frac{1}{2}$ (where ν is the drained Poisson ratio) and $0 \leq B \leq 1$; the upper limits are approached in the case of a fully saturated material with effectively incompressible fluid and solid constituents, the lower limits for a highly compressible pore fluid. Relations between the constants are

$$(8.12) \quad B = (K_u - K)/\zeta K_u,$$

$$(8.13) \quad \nu_u = \frac{3\nu + \zeta B(1 - 2\nu)}{3 - \zeta B(1 - 2\nu)}.$$

Further, RICE and CLEARY [99] express B in terms of K , porosity (m/ρ in the reference state), fluid bulk modulus K_f , K'_s and a further modulus K''_s , which, like K'_s , reduces to K_s in the special cases discussed earlier. Hence, in these

special cases the additional constants ζ ; K_u (or ν_u, B) can be calculated directly from measured values of the drained elastic constants K and G , from the porosity and from the bulk moduli K_f and K_s of the fluid and solid constituents.

The parameters which control the magnitude of effects to be discussed in subject. 8'2-8'4 are the Poisson ratios ν and ν_u (and particularly the difference between them), whereas the time scale of the effects is controlled by c . Table II shows values of ν and ν_u from a tabulation of properties for intact rocks by RICE and CLEARY [99], assuming full saturation, and from a tabulation by RICE and RUDNICKI [123] based on self-consistent model calculations of O'CONNELL and BUDIANSKY [132] for a solid of Poisson ratio 0.25 containing N narrow, fluid-filled cracklike pores of radius r per unit volume, assumed to be capable of fluid communication. In general the Poisson ratio associated with stress wave propagation is intermediate to ν and ν_u , sometimes approaching the latter, and examinations of wave speed data by O'CONNELL and BUDIANSKY [132] suggest a range of Nr^3 from 0.1 to 0.3 as being representative of field conditions in the vicinity of the 1971 San Fernando earthquake. The last three columns of table II contain various ratios of undrained to drained rock stiffness that arise in applications. The last two of these columns refer to the expressions for ξ given in (7.16) for axisymmetric narrow ellipsoidal inclusions and in (7.15) for spherical inclusions; ξ is calculated from ν , ξ_u from ν_u .

TABLE II. — Values of the drained and undrained Poisson ratios, ν and ν_u , and of various ratios of undrained to drained stiffness based upon them. The intact-rock results are from a tabulation by RICE and CLEARY [99]. The results given in terms of the crack density parameter Nr^3 are from a tabulation by RICE and RUDNICKI [123], based on self-consistent model calculations by O'CONNELL and BUDIANSKY [132] for a solid with Poisson ratio 0.25 containing N cracklike pores of radius r per unit volume.

| | ν | ν_u | $\frac{1-\nu}{1-\nu_u}$ | ξ/ξ_u for axisymmetric narrow ellipse | ξ/ξ_u for sphere |
|-------------------------------------|-------|---------|-------------------------|---|------------------------------|
| <i>Intact rock type [99]</i> | | | | | |
| Charcoal granite | 0.27 | 0.30 | 1.04 | | |
| Westerly granite | 0.25 | 0.34 | 1.14 | | |
| Ruhr sandstone | 0.12 | 0.31 | 1.28 | | |
| Berea sandstone | 0.20 | 0.33 | 1.19 | | |
| Clay soil | 0.12 | 0.50 | 1.76 | | |
| <i>Nr^3 [123, 132]</i> | | | | | |
| 0 | 0.25 | 0.25 | 1.00 | 1.00 | 1.00 |
| 0.1 | 0.21 | 0.28 | 1.11 | 1.06 | 1.07 |
| 0.2 | 0.17 | 0.32 | 1.22 | 1.12 | 1.15 |
| 0.3 | 0.12 | 0.36 | 1.37 | 1.20 | 1.25 |
| 0.4 | 0.08 | 0.41 | 1.56 | 1.29 | 1.39 |

The values of diffusivity c for intact rocks with water as the pore fluid are [99] $7 \cdot 10^{-6}$ and $2.2 \cdot 10^{-5}$ m^2/s for the two granites and $5.3 \cdot 10^{-4}$ and 1.6 m^2/s for the two sandstones of table II. But fluid transport in rocks under field conditions is expected to be dominated by large-scale joints and faults. Indeed, various field observations in earthquake regions as summarized by ANDERSON and WHITCOMB [133] suggest values of c in the range of 1 m^2/s , although measurements based on well response near the San Andreas fault by KOVACH *et al.* [134] suggest a range of 0.01 to 0.1 m^2/s . Typically, results on pore fluid effects in rupture models have been given for $c = 0.1$ and 1.0 m^2/s [11, 123].

It is to be expected that c and the differences between drained and undrained moduli reduce with depth in the Earth, owing to increased overburden pressure.

§2. Stress field of a dislocation; aftershock processes. — BOOKER [125] gave the plane-strain solution of the Biot equations for a suddenly introduced discrete dislocation, corresponding to mode-II slip, in the case of incompressible constituents ($\nu_u = 0.5$), and RICE and CLEARY [99] gave the solution for arbitrary ν_u . If a dislocation of Burger's vector b_1 is introduced at point x'_1 of the x_1 -axis at time t' , *i.e.* the slip distribution is

$$(8.14) \quad \Delta u_1(x_1) = b_1 U(x'_1 - x_1) U(t - t'),$$

the resulting shear stress $\sigma_{21}(x_1, x_2, t)$ along the axis ($x_2 = 0$) is [99]

$$(8.15) \quad \sigma_{21}(x_1, 0, t) = \frac{Gb_1 U(t - t')}{2\pi(1 - \nu_u)(x_1 - x'_1)} F[(x_1 - x'_1)^2/4c(t - t')],$$

where

$$(8.16) \quad F(\lambda) = 1 - \left[1 - \frac{1 - \nu_u}{1 - \nu} \right] \frac{1 - \exp[-\lambda]}{\lambda}.$$

At short times after dislocation introduction, $F = 1$, whereas, at long times, $F = (1 - \nu_u)/(1 - \nu)$, which is required in order for the solution to reduce to that based on drained elastic properties.

The significance of this solution for aftershock processes was recognized by NUR and BOOKER [124] and BOOKER [125]. For example, suppose that a region of the x_1 -axis sustains a sudden mode-II slip so that a stress drop $\Delta\sigma (= \sigma_{21}^0 - \sigma_{21}^f)$ results in the slipped region, and that afterwards the slip distribution remains fixed in time. Because the slip can be regarded as a distribution of dislocations, the stress drop quantity $\Delta\sigma (= \sigma_{21}^0 - \sigma_{21})$ diminishes in time, ultimately by the factor $(1 - \nu_u)/(1 - \nu)$, within the slipped region but increases outside it. This means that the total shear stress σ_{21} increases in time within the slipped region, and decreases outside it. This is consistent with a pattern of aftershock activity which is confined to the slipped region, rather than the (presumably) more highly stressed region outside of it, and with a time scale controlled by pore fluid diffusion.

The magnitude $(1 - \nu_u)/(1 - \nu)$ of the long-time fractional reduction in stress drop is the inverse of the quantity tabulated in the third column of table II, and these figures suggest that 10 to 30% reductions may be typical. On the other hand, if the ruptured region is in the form of a circular shear crack, the long-time reduction is given by the inverse of the quantity tabulated in the fourth column, suggesting reductions of 5 to 15%. In either case, the stress changes motivating aftershock activity seem significant. Of course, the aftershocks themselves alter the slip distribution. If the stress drop on the fault is to remain constant in time, the figures would imply a further slip of perhaps 5 to 20% on a circular rupture after the main event, either aseismically or with aftershocks.

An estimate of the time scale for stress redistribution may be made by considering the sudden slip distribution (eq. (5.10))

$$(8.17) \quad \Delta u_1 = 2(1 - \nu_u)(\Delta\sigma)_{t=0^+} \sqrt{a^2 - x_1^2}/G$$

for a mode-II plane-strain shear crack of length $2a$, sustaining a uniform stress drop $(\Delta\sigma)_{t=0^+}$ immediately after rupture. For purposes of calculating approximately the time-dependent stress drop $\Delta\sigma$ at the center of the rupture ($x_1 = 0$), this distribution may be regarded as being created by two oppositely signed discrete dislocations placed at the centroids $x_1 = \pm 2a/\pi$ of the right ($0 < x_1 < a$) and left ($-a < x_1 < 0$) continuous dislocation distributions of density $-d\Delta u_1/dx_1$. Hence

$$(8.18) \quad \Delta\sigma \approx (\Delta\sigma)_{t=0^+} F(a^2/\pi^2 ct).$$

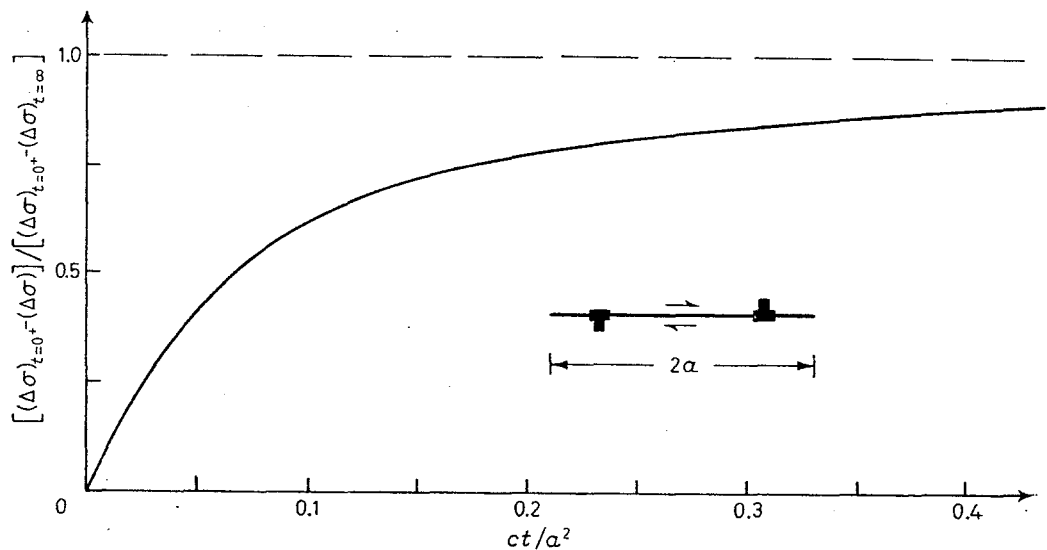


Fig. 17. - Time dependence of the stress drop $\Delta\sigma$ at the center of a suddenly introduced shear fault, sustaining a uniform stress drop $(\Delta\sigma)_{t=0^+}$, in a fluid-infiltrated solid. The growth in time of the total shear stress σ_{21} acting on the slipped region may contribute to the time scale of aftershock processes.

The result is plotted in fig. 17 in the dimensionless form

$$[(\Delta\sigma)_{t=0^+} - \Delta\sigma]/[(\Delta\sigma)_{t=0^+} - (\Delta\sigma)_{t=\infty}] \text{ vs. } ct/a^2.$$

The reduction in $\Delta\sigma$ is rapid at first and a characteristic time of aftershock activity can be defined by $a^2/14c$, corresponding to half of the full reduction. However, the effect continues over long time periods, with the dimensionless stress quantity in fig. 17 approaching slowly to unity, as $1 - a^2/2\pi^2ct$, at large times. As an example, if the rupture length $2a$ is 4 km and c lies in the range 0.1 to 1 m²/s suggested earlier, the characteristic time ranges from 3.5 to 35 days, although the shape of the curve in fig. 17 suggests continuing effects over periods that are several times longer.

8.3. Pore fluid stabilization of quasi-statically propagating shear cracks. — The complicated nature of the Biot equations has thus far prohibited their solution for realistic crack models, in which a zone of slip is initiated at some location and spreads, at first quasi-statically, along a fault. However, a simpler crack model solved by RICE and SIMONS [75] suggests a significant effect of pore fluids in stabilizing shear cracks. They considered a semi-infinite mode-II crack, moving quasi-statically at uniform speed v under the action of a stress drop $\Delta\sigma$ that acts only over distance l behind the crack tip, where the region of stress drop moves also at uniform speed v . This simulates a moving finite crack of comparable length, for which slip is arrested at the trailing end.

First neglecting any zone of strength degradation at the tip, they showed that the near-tip stress and strain field was of exactly the same inverse-square-root singular form as for an ordinary elastic solid having a Poisson ratio equal to the drained value, ν , and that the pore pressure vanished at the tip. They showed that the stress intensity factor K of this singular field was given by

$$(8.19) \quad K = K_{\text{nom}} h(vl/c),$$

where

$$(8.20) \quad K_{\text{nom}} = \Delta\sigma \sqrt{8l/\pi}$$

is the nominal intensity factor, *i.e.* that which would result from the same loading on an ordinary elastic solid, and $h(vl/c)$ is a monotonically decreasing function of its argument (and defined by an integral in eq. (41) of [75]), equal to unity when $vl/c = 0$ and approaching $(1 - \nu_u)/(1 - \nu)$ when $vl/c \rightarrow \infty$. This high-speed limit of $h(vl/c)$ is again the inverse of the stiffness ratio given in the third column of table II. For this crack model the criterion for crack advance is that

$$(8.21) \quad (1 - \nu) K^2/2G = \mathcal{J}_{\text{crit}},$$

where \mathcal{J}_{crit} is the critical energy release rate, and thus by (8.19) the nominal value of the energy release rate necessary to drive the crack at speed v is

$$(8.22) \quad \mathcal{J}_{nom} \equiv (1 - \nu) K_{nom}^2 / 2G \equiv 4(1 - \nu)(\Delta\sigma)^2 l / \pi G = \mathcal{J}_{crit} / [h(vl/c)]^2.$$

Hence, according to this model, $\mathcal{J}_{nom} = \mathcal{J}_{crit}$ at $v = 0^+$, but \mathcal{J}_{nom} must increase to drive the fault at increasing speeds, and

$$(8.23) \quad \mathcal{J}_{nom} \rightarrow [(1 - \nu)/(1 - \nu_u)]^2 \mathcal{J}_{crit} \quad \text{as } vl/c \rightarrow \infty.$$

If we judge from the values tabulated in table II, this is a substantial effect, with values of the coefficient \mathcal{J}_{crit} ranging from 1.23 to 1.88 for values of Nr^3 between 0.1 and 0.3. The result is plotted in a dimensionless form as the curve labelled $\omega/l = 0$ in fig. 18. (The curve is drawn for $(1 - \nu)/(1 - \nu_u) = 1.33$, but, in the dimensionless form presented, it is not very sensitive to the numerical value chosen.)

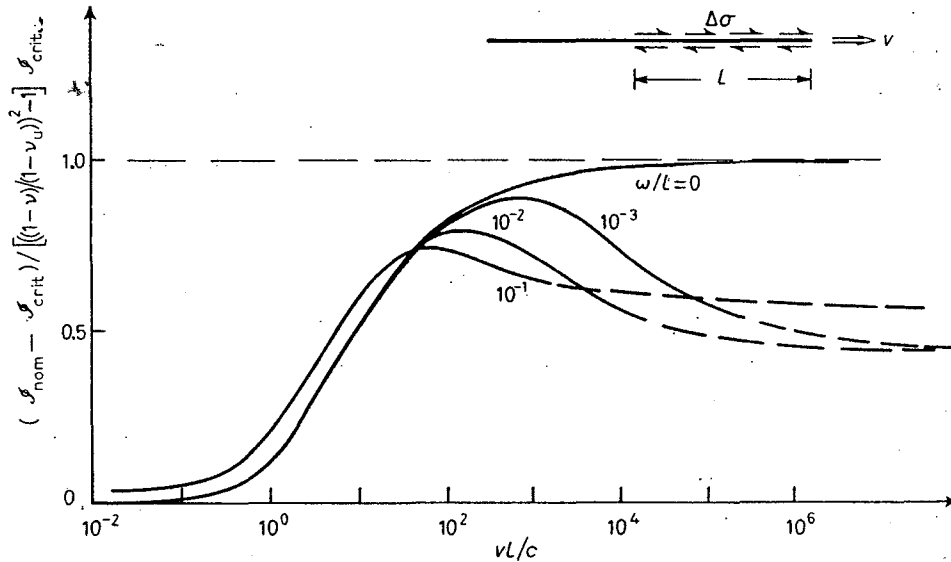


Fig. 18. — The nominal energy release rate ($\mathcal{J}_{nom} = 4(1 - \nu)(\Delta\sigma)^2 l / \pi G$) required to drive a mode-II shear crack at speed v in a fluid-infiltrated elastic solid. \mathcal{J}_{crit} is the actual fracture energy. Size of the slip-weakening zone is ω ; $\omega = 0$ corresponds to singular crack model.

This is, however, a case in which the singular crack model leads to results which become unrealistic physically at high speeds (when the diffusion penetration scale c/v of the drained elastic singularity shrinks to zero), and has been discussed by RICE [135] as one of several examples in which an energy balance fracture criterion for a singular crack model leads to paradoxical results. A more realistic estimate of the effect is described by a slip-weakening model

analyzed by RICE and SIMONS [75], and corresponding to a constant resistance over the size ω of the end region (like in the dashed-line plots of fig. 11). Results are shown for several ratios ω/l ; the effect is seen to lead to a peak in the required value of \mathcal{J}_{nom} to drive the fault and, very approximately, this peak occurs when the speed is sufficiently large for the diffusion penetration distance c/v to become comparable to ω .

The results of fig. 18 show a substantial effect of pore fluids in stabilizing a shear rupture, in that \mathcal{J}_{nom} must be increased continuously, at least up to the peak in the curves, to drive the fault at increasing speed. As RICE and SIMONS [75] observed, the stabilizing effect may be a critical factor in allowing the existence of slowly propagating slip events along faults (time-dependent frictional resistance may be involved also). For example, KING *et al.* [78] and NASON and WEERTMAN [136] report that creep events on the San Andreas fault in central California propagate at speeds ranging from 1 to 10 km/day (sometimes faster) and have rupture lengths ranging from 0.1 to 10 km. Since there seems to be an inverse relation between speed and length, these events may be considered to correspond to values of vl ranging from approximately 1 to 10 km²/day. Hence, for values of c suggested earlier these events correspond to a range of values of vl/c between 10 and 10² when $c = 1$ m²/s and between 10² and 10³ when $c = 0.1$ m²/s. These ranges of vl/c coincide generally with the portion of the vl/c axis in fig. 18 for which the pore fluid effects should be active in stabilizing the ruptures, although the range for the smaller value of c extends somewhat beyond the maxima in the curves for the slip-weakening model.

The results suggest that large-scale slip events, for example, as studied by STUART [57, 58] and STUART and MAVKO [59], are given some extra margin of stability by the presence of pore fluids, and that they can sustain modest increases in their effective fracture energies (\mathcal{J}_{nom}), at least up to the level corresponding to the peak in the \mathcal{J}_{nom} vs. v relation. This may be important in leading to a less abrupt instability than that expected when pore fluid effects are neglected, and may be a source of short-time earthquake precursors in the form of accelerating fault creep toward instability.

§4. Effects on elastic unloading stiffness of the surroundings of a strain-weakening zone. — Similar stabilizing effects of pore fluids are predicted for the strain-weakening inclusion model of subsect. 7.3. As shown in fig. 16, the inclusion becomes unstable at point B' when the slope of its softening stress-strain relation decreases to a value equal to the elastic unloading stiffness of the surroundings, namely G/ξ , where ξ is a function of the Poisson ratio of the surroundings and shape of the inclusion, eqs. (7.15), (7.16). For slow tectonic loadings the surroundings may be assumed to deform in a nearly drained fashion. But, when the instability point B' , based on the drained value of ξ , is reached, the inclusion cannot become dynamically unstable, because

the surroundings respond to rapid deformations in an undrained fashion, and thus with a larger stiffness G/ξ_u , where ξ_u is the value of ξ corresponding to ν_u . (Hence the ratio of undrained to drained stiffness of the surroundings is ξ/ξ_u , and this is tabulated in the last two columns of table II.) Instead, a process of self-driven creep begins at B' , which may, in general, be expected to accelerate toward a seismic instability when the softening slope reduces to G/ξ_u , but which may under some conditions allow an aseismic progression of rupture.

The process has been analyzed in an approximate manner by RICE [11] and RICE and RUDNICKI [123]. Their work is based on a solution developed by RICE *et al.* [127] for the time-dependent straining of a fluid-infiltrated solid containing a highly permeable spherical inclusion. Under shear loading, and for nondilatant shearing of the inclusion, the resulting pore pressure perturbation vanishes within the inclusion, but diffusive flows are established in the surroundings in their transition from undrained to drained response. RICE *et al.* [127] showed that the inclusion deforms homogeneously under these conditions and the Eshelby relation of (7.14) generalizes to

$$(8.24) \quad \gamma_{inc}(t) - \gamma_{\infty}(t) = \gamma_{inc}(0) - \gamma_{\infty}(0) + \frac{1}{G} \int_0^t \{ \xi_u + (\xi - \xi_u) f[ct/a^2] \} [\dot{\tau}_{\infty}(t') - \dot{\tau}_{inc}(t')] dt',$$

where $t = 0$ is some time at which the system is at equilibrium under fully drained conditions, and where $f(ct/a^2)$ is a function that they determine, which increases from 0 to 1 with a time history very similar to that for the function plotted in fig. 17.

RICE and RUDNICKI [123] present results for the deformation to instability of strain-weakening inclusions, assumed to exhibit a stress-strain relation near peak strength ($\tau_{inc} = \tau_p$, $\gamma_{inc} = \gamma_p$) in the form

$$(8.25) \quad \tau_{inc} = \tau_p - G(\gamma_{inc} - \gamma_p)^2/2\lambda,$$

where 2λ (which they choose as 0.005, approximately consistent with data like those in fig. 13) is a measure of the width of the strength peak. They show results for the time-dependent inclusion strain, assuming a uniform tectonic stress rate $\dot{\tau}_{\infty}$, and define a precursor time t_{pr} as the time of the self-driven accelerating creep period from point B' in fig. 16 to the final seismic instability. For $\dot{\tau}_{\infty} = 1$ bar/y, $c = 0.1$ m²/s and $\xi/\xi_u = 1.10$ (which seems reasonable from table II), they find $t_{pr} = 37$ days for a spherical inclusion of 1 km radius, 83 days for 3 km radius and 122 days for 5 km radius. The times decrease by about a factor of 1/2 for $c = 1$ m²/s. Also, estimates of t_{pr} for a very flat inclusion zone in the form of an axisymmetric ellipsoid with 18:1 aspect ratio are generally 1/10 to 1/15 of those for a spherical zone. An increased undrained to

drained stiffness ratio increases t_{pr} , for example by about a factor of 3 when $\xi/\xi_a = 1.25$. Although these estimates of t_{pr} vary widely according to the assumptions made, they are generally consistent as to order of magnitude with those for earthquake precursors associated with events of comparable rupture size by SCHOLZ *et al.* [137] and WHITCOMB *et al.* [138].

8.5. *Constitutive response for inelastic dilatancy of fluid-infiltrated solids.* — Inelastic dilatancy is a characteristic feature of brittle rock deformation as observed in the laboratory at loadings near or to failure (*e.g.* [71, 72]), and is also observed to accompany shearing of rock surfaces in contact [100]. In nominally coherent rock, dilatancy is a consequence of the opening of cracks. The effects of such processes, distributed over regions near faults, have been cited as a possible source of precursory variations in seismic and transport properties (*e.g.* [137-141]).

Here we consider dilatancy of fluid-infiltrated rocks, and note that this provides another means for the stabilization of rupture processes since the strength of brittle rock is largely frictional in origin, and frictional resistance is enhanced by the suctions developed in pore fluids by dilatant deformation. The effect was first discussed in relation to granular materials by REYNOLDS [142]. It is a basic concept in interpreting the mechanical response of soils, and has been demonstrated for initially intact saturated rocks by BRACE and MARTIN [143].

For elastic response, eq. (8.1) shows that the strain is determined by $\sigma_{\alpha\beta} + \zeta p \delta_{\alpha\beta}$, where $0 < \zeta < 1$. But is it generally agreed that inelastic-strain increments are governed by the Terzaghi [144] « effective » stress $\sigma_{\alpha\beta} + p \delta_{\alpha\beta}$. RICE [145] has shown that this form must apply when inelasticity arises from frictional slip at isolated asperity contacts and/or from the growth of sharp cracks in fully saturated rock, and in these same circumstances the inelastic change $d^p v$ in the porosity $v (= m/\rho)$ is equal to the inelastic dilatant strain. Thus, assuming conditions as discussed earlier are met for the moduli K'_s, K''_s to reduce to the bulk modulus of the solid, K_s , RICE [11] showed that the constitutive relations of eqs. (7.1), (7.2) generalize in the case of fluid saturation to

$$(8.26) \quad \begin{cases} d\gamma = d\tau/G + d^p\gamma, & d\varepsilon = -[d\sigma - (1 - K/K_s) dp]/K + d^p\varepsilon, \\ d^p\gamma = [d\tau - \mu(d\sigma - dp)]/h, & d^p\varepsilon = \beta[d\tau - \mu(d\sigma - dp)]/h. \end{cases}$$

Further, just as for the elastic case, it is necessary to append a constitutive relation for the fluid mass content, which is

$$(8.27) \quad dm/\rho = v dp/K_s - (1 - K/K_s)(d\sigma - dp)/K - v dp/K_s + d^p\varepsilon.$$

These equations imply that, for drained deformation (p constant) at constant σ ,

$$(8.28) \quad (d\tau/d\gamma)_{\text{drained}} = h/[1 + h/G],$$

whereas, for undrained deformation (m constant) at constant σ ,

$$(8.29) \quad (d\tau/d\gamma)_{\text{undrained}} = (h + \mu\beta K')/[1 + (h + \mu\beta K')/G],$$

where

$$(8.30) \quad 1/K' = 1/K + \nu/K_t - (1 + \nu)/K_s.$$

Equation (8.29) illustrates the effect of dilatancy hardening; the plastic modulus h for drained response is increased to an effective modulus $h + \mu\beta K'$ for undrained response. The corresponding rate of development of suction in the pore fluid is

$$(8.31) \quad (dp/d\tau)_{\text{undrained}} = -\beta K'/(h + \mu\beta K').$$

The strengthening of shear resistance which can be obtained in this way is potentially large since K' will generally be of the order of the smaller of K or K_t/ν . But it is limited by the following factors:

i) As large suctions are induced, the effective compression $\sigma - p$ increases and this generally tends to inhibit dilatancy and, if $\beta \rightarrow 0$, the effect ceases.

ii) The suctions may reach a level such that the total pore pressure (initial ambient pressure minus suction) reduces sufficiently that a liquid to vapor transition occurs in the pore fluid or dissolved substances come out of solution as gases. In this case $K_t \rightarrow 0$, which implies that $K' \rightarrow 0$ and again limits the effect.

iii) The plastic constitutive moduli for the underlying drained response may reduce sufficiently with continuing deformation so that the drained response meets conditions for a localization instability as discussed in subsect. 7.1. RICE [146] showed that, despite the fact that $h + \mu\beta K'$ may be large and positive at such a state, dilatant hardening then becomes unstable in the sense that any small nonuniformities in the pore pressure distribution grow exponentially in time, the implication being that the localization instability will occur in the undrained condition as well.

The effects of dilatancy within slip-weakening fault models have been indicated in fig. 10. In particular, if slip during the strength degradation process is accompanied by dilatant opening over a time scale that is too short for full alleviation of the associated suctions by diffusion, the effective compressive stress ($-\sigma_{22} - p$ in fig. 10c) will increase, thus increasing the shear resistance and the effective fracture energy.

Estimates of the effects of dilatancy on shear crack propagation with a dilating end region have been made by RICE [11] (based on an earlier study [147] of analogous phenomena in clay soils), and on a strain-weakening inclusion

model by RICE and RUDNICKI [123]. Unfortunately the calculations rely on many parameters for which the values under field conditions are uncertain within wide ranges. However, the use in these calculations of even minimal dilatancy parameters as inferred from laboratory studies (*e.g.* [71, 100]) suggests strong effects of dilatancy in stabilizing the rupture process. The effects are similar in kind to the analogous effects due to Biot elastic response as discussed in subsect. 8'3 and 8'4.

8'6. *Dilatancy effects during the slip-weakening process in shear crack propagation.* – To examine the effect of dilatancy during fault slippage, consider first an infinite fault occupying the plane $x_2 = 0$ and suppose that this is slipped uniformly in shear under constant compressive stress ($-\sigma_{22}$). In this case the $\mathbf{u} = \mathbf{u}(x_2, t)$ and eqs. (8.9), (8.10) imply that

$$(8.32) \quad c \partial^2 p / \partial x_2^2 = \partial p / \partial t.$$

Let $H(t)$ be the dilatant opening of the fault. This opening must be supplied with pore fluid so that the boundary condition on $x_2 = 0$ is

$$(8.33) \quad \frac{1}{\rho} [q_2(0^-, t) - q_2(0^+, t)] = \kappa \left[\frac{\partial p}{\partial x_2}(0^+, t) - \frac{\partial p}{\partial x_2}(0^-, t) \right] = \dot{H}(t).$$

The solution of the diffusion equation (8.32) is straightforward under these boundary conditions and one finds that the suction induced on the plane of the fault is

$$(8.34) \quad -p(0, t) = \frac{c}{2\kappa} \int_{-\infty}^t \frac{\dot{H}(t') dt'}{\sqrt{\pi c(t-t')}}.$$

Now consider a quasi-statically propagating shear crack moving at uniform speed v (fig. 19a) and assume that dilatant opening occurs at a uniform rate Hv/ω within the slip-weakening zone, so that a total dilatant opening H results at $x_1 = -\omega$, and remains constant thereafter. The resulting pore pressure distribution on the fault plane may be estimated approximately by (8.34) and is

$$(8.35) \quad -p = s [U(-x_1) \sqrt{-x_1/\omega} - U(-x_1 - \omega) \sqrt{-(x_1 + \omega)/\omega}],$$

where U is the unit step function and

$$(8.36) \quad s = (cH/\kappa\omega) \sqrt{v\omega/\pi c}$$

is the maximum suction (fig. 19a). The distribution would be less sharply peaked if the fault itself is a high-diffusivity path. The effect of the suction

is to augment the shear resistance σ_{21} by $\mu(-p)$, where μ is the friction coefficient (*i.e.* the slope of the curves in fig. 10c), where the resistive stress is shown as a function of $-\sigma_{22} - p$, and this means that the stresses required to drive the crack are increased.

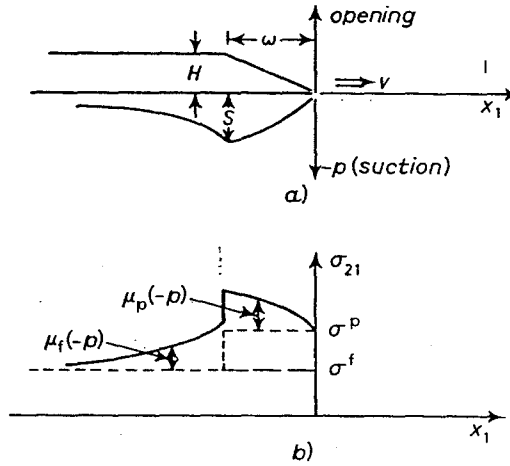


Fig. 19. - Effect of dilatant opening during fault slippage: a) a maximum suction s is induced in the pore fluid and b) the stress-resisting slip is augmented by $\mu(-p)$, where μ is the friction coefficient.

RICE [11, 147] gave an approximate estimate of the effect by idealizing the slip-weakening stress distribution in the absence of suctions, as shown by the dashed line in fig. 19b). The total shear resistance is shown by the solid line and the friction coefficient is written as μ_p within the zone of peak strength and μ_t outside it. In analyzing the problem, he actually replaced $\sigma^p - \sigma^f$ with $(2/3) \cdot (\sigma^p - \sigma^f)$ and $\overline{\Delta u}$ with $(3/2) \overline{\Delta u}$ to preserve the same fracture energy \mathcal{S} in the absence of fluid suction but to make the size ω of the end region agree with the more realistic estimate ω_0 of (6.12) in that case. The surrounding material was treated as an ordinary elastic solid, so that the additional stabilization resulting from Biot elasticity (subsect. 3'3) is neglected. Assuming that the overall crack length is large compared to the size ω , he finds that

$$(8.37) \quad \omega = \omega_0 [\sqrt{1 + \beta^2} - \beta]^2, \quad \text{where } \beta = 3s[\mu_p(1 - \ln 2) - \mu_t \ln 2]/8(\sigma^p - \sigma^f).$$

This is an implicit equation because β depends (through s) on ω . The resulting energy release rate \mathcal{S} required to drive the fault at the assumed speed v (obtained from the corresponding expression for K in eq. (22) of [147], also given as eq. (38) of [11]) is

$$(8.38) \quad \mathcal{S} \approx (\sigma^p - \sigma^f) \overline{\Delta u} [\sqrt{1 + \beta^2} - \beta]^2 \left[1 + \frac{3s}{4(\sigma^p - \sigma^f)} (\mu_p + \mu_t \ln \sqrt{4l/e\omega}) \right]^2,$$

where e is the natural-logarithm base and l is the total length over which the crack has propagated. For nonuniform, accelerating propagation it should be reasonable to choose l as the length over which the fault has propagated at speeds comparable to the current speed. Fortunately, the dependence on l is not strong.

The result simplifies considerably when $\mu_p = 0.44 \mu_t$, which means that $\beta = 0$ and $\omega = \omega_0$. In this case, after using (8.36) and (6.12) with $\nu = 0.25$, the expression for \mathcal{J} can be put in the form

$$(8.39) \quad \mathcal{J} = (\sigma^p - \sigma^t) \overline{\Delta u} [1 + (\mu_t/\pi)(c/\kappa G)(H/\overline{\Delta u})\sqrt{v\omega_0/\pi c} \ln(1.9\sqrt{l/\omega_0})]^2.$$

To discuss the terms in the bracket, note that $H/\overline{\Delta u}$ is a dilatancy factor. BARTON [100] gives $dH/d(\Delta u)$ at peak strength of rough natural rock surfaces as the tangent of a dilatancy angle d_n and suggests that

$$(8.40) \quad d_n \approx 10^\circ \log [(\sigma_1 - \sigma_3)/\sigma_n],$$

where σ_n is the effective normal stress on the fault and $\sigma_1 - \sigma_3$ is the compressive fracture strength of intact specimens of the adjoining material at the same confining stress σ_3 as in the fault sliding experiment. He suggests that d_n values of 1° to 3° will persist at the transition from slip with strength degradation to stable slip (right end of fig. 10c). Thus, if $H/\overline{\Delta u}$ is identified as $(1/2) \operatorname{tg} d_n$, values of $H/\overline{\Delta u}$ equal at least to 0.008 to 0.026 are expected, and typically perhaps 2 to 3 times larger in the range of slip with large strength degradation. Accordingly, the following numerical example takes $H/\overline{\Delta u} = 0.04$ (i.e. $d_n = 4.6^\circ$). The ratio $c/\kappa G$ is independent of permeability and can be expressed as [99]

$$(8.41) \quad c/\kappa G = 2B^2(1 + \nu_u)^2(1 - \nu)/9(1 - \nu_u)(\nu_u - \nu),$$

where typical values of B for intact rock are [99] 0.5 to 0.9. B may be larger under field conditions than for intact rock due to joints and faults, and has a maximum value of 1; $B = 0.8$ is used. If we choose the ν, ν_u values for $Nr^3 = 0.2$ in table II as representative, this gives $c/\kappa G = 2.0$.

The logarithmic term in (8.39) is taken as 2.6, corresponding to $l = 50 \omega_0$ (e.g. 5 km rupture length with 100 m end region). Factor of 10 increases or decreases in l/ω_0 would change the 2.6 to 3.7 or 1.4, respectively. Hence, for the case considered, with friction coefficient $\mu_t = 0.6$,

$$(8.42) \quad \mathcal{J} \approx (\sigma^p - \sigma^t) \overline{\Delta u} [1 + 0.02\sqrt{v\omega_0/c}]^2$$

and the corresponding value of the maximum suction is

$$(8.43) \quad s = (4/3\pi)(c/\kappa G)(H/\overline{\Delta u})(\sigma^p - \sigma^t)\sqrt{v\omega_0/\pi c} \approx 0.02(\sigma^p - \sigma^t)\sqrt{v\omega_0/c}.$$

These expressions are plotted in fig. 20. Evidently, very large increases in \mathcal{F} are possible. Depending on the size of the strength degradation zone ω_0 (which is unknown to within very wide limits, subsect. 6'2) the middle range

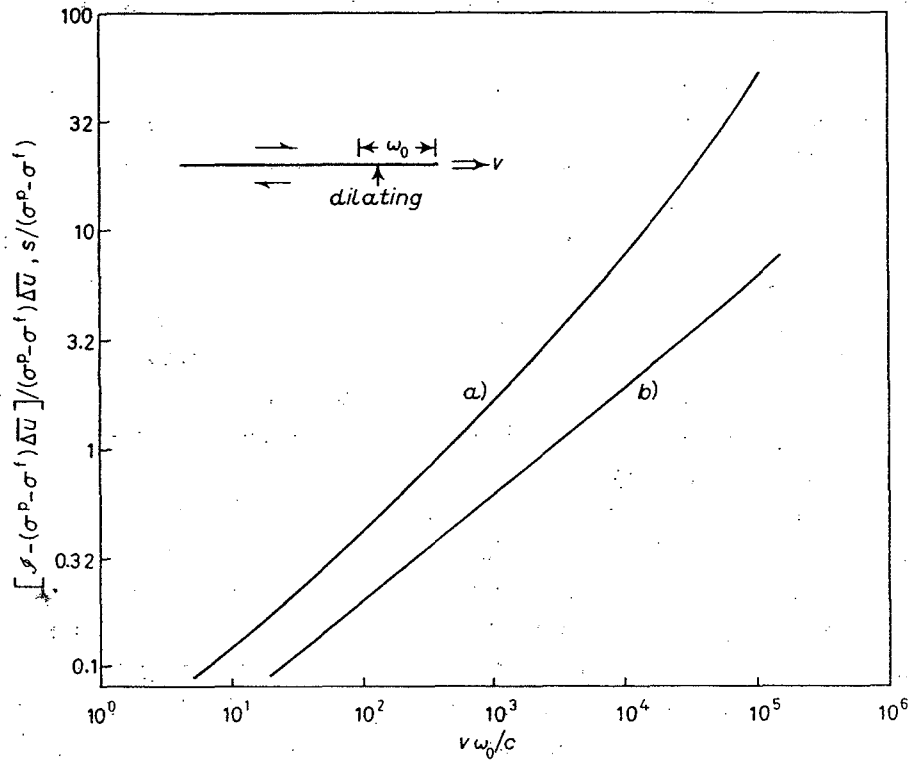


Fig. 20. - Fracture energy and maximum suction induced for stabilization of propagating shear crack by dilatant hardening: curve *a*) fracture energy \mathcal{F} , curve *b*) suction s . Computation assumed dilatant opening $H = 0.04 \Delta \bar{u}$, rupture length $l = 50 \omega_0$, frictional coefficient $\mu_t = 0.6$.

of the velocity scale in fig. 20 (say, 10^2 to 10^4) may correspond to slow creep propagation or to rapid crack propagation, perhaps in the early stages of dynamic rupture. For example, if $\omega_0 = 1$ km (the largest estimate in subsect. 6'2), the middle range of the velocity axis corresponds to $v = 4$ to 400 km/day. This estimate of ω_0 was associated with a strength drop of 100 bar (and a fracture energy of 10^6 J/m²), so that the suctions are of order 20 to 200 bar over this range. But, if $\omega_0 = 1$ m, the middle range of the velocity axis is 3 to 300 km/min.

8'7. Dilatant hardening stabilization of rupture in the strain-weakening inclusion model. - A related study of dilatancy effects was made by RICE and RUDNICKI [123], who applied the constitutive formulation of eqs. (8.26), (8.27) to the strain-weakening inclusion model of fig. 16. This analysis was complementary to that based on Biot elastic effects in the surroundings and discussed in sub-

sect. 8'4. The inclusion was taken to be spherical in shape and was assumed to sustain a spatially uniform but (because of the dilatant deformation) time-varying pressure p , and fluid flow into the inclusion, in order to alleviate the continually generated suction, was calculated according to the solution for an arbitrary pressure variation on the wall of the spherical cavity in fluid-infiltrated elastic surroundings [99, 127].

Again, instability cannot occur abruptly when state B' is reached in fig. 16, because the rapid deformations of the inclusion are undrained and hence stiffer than those of the (drained) stress-strain relation in the figure. Hence the system enters a period of self-driven accelerating creep at B' .

RICE and RUDNICKI modelled the processes by assuming that the drained, *in situ* stress-strain relation in shear had the form of eq. (8.25) near peak, and solved for the time histories of strain and pore pressure within the inclusion due to a uniform rate of remote stressing. Over the range of parameters studied, suction in excess of a few tens of bar were found to result only very late in the precursory period (again defined as the time between reaching state B' and final seismic instability).

Assuming a tectonic loading rate $\dot{\tau}_\infty = 1$ bar/y, friction factor $\mu = 0.6$, dilatancy factor $\beta = 0.3$, peak width stress-strain parameter $2\lambda = 0.005$, fluid compressibility $K_f = 22$ kbar and initial porosity $v = 0.01$, they compute precursory times $t_{pr} = 55, 230$ and 410 days when $c = 1$ m²/s and the zone radius is $a = 1, 3$ and 5 km, respectively. The corresponding figures are $t_{pr} = 240, 840$ and 1420 days, respectively, when $c = 0.1$ m²/s. Also, decreases in β result in approximately proportional decreases in t_{pr} , whereas a factor of 10 decrease in K_f is required to decrease t_{pr} by a half. A flattened shape of the strain-weakening zone should reduce t_{pr} , as for the model in subsect. 8'4, but results for t_{pr} have not been obtained for this case.

Contrary to popular conceptions of the dilatancy-diffusion model, t_{pr} does not scale in proportion to a^2/c . This is because diffusion is not the only source of the time scale in the process. The tectonic loading rate is important as well, particularly since this determines how far removed the system is from drained equilibrium when the stage of self-driven accelerating creep is entered. The results also do not support the conception that dilatancy must necessarily be associated with large changes in wave speeds and, conversely, that the absence of wave speed anomalies means an absence of dilatancy. Such wave speed effects can result [139], but, as remarked, the suction induced in the pore fluid seem generally to be small, even though the mechanism seems capable of producing long-time precursory effects of accelerating creep. Significant wave speed alterations can occur only if the suction is large enough to induce a liquid to vapor transition or release of dissolved gases over large regions of rock. The model suggests that this need not happen until very late in the precursory period, if at all, although it is certainly possible that such phenomena could occur locally through strong nonuniformities of deformation that are neglected

in the simple model of a homogeneously deforming inclusion. Perhaps more direct evidence on large-scale dilatancy effects may be sought in effects on transport properties, *e.g.* electro-kinetic effects [148, 149], which are sensitive to the dilatant opening of cracks but do not require a lack of liquid-phase infiltration.

PART III

Processes on a tectonic scale leading to earthquake instabilities.

9. – Space and time sequences of earthquake activity and viscous coupling to the asthenosphere.

The earthquake instability models considered in part II are local in character. In different forms, they assume that the surroundings of the focal region are essentially elastic and are subjected to a remotely uniform tectonic stress, typically taken to increase at a constant rate, that induces instability after some process of stable fault slippage (subsect. 6'1) or distributed inelastic straining (subsect. 7'3), possibly influenced by time-dependent frictional slip (subsect. 6'4) and/or by mechanical interactions with pore fluids (sect. 8). These considerations provide a framework for relatively short-term earthquake precursory processes in the vicinity of the focal region. But to understand earthquake processes over longer time and spatial scales, it is useful to consider in more detail the tectonic stressing process itself. This stressing is, of course, attributed to large-scale tectonic plate motions that are accommodated by some combination of stable slippage and discontinuous brittle rupture, *i.e.* earthquakes, along plate boundaries or seismic belts.

Here we examine the time- and position-dependent stressing of crustal material that arises from coupling of an essentially elastic lithosphere to an asthenosphere that responds viscously under long-term sustained stress. This coupling seems relevant to understanding the recurrence times of great earthquakes as well as the processes of transmission of earthquake activity along seismic belts and the time-dependent stressing to rupture of seismic gap zones that have not accommodated as much (or as recently) as neighboring zones of the belt to imposed plate motions.

Some aspects of this viscoelastic coupling have been considered in models as initiated by BUDIANSKY and AMAZIGO [13] for the periodic occurrence of great earthquakes. They examine a model for strike slip faulting in which the fault extends vertically downwards from the Earth's surface in a lithospheric plate, and in which displacement is uniform along the direction of strike as if the length of the surface breaks was indefinitely long, with uniform offset,

in the strike direction (*i.e.* two-dimensional mode-III crack model). BUDIANSKY and AMAZIGO neglected coupling at the upper asthenosphere boundary and instead modelled creep effects approximately by assuming that the crust behaved as a homogeneous Maxwell linear viscoelastic body (elastic and viscous element in series). More realistic treatments of the coupling, in which an elastic plate subject to remote velocity boundary conditions is joined to a viscoelastic substrate, were developed subsequently by SAVAGE and PRESCOTT [150] for a distributed dislocation fault model and in the context of crack models with prescribed stress drops by SPENCE and TURCOTTE [151] and TURCOTTE *et al.* [14].

As first noted in the simple model of Budiansky and Amazigo [13], this class of models exhibits a limit cycle response consisting of indefinitely repeated sequences of seismic-stress drop in rapid slip on the fault, that shifts stress down toward the asthenosphere, causing initially rapid creep there which gradually accommodates the earthquake slip and, together with the continually imposed plate motions, re-stresses the fault and repeats the cycle. Further, the correlation of such models with observations on plate motion rates, earthquake stress drops and recurrence times, or with observations on surface deformation during the post-seismic adjustment period, permits an approximate estimate of asthenosphere rheological properties. For example, NUR and MAVKO [152] generalized by correspondence methods a solution of Rybicki [153] for a dislocation in a layered elastic medium to the viscoelastic case, and predicted post-seismic deformations due to the viscoelastic coupling with a homogeneous Maxwell asthenosphere. Fitting of results to observed deformation following the 1946 Nankaido earthquake suggested a viscosity η on the order of $5 \cdot 10^{18}$ Pa·s ($= 5 \cdot 10^{19}$ poise), so that the relaxation time η/G is of the order of 5 years. This viscosity estimate is within the range ($4 \cdot 10^{18}$ to $6 \cdot 10^{20}$ Pa·s) predicted by McCONNELL [154] from Fennoscandian uplift data, but somewhat lower than more recent estimates ($4 \cdot 10^{19}$ Pa·s) from those data by CATHLES [155] and STACEY [25], and also from very approximate estimates by STACEY [25] based on energy balances in plate motion ($3 \cdot 10^{19}$ Pa·s under oceanic crust, $5 \cdot 10^{20}$ Pa·s under continental crust). However, as noted in a somewhat different context by RUDNICKI [8], if the actual asthenosphere rheology is non-linearly viscous (*e.g.* [25, 156]), a somewhat reduced effective linear viscosity may be appropriate for the response to large stress alterations created in the asthenosphere by great earthquakes.

The cyclic earthquake models just discussed consider variations in time of crustal-stress levels, but neglect nonuniformities in space. In fact, the examination of earthquake activity over long sections of seismic belts suggests that there may be relatively well-organized spatial patterns of stress accumulation and relief, so that the stressing at one segment along a belt is not independent of, but rather is influenced strongly by, the time-dependent transmission of stress from the rupture of neighboring segments. This seems to be particularly true for the occurrence of great earthquakes (say, magnitude 7 or larger) as studied

on the northwestern circum-Pacific belt by FEDOTOV [157] and MOGI [158, 159], and along the North Anatolian fault zone in Turkey by RICHTER [160], MOGI [159] and AMBRASEYS [161]. Successive major ruptures, extending over distances on the order of 200 km along the Earth's surface, tend to abut rather than overlap; for example, MOGI [158] observes that the circum-Pacific belt is covered in a nearly continuous manner by the aftershock areas of great shallow earthquakes without any appreciable overlap of the aftershock zones.

Although the fit to a simple propagation model is far from perfect, the observations suggest the propagation of a « triggering » process for great earthquakes along seismic belts, with speeds on the order of 50 to 100 km/y (ignoring the discontinuities of individual events) for the North Anatolian zone and of 150 to 270 km/y for the circum-Pacific belt [159].

SAVAGE [162] has hypothesized the presence of a propagating creep wave of stress that triggers major ruptures along the northeastern Pacific boundary. Further, SCHOLZ [163], in an analysis of various observations before the 1975 Haicheng earthquake, has presented strong evidence for a propagating « deformation front », with width (in terms of induced seismic activity) on the order of 100 to 300 km, that travelled approximately 1000 km through northeast China at a speed on the order of 110 km/y.

These observations of propagation effects are most marked by the occurrence of major ruptures, while lower-magnitude seismic activity seems to be occurring in a much less systematic way [159]. The picture which emerges is that plate boundaries or seismic belts may be ruptured by large-scale, through-crust, crack-propagation-like processes. In other words, the accommodation of plate boundaries to imposed plate motions does not seem to occur in a random fashion in space through process of stress build-up to instability and release. Rather, the stress intensification seems to be dictated in large part by processes of slip on adjoining segments of the seismic belt, which reduces stress locally but thereby transmits stress, and hence new seismic activity, to neighboring segments.

The most likely factor controlling the time scale of these processes is, of course, the viscous coupling between the lithosphere and the asthenosphere. The simple Elsasser [164] model of a semi-infinite elastic plate riding on a layer of viscous material shows that uniform stress drops along a plate boundary create deformation waves of stress relief which propagate outward in the plate as a diffusion process. This process, as noted by BOTT and DEAN [165] and ANDERSON [12], may provide a mechanism by which stress alterations and hence seismic activity is transmitted along plate boundaries. Consider, for example, the rupture of a long but finite segment of the crust in a great earthquake. The sudden drop in stress along the fault transfers stress both to the upper asthenosphere and to the adjoining sectors of the plate boundary. But, as the asthenosphere relaxes in time, more of the stress alteration is shifted to the adjoining segments of plate boundary, and this provides an in-

creased tectonic stressing rate on those segments, making them likely sites for the location of the next major rupture. The process is complicated to describe in mathematical terms. An approximate formulation is outlined in sect. 10 based on a generalization of the Elsasser model, which has been applied recently by LEHNER *et al.* [166] to analyze time-dependent crustal stressing following major ruptures or associated with propagating deformation fronts of the kind discussed by SAVAGE [162] and SCHOLZ [163].

These considerations are, of course, relevant also to the description of the time-dependent stressing of seismic gap zones adjoining major ruptures along active earthquake belts. Such zones are a natural focus for studies of impending earthquakes (*e.g.* [15]). They have, presumably, been stressed to high levels at the times of rupture of adjoining sections of the belt, and the process of asthenosphere relaxation is expected to cause further time-dependent stress increases with gap zones at rates which may greatly exceed average tectonic stressing rates.

10. — Generalized Elsasser model and time-dependent stressing associated with major ruptures.

Consider an elastic lithosphere plate of uniform thickness H which rides on a viscoelastic asthenosphere; x_1, x_2 are co-ordinates on the upper plate surface. Let

$$(10.1) \quad \sigma_{\alpha\beta}(x_1, x_2) = \frac{1}{H} \int_{-H}^0 \sigma_{\alpha\beta}(x_1, x_2, x_3) dx_3$$

be thickness-averaged stresses. Then the three-dimensional stress equilibrium equations integrate to

$$(10.2) \quad \partial \sigma_{\alpha\beta} / \partial x_\alpha = \tau_\beta / H, \quad \alpha, \beta = 1, 2,$$

in terms of the thickness-averaged stresses, where $\tau_\beta = \sigma_{3\beta}(x_1, x_2, -H)$ is the shearing traction acting in the negative β -direction on the lower plate surface. Let $u_\alpha(x_1, x_2)$, $\alpha = 1, 2$, be the corresponding thickness-averaged displacements in the plane of the plate. Then the « plane stress » relations between stress and displacement gradients are

$$(10.3) \quad \sigma_{\alpha\beta} = G \{ \partial u_\alpha / \partial x_\beta + \partial u_\beta / \partial x_\alpha + [2\nu / (1 - \nu)] \delta_{\alpha\beta} \partial u_\gamma / \partial x_\gamma \}.$$

These follow from the three-dimensional isotropic stress-strain relations when it is assumed that the changes in thickness average stress σ_{33} due to deformation are negligible. Such will be the case for disturbances of dominant wavelengths that are comparable to or greater than H , although even for very-short-wavelength

disturbances (for example, crack tips or dislocations in plates) comparison between plane-stress and plane-strain (the extreme limit of thickness direction constraint) solutions suggests that the errors in prediction of the thickness average fields will generally be small, involving errors of the order $\nu^2 \approx 10\%$.

The model of Elsasser [164] (formulated for one- vs. two-dimensional displacement fields) takes

$$(10.4) \quad \tau_\alpha = \eta \dot{u}_\alpha / h,$$

where h is the thickness of the asthenosphere and η is its average viscosity. This should be especially appropriate if, as is widely suspected (*e.g.* [25, 155]), the asthenosphere is a channel of material of the same order of thickness as H and of much lower viscosity than the adjoining material. Otherwise η/h is to be regarded as some effective upper-mantle coupling parameter, although it would have to depend on the dominant wavelength of the disturbances. MELOSH [156] adopts a nonlinear viscous relation instead of (10.4), but, in order to deal simply with some otherwise complex problems, nonlinearity is neglected here.

A weakness of the Elsasser model is that in it the asthenosphere responds rigidly to sudden loadings, and this can be corrected in a manner consistent with the simplicity of the model by using the Maxwell form

$$(10.5) \quad \dot{u}_\alpha b / G + \tau_\alpha h / \eta = \dot{u}_\alpha.$$

That is, $\tau_\alpha = Gu_\alpha/b$ is the resistance of the asthenosphere to a sudden displacement u_α . This is less suitable than the corresponding approximation for the viscous part of the resistance. LEHNER *et al.* [166] show that the choice $b \approx (\pi/4)^2 H$ causes this model to give the same instantaneous elastic relation between $\Delta\sigma$ and Δu for a sudden, uniform through-thickness stress drop as would be the case for a mode-III crack in a half-space of uniform elastic modulus G . (However, the instantaneous displacements attenuate somewhat too rapidly in the direction perpendicular to the fault.)

If we combine eqs. (10.2), (10.3) and (10.5), the thickness average displacement field is governed by

$$(10.6) \quad (\alpha + \beta \partial/\partial t) \{ \partial^2 u_\gamma / \partial x_e \partial x_e + [(1 + \nu)/(1 - \nu)] \partial^2 u_e / \partial x_e \partial x_\gamma \} = \partial u_\gamma / \partial t, \\ \gamma, e = 1, 2,$$

where

$$(10.7) \quad \alpha = hHG/\eta, \quad \beta = bH.$$

The parameter α is a diffusivity. Taking $h = 100$ km [25, 155], $G = 5.5 \cdot 10^{10}$ Pa as a lithosphere average shear modulus [25], $H = 90$ km as an average of

oceanic and continental lithosphere thickness [25], and using the range of η from $5 \cdot 10^{18}$ Pa·s [152] to $4 \cdot 10^{19}$ Pa·s [155], one finds

$$(10.8) \quad \alpha \approx 3 \cdot 10^3 \text{ to } 3 \cdot 10^2 \text{ km}^2/\text{y}.$$

Using $b \approx (\pi/4)^2 H$ as suggested earlier, we have

$$(10.9) \quad \sqrt{\beta} \approx 70 \text{ km},$$

and the characteristic relaxation time of the Maxwell model is

$$(10.10) \quad \beta/\alpha \approx 1.5 \text{ to } 15 \text{ y}.$$

For times which are large compared to this relaxation time, the Maxwell model can be replaced by Elsasser's purely viscous model.

10.1. Response to sudden stress drops and slips on long segments of a plate boundary. — Consider a very long section of plate boundary, coincident with the x_1 -axis, and suppose that faulting takes place uniformly along the boundary so that $\mathbf{u} = \mathbf{u}(x_2, t)$. The equations for u_1, u_2 then decouple to

$$(10.11) \quad (\alpha + \beta \partial/\partial t)(\partial^2/\partial x_2^2)[u_1, 2u_2/(1-\nu)] = (\partial/\partial t)[u_1, u_2].$$

If the slip is of a strike slip type, only u_1 is nonzero and it is related to the stress alteration (from the stress field $\sigma^0(x_2, t)$ which would result in the plate due to large-scale tectonic processes if no slip had taken place) by

$$(10.12) \quad \sigma_{21} - \sigma_{21}^0 = G \partial u_1 / \partial x_2.$$

For a thrust type of slip, which is regarded as a normal discontinuity Δu_2 in displacement within the plane-stress model, with stress drop expressed in terms of $\Delta \sigma_{22}$, the only nonvanishing displacement is u_2 and

$$(10.13) \quad \sigma_{22} - \sigma_{22}^0 = [2G/(1-\nu)] \partial u_2 / \partial x_2.$$

Equations (10.11)-(10.13) may be solved by Laplace transformation. This is done for the strike-slip case and the solution for the thrust case be constructed from it by an easy change of variables. Let

$$(10.14) \quad \hat{u}_1(x_2, s) = \int_0^{\infty} u_1(x_2, t) \exp[-st] dt.$$

Then, if $\Delta\hat{u}_1(s)$ is the transform of the slip displacement on the fault, we have, for $x_2 > 0$,

$$(10.15) \quad \begin{cases} \hat{u}_1(x_2, s) = [\Delta\hat{u}_1(s)/2] \exp[-\lambda(s)x_2], \\ \hat{\sigma}_{21}(x_2, s) - \hat{\sigma}_{21}^0(x_2, s) = -\lambda(s)G[\Delta\hat{u}_1(s)/2] \exp[-\lambda(s)x_2], \end{cases}$$

where

$$(10.16) \quad \lambda(s) = \sqrt{s/(\alpha + \beta s)}.$$

Thus the stress drop $\Delta\sigma_1(t) = \sigma_{21}^0(0, t) - \sigma_{21}(0, t)$ is related to the slip $\Delta u_1(t)$ by

$$(10.17) \quad \Delta\hat{\sigma}_1(s) = G\lambda(s)\Delta\hat{u}_1(s)/2.$$

The following special cases are of interest:

i) If the plate boundary undergoes a step function slip $\Delta u_1 U(t)$, where now Δu_1 is a constant, and is constrained subsequently from further slip, standard Laplace inversion procedures show that the stress drop is

$$(10.18) \quad \Delta\sigma_1(t) = [G\Delta u_1/2\sqrt{\beta}] \exp[-\alpha t/2\beta] I_0(\alpha t/2\beta),$$

where $I_0(\dots)$ is the modified Bessel function of zero order and $I_0(0) = 1$. For long times (*i.e.* $t \gg \beta/\alpha \approx 1.5$ to 15 years, eq. (10.10)) this reduces to

$$(10.19) \quad \Delta\sigma_1(t) = G\Delta u_1/2\sqrt{\pi\alpha t},$$

which would be valid for all time within the simple Elsasser model (*i.e.* for $\beta = 0$). The solution given by eq. (10.18) is plotted in fig. 21, where the time axis is scaled by the Maxwell relaxation time.

The displacement $u_1(x_2, t)$ at points within the plate is given by a complicated integral, but for large times this reduces to

$$(10.20) \quad u_1(x_2, t) = (\Delta u_1/2) \operatorname{erfc}[x_2/2\sqrt{\alpha t}],$$

which shows that the slip propagates out into the plate as a spreading diffusion wave. The average penetration distance of the disturbance is $x_2 \approx 2\sqrt{\alpha t}$ and the portion of the plate in which the major deformations are concentrated spreads over a distance of approximately $3\sqrt{\alpha t}$. Thus, for example, if we use the lower viscosity estimate, the penetration of the stress wave is $x_2 \approx 70$ km for $t = 0.5$ y, 100 km for 1 y, 170 km for 3 y, 320 km for 10 y and 1000 km for 100 y; the distances x_2 decrease by a factor of 3 for the larger viscosity estimate. These figures illustrate the manner in which stress redistributions from great earthquakes are propagated through the crust. For thrust boundaries, eq. (10.11) shows that α should be replaced by $2\alpha/(1 - \nu)$, so that the penetration distances x_2 are approximately 1.6 times greater at any given time.

The stress drop $\Delta\sigma_1(t)$ on the plate boundary decreases to zero for long times because the asthenosphere ultimately relaxes completely and is able to sustain no part of the stress drop. This is a deficiency of the infinitely-long-fault model. The actual long-term stress drop should be identified with the $\Delta\sigma_1$ that would remain in a plate uncoupled to its foundation and subject to the same slip. Since the actual rupture lengths in great earthquakes are seldom more than a

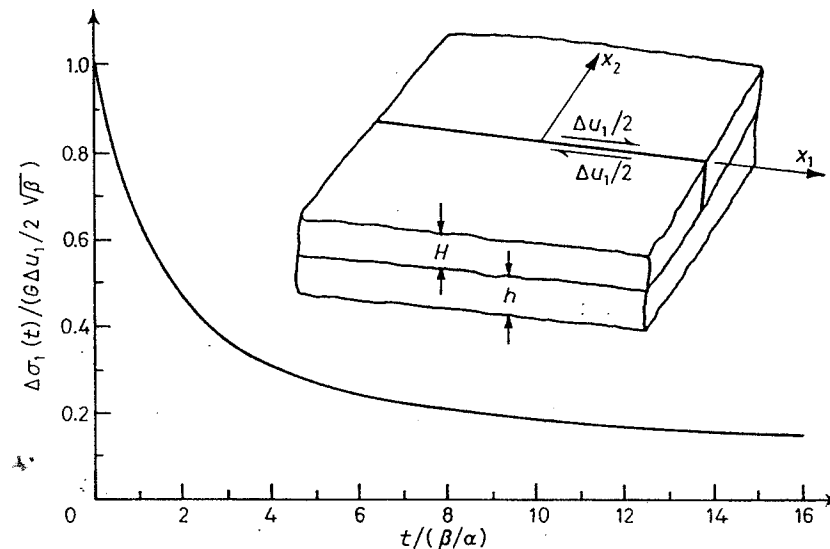


Fig. 21. - Thickness average shear stress drop $\Delta\sigma_1(t)$ associated with sudden thickness average slip Δu_1 which takes place at $t=0$ and is held fixed for subsequent time on infinitely long strike slip boundary; $\sqrt{\beta} \approx \pi H/4 \approx 70$ km, $\beta/\alpha =$ Maxwell relaxation time ≈ 1.5 y for $\eta = 5 \cdot 10^{18}$ Pa·s, 15 y for $\eta = 5 \cdot 10^{19}$ Pa·s.

few times H , the long-term value of $\Delta\sigma_1$ is of the same order but smaller than the initial stress drop. On the other hand, for the sequential occurrence of neighboring great earthquakes over a relatively short time period, compared to earthquake recurrence times, the infinite-fault model may be approximately valid.

Despite these deficiencies, the solution does illustrate the effects of asthenosphere coupling on shifting back onto the plate boundary the stress which is shed from it during the earthquake, as viscous relaxation processes take place. That is, σ_{21} increases in time, rather rapidly at first, as $\Delta\sigma_1$ decreases. This is an effect analogous to that of pore fluids discussed in subsect. 8'1, although of typically longer time scale (an analogously defined characteristic time for the process is $\approx 1.8 \beta/\alpha \approx 2.7$ to 27 years), and may be important as a factor causing aftershocks following great earthquakes.

ii) The complementary problem, which is that treated by ELSASSER [164] and BOTT and DEAN [165], considers the stress drop $\Delta\sigma_1$ to be constant on the

plate boundary. In this case the solution by Laplace inversion of (10.17) for the slip on the boundary is

$$(10.21) \quad \Delta u_1(t) = [2 \Delta \sigma_1 \sqrt{\beta/G}] \exp[-\alpha t/2\beta] [(1 + \alpha t/\beta) I_0(\alpha t/2\beta) + (\alpha t/\beta) I_1(\alpha t/2\beta)],$$

where $I_1(z) = dI_0(z)/dz$. For long times this reduces to

$$(10.22) \quad \Delta u_1(t) = (4 \Delta \sigma_1/G) \sqrt{\alpha t/\pi},$$

which is Elsasser's [164] solution; it applies for all time if $\beta = 0$. The corresponding long-time solution for the propagation of the stress relief into the plate is

$$(10.23) \quad \sigma_{21}^0 - \sigma_{21} = \Delta \sigma_1 \operatorname{erfc}(x_2/2\sqrt{\alpha t})$$

and this has a penetration history identical to that discussed earlier.

This solution is unrealistic in the sense that it allows slip to take place for all subsequent time on the plate boundary. However, unless the gain in strength following rupture is rapid by comparison to characteristic times of the solution, some of the implied post-seismic slip on the boundary may in fact actually occur. To address the problem further it is necessary to describe the time-dependent restrengthening process in more detail than is presently possible.

10'2. *A model of a propagating deformation front.* — LEHNER *et al.* [166] apply the generalized Elsasser model to an analysis of propagating through-crust deformation fronts. They first show that the governing equations (10.6) can be replaced, for strike-slip motions, by the simpler uncoupled model equation

$$(10.24) \quad (\alpha + \beta \partial/\partial t) [(1 + \nu)^2 \partial^2 u_1/\partial x_1^2 + \partial^2 u_1/\partial x_2^2] = \partial u_1/\partial t$$

for u_1 , with the associated stress alteration being given by (10.12). They show that the solutions of this equation reproduce closely the solutions of (10.6) relating arbitrary distributions of $\Delta u_1(x_1, t)$ along plate boundary to the associated distributions $\Delta \sigma_1(x_1, t)$ of stress drop, and do so exactly in the limits of short- and long-wavelength disturbances, as well as in all cases for which the foundation is relaxed ($\tau_\alpha = 0$). A model equation with analogous features for thrust boundaries is [166]

$$(10.25) \quad (\alpha + \beta \partial/\partial t) \{ [(1 + \nu)^2 (1 - \nu)/2] \partial^2 u_2/\partial x_1^2 + [2/(1 - \nu)] \partial^2 u_2/\partial x_2^2 \} = \partial u_2/\partial t$$

with stress alterations given by (10.13).

LEHNER *et al.* [166] model propagating deformation fronts of the strike slip type by seeking solutions of (10.24) in the steady-state form $u_1 = u_1(x_1 - vt, x_2)$ corresponding to uniformly moving dislocations and uniformly moving cracks

under prescribed stress drops. The work is intended to examine the hypothesis that viscous coupling to the asthenosphere might control the kinds of sequential occurrence of great earthquakes and crustal deformations discussed in sect. 9. The full details of solution are rather complicated. Here the results are reported only for the case of a zone of length l that moves uniformly along the plate boundary in a strike-slip mode and sustains a uniform thickness average stress drop $\Delta\sigma$. For simplicity of analysis the problem is modelled in the same manner as discussed in subsect. 8'3, namely as a uniform stress drop $\Delta\sigma$ acting only over a length l near the tip of a uniformly moving, semi-infinite mode-II crack (see inset diagram of fig. 22).

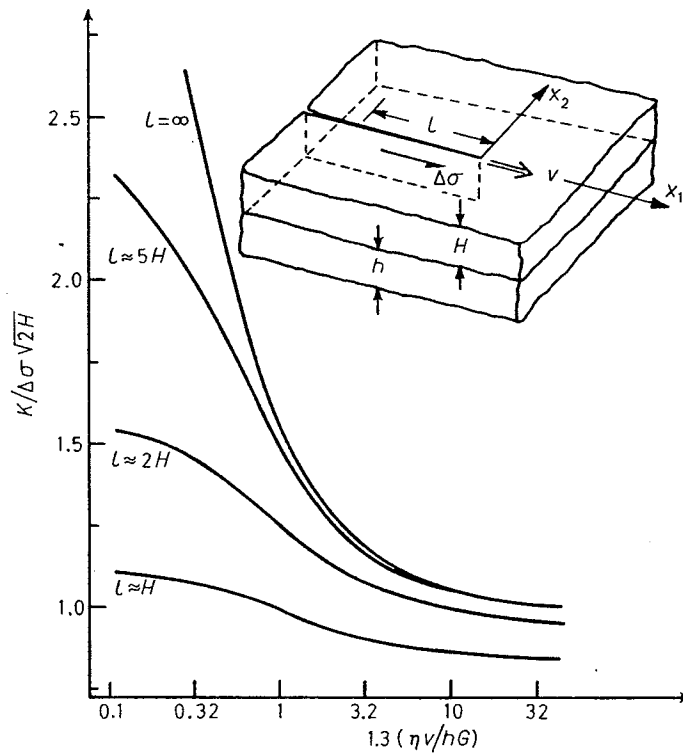


Fig. 22. - Concentration of stress (as measured by thickness average stress intensity factor K) at leading edge of a propagating through-crust deformation front, modelled by uniform stress drop $\Delta\sigma$ over length l .

A measure of the concentrated stress near the tip of the propagating zone is provided by the mode-II stress intensity factor, and this is found by solution of (10.24) under the stated boundary conditions to be given by [166]

$$(10.26) \quad K = \Delta\sigma\sqrt{2/a(v)} \operatorname{erf}[\sqrt{a(v)l}],$$

where $a(v)$ is a function of velocity given by

$$(10.27) \quad 2a(v) = \sqrt{(\alpha/\beta v)^2 + 4/\beta(1+v)^2} - \alpha/\beta v.$$

In the limit $v \rightarrow 0$, $a(v) \rightarrow 0$ and the foundation is completely relaxed. In that case the solution for K reduces to

$$(10.28) \quad K = \Delta\sigma\sqrt{8l/\pi},$$

which is the known solution for a similar loading on an elastic plate with traction-free lower surfaces. In the opposite limit, $v \rightarrow \infty$, the foundation is unrelaxed and responds only elastically; $a(v) \rightarrow 1/(1+v)\sqrt{\beta}$ in that limit and

$$(10.29) \quad K = \Delta\sigma\sqrt{2(1+v)\sqrt{\beta}} \operatorname{erf} \left[\sqrt{l/(1+v)\sqrt{\beta}} \right].$$

Note that, when the length l of the zone of stress drop is large compared to $(1+v)\sqrt{\beta}$ ($\approx H$), K becomes independent of l and is given by $K \approx \Delta\sigma\sqrt{2H}$. By comparison, the relaxed result of (10.28) has no limit as l increases.

The full solution of (10.26) for K has been plotted in fig. 22 as a function of v for various lengths l of the deformation zone. Here v is taken as 0.25 and for simplicity of interpretation $(1+v)\sqrt{\beta} \approx (1+v)\pi H/4$ has been replaced by H , and eq. (10.7) for α has been used so that the parameter $2v\sqrt{\beta}/(1+v)\alpha$ is written as $1.3\eta v/hG$. The stress concentration decreases with v as expected, because the foundation has less time for relaxation at higher speeds. For values of the dimensionless velocity parameter in excess of about 30, the result for K is within approximately 1% of the completely unrelaxed limit of (10.29), whereas significant increases in K (most marked for the great rupture lengths) occur as the velocity parameter decreases.

The results suggest that values of the velocity parameter between, say, 1 and 30 might correspond to the speeds of propagating rupture events of the type discussed in sect. 9. This is in good agreement with the reported speeds, which range from 50 to 100 km/y on the Anatolian fault, 100 km/y in northeast China and 150 to 270 km/y on the circum-Pacific belt. If one uses the crustal average shear modulus $G = 5.5 \cdot 10^{10}$ Pa and $h = 100$ km as before, and the Nur and Mavko [152] viscosity of $\eta = 5 \cdot 10^{18}$ Pa·s, the reported crustal propagation events correspond to values of the dimensionless velocity parameter $1.3\eta v/hG$ in fig. 22 ranging from 2 to 11, which falls into the anticipated range. The fit is a little less good but still convincing when the larger Cathles [155] viscosity of $4 \cdot 10^{19}$ Pa·s is used, in which case the reported crustal events correspond to values of the velocity parameter between 16 and 85. For the thrust-slip model, corresponding variations in K occur over a range of the dimensionless velocity parameter which is increased by a factor of $2/(1-v) \approx 8/3$. Hence the range of 1 to 30 for the strike-slip model is equivalent to a range of 3 to 80 for the thrust-slip model, and all the values inferred above from reported speeds fall essentially into this range.

These results support the concept that coupling between the elastic lithosphere and viscoelastic asthenosphere is a major process in controlling the progression of great earthquake ruptures along plate boundaries. They also

suggest that viscosities of the order 1 to $2 \cdot 10^{19}$ Pa·s are appropriate for earthquake processes. As remarked earlier, the effective viscosity associated with response to great earthquakes may be lower than that for processes which generate less stress in the asthenosphere, because of possible nonlinearities in actual asthenosphere rheology.

10.3. Stressing of segments of plate boundaries adjoining great earthquake ruptures. — For simplicity of discussion, the time-dependent concentration of stress on segments of a plate boundary adjoining a great earthquake rupture is measured here in terms of the thickness average stress intensity factor K , assuming a uniform thickness average stress drop $\Delta\sigma$ along a rupture length l . LEHNER *et al.* [166] analyze the time dependence of this stressing by developing appropriate solutions of (10.24). The intensity factor immediately after rupture is given by (10.29), which corresponds to unrelaxed, purely elastic asthenosphere response. The derivation of the long-time limit, for complete relaxation of the asthenosphere, is difficult and must be carried out in conjunction with some model which tells when post-seismic slip stops so that the offset Δu remains fixed for subsequent time. However, an upper bound to the relaxed value, which corresponds to the maintenance of a constant stress drop (and hence of continued post-seismic slip), is given by (10.28).

The ratio of this upper-bound relaxed value of K to the unrelaxed value immediately after rupture is approximately 1.34 when $l = H$, 1.67 when $l = 2H$ and 2.51 when $l = 5H$. The actual time dependence of the transition from the unrelaxed to relaxed limit will, of course, depend on the processes of viscous asthenosphere response, as embodied in (10.6), (10.24) and (10.25).

The results suggest that viscous coupling processes be explored further as a basis for determining time-dependent stress accumulation in regions adjoining great earthquakes, and similar concepts should be useful for the analysis of stress accumulation within seismic gap zones along earthquake belts.

* * *

The preparation of this review was supported by the NSF Geophysics Program and USGS Earthquake Hazards Reduction Program. I am grateful to P. G. RICHARDS (Lamont) for making available portions of the manuscript for his forthcoming book with AKI [1], and to J. W. RUDNICKI (University of Illinois) for a pre-publication copy of his fracture review [8]. Also, I am grateful for discussions with R. DMOWSKA (Polish Academy of Sciences) on elastodynamic spectra of earthquakes, with L. B. FREUND (Brown University) on dynamic crack tip stress fields, with F. K. LEHNER and V. C. LI (Brown University) on earthquake migration along plate boundaries, and with A. L. RUINA (Brown University) and J. H. DIETERICH (USGS) on constitutive models for frictional slip. Further, I am grateful to S. MANCINO (Brown University) for careful preparation of the typewritten manuscript.

REFERENCES

- [1] K. AKI and P. G. RICHARDS: *Quantitative Seismology* (in publication, San Francisco, Cal., 1980).
- [2] R. BURRIDGE and L. KNOPOFF: *Bull. Seismol. Soc. Am.*, **54**, 1875 (1964).
- [3] B. V. KOSTROV: *Publ. Inst. Geophys. Polish Acad. Sci.*, **62**, 25 (1973); also, *Izv. Akad. Nauk SSSR Fiz. Zemli*, **23**, 23 (1974).
- [4] S. DAS and K. AKI: *J. Geophys. Res.*, **82**, 5658 (1977).
- [5] J. D. ACHENBACH: *Wave Propagation in Elastic Solids* (Amsterdam, 1973).
- [6] J. R. RICE: *Fracture, an Advanced Treatise*, edited by H. LIEBOWITZ, Vol. 2 (New York, N. Y., 1968), p. 191.
- [7] L. B. FREUND: *J. Geophys. Res.*, **84**, 2199 (1979).
- [8] J. W. RUDNICKI: *Annual Review of Earth and Planetary Science*, edited by F. A. DONATH, Vol. 8 (in publication, Palo Alto, Cal., 1980).
- [9] T. C. HANKS and H. KANAMORI (special-issue associate editors): *J. Geophys. Res.*, **84**, No. B 5 (1979).
- [10] J. D. BYERLEE and M. WYSS (special-issue editors): *Pure Appl. Geophys.*, **116**, No. 4/5 (1978).
- [11] J. R. RICE: *Gerlands Beitr. Geophys.*, **88**, 91 (1979).
- [12] D. L. ANDERSON: *Science*, **187**, 1077 (1975).
- [13] B. BUDIANSKY and J. C. AMAZIGO: *J. Geophys. Res.*, **81**, 4897 (1976).
- [14] D. L. TURCOTTE, R. T. CLANCY, D. A. SPENCE and F. H. KULHAWY: *J. Geophys. Res.*, **84**, 2273 (1979).
- [15] J. EVERNDEN (Editor): USGS Open File Report 78-943 (U. S. Geological Survey, Menlo Park, Calif., 1978).
- [16] J. D. ESHELBY: *Progress in Solid Mechanics*, edited by I. SNEDDON and R. HILL, Vol. 2 (Amsterdam, 1961), p. 89; also, *Proc. R. Soc. London Ser. A*, **241**, 376 (1957).
- [17] G. BACKUS and M. MULCAHY: *Geophys. J. R. Astron. Soc.*, **46**, 341 (1976); **47**, 301 (1976).
- [18] A. T. DEHOOP: Doctoral Thesis (Delft University of Technology, Delft, 1958).
- [19] S. P. TIMOSHENKO and J. N. GOODIER: *Theory of Elasticity*, 2nd edition, Chap. 14 (New York, N. Y., 1951).
- [20] F. R. N. NABARRO: *Philos. Mag.*, **42**, 313 (1951).
- [21] A. V. VVEDENSKAYA: *Izv. Acad. Nauk SSSR Ser. Geofiz.*, No. 3, 277 (1956).
- [22] J. A. STEKETEE: *Can. J. Phys.*, **36**, 1168 (1958).
- [23] L. M. BALAKINA, E. F. SAVERENSKY and A. V. VVEDENSKAYA: *Physics and Chemistry of the Earth*, edited by L. H. AHRENS *et al.*, Vol. 4 (London, 1961), p. 211.
- [24] K. KHATTRI: *Earth Sci. Rev.*, **9**, No. 1, 19 (1973).
- [25] F. D. STACEY: *Physics of the Earth*, 2nd edition (New York, N. Y., 1977).
- [26] H. KANAMORI: *J. Geophys. Res.*, **82**, 2981 (1977).
- [27] N. HASKELL: *Bull. Seismol. Soc. Am.*, **54**, 1811 (1964); **56**, 25 (1966).
- [28] A. BEN-MENAHEN: *Bull. Seismol. Soc. Am.*, **51**, 401 (1961).
- [29] J. C. SAVAGE: *J. Geophys. Res.*, **77**, 3788 (1972).
- [30] J. N. BRUNE: *J. Geophys. Res.*, **75**, 4997 (1970); **76**, 5002 (1971).
- [31] J. N. BRUNE, R. J. ARCHULETA and S. HARTZELL: *J. Geophys. Res.*, **84**, 2262 (1979).
- [32] R. MADARIAGA: *Bull. Seismol. Soc. Am.*, **66**, 639 (1976).
- [33] R. MADARIAGA: *Geophys. J. R. Astron. Soc.*, **51**, 625 (1977).

- [34] P. G. RICHARDS: *Int. J. Solids Struct.*, **9**, 843 (1973); *Bull. Seismol. Soc. Am.*, **66**, 1 (1976).
- [35] S. DAS and K. AKI: *Geophys. J. R. Astron. Soc.*, **50**, 643 (1977).
- [36] D. J. ANDREWS: *J. Geophys. Res.*, **81**, 5679 (1976).
- [37] R. BURRIDGE, G. CONN and L. B. FREUND: *J. Geophys. Res.*, **84**, 2110 (1979).
- [38] B. V. KOSTROV: *J. Appl. Math. Mech. (USSR)*, **28**, 1077 (1964).
- [39] L. B. FREUND: *Mechanics Today*, edited by S. NEMAT-NASSER, Vol. **3** (New York, N. Y., 1976), p. 55; also, *The Mechanics of Fracture*, edited by F. ERDOGAN, ASME Appl. Mech. Div., Vol. **19** (New York, N. Y., 1976), p. 105.
- [40] R. MADARIAGA: *J. Geophys. Res.*, **84**, 2243 (1979).
- [41] A. MCGARR, S. M. SPOTTISWOODE, N. C. GAY and W. D. ORTLEPP: *J. Geophys. Res.*, **84**, 2251 (1979).
- [42] V. I. KEILIS-BOROK: *Ann. Geofis.*, **12**, 205 (1959).
- [43] J. H. DIETERICH: *J. Geophys. Res.*, **84**, 2161, 2169 (1979).
- [44] B. A. BILBY and J. D. ESHELBY: *Fracture, an Advanced Treatise*, edited by H. LIEBOWITZ, Vol. **1** (New York, N. Y., 1968), p. 99.
- [45] B. R. LAWN and T. R. WILSHAW: *Fracture of Brittle Solids* (Cambridge, 1975).
- [46] H. D. BUI: *Mécanique de la rupture fragile* (Paris, 1978).
- [47] N. I. MUSKHELISHVILI: *Some Basic Problems in the Mathematical Theory of Elasticity*, translated by J. R. M. RADOCK (Groningen, 1953); also, *Singular Integral Equations*, translated by J. R. M. RADOCK (Groningen, 1953).
- [48] G. R. IRWIN: *Structural Mechanics*, edited by J. N. GOODIER and N. J. HOFF (New York, N. Y., 1960), p. 557.
- [49] P. C. PARIS and G. C. SIH: *Fracture Toughness Testing and Its Applications*, ASTM Spec. Tech. Publ. 381 (Philadelphia, Penna., 1965), p. 30.
- [50] M. L. WILLIAMS: *J. Appl. Mech.*, **28**, 78 (1957).
- [51] H. TADA, P. C. PARIS and G. R. IRWIN: *The Stress Analysis of Cracks Handbook* (Hellertown, Penna., 1973).
- [52] B. A. BILBY, A. H. COTTRELL and K. H. SWINDEN: *Proc. R. Soc. London Ser. A*, **272**, 304 (1963).
- [53] J. WEERTMAN and J. R. WEERTMAN: *Elementary Dislocation Theory* (New York, N. Y., 1964).
- [54] R. DMOWSKA and B. V. KOSTROV: *Arch. Mech. Stosow.*, **25**, 421 (1973).
- [55] D. M. BARNETT and L. B. FREUND: *Bull. Seismol. Soc. Am.*, **66**, 667 (1967).
- [56] M. P. CLEARY: *Int. J. Num. Meth. Eng.*, **10**, 679 (1976).
- [57] W. D. STUART: *J. Geophys. Res.*, **84**, 1063 (1979).
- [58] W. D. STUART: *Science*, **203**, 907 (1979).
- [59] W. D. STUART and G. M. MAVKO: *J. Geophys. Res.*, **84**, 2153 (1979).
- [60] J. WEAVER: *Int. J. Solids Struct.*, **13**, 321 (1979).
- [61] B. BUDIANSKY and J. R. RICE: *Wave Motion*, **1**, 187 (1979).
- [62] J. R. RICE: *J. Appl. Mech.*, **35**, 379 (1968).
- [63] J. D. ESHELBY: *Inelastic Behavior of Solids*, edited by M. F. KANNINEN *et al.* (New York, N. Y., 1970), p. 77.
- [64] G. P. CHEREPANOV: *Int. J. Solids Struct.*, **4**, 811 (1968).
- [65] C. ATKINSON and J. D. ESHELBY: *Int. J. Fract. Mech.*, **4**, 3 (1968).
- [66] A. C. PALMER and J. R. RICE: *Proc. R. Soc. London Ser. A*, **332**, 527 (1973).
- [67] E. H. YOFFE: *Philos. Mag.*, **42**, 739 (1951).
- [68] B. COTTERELL and J. R. RICE: *Int. J. Fract. Mech.*, in publication (1980).
- [69] F. ERDOGAN and G. C. SIH: *ASME J. Basic Eng.*, **85**, 519 (1963).
- [70] W. F. BRACE and E. G. BOMBOLAKIS: *J. Geophys. Res.*, **68**, 3709 (1963).
- [71] W. F. BRACE, B. W. PAULDING and C. H. SCHOLZ: *J. Geophys. Res.*, **71**, 3939 (1966).

- [72] F. RUMMEL, H. J. ALHEID and C. FROHN: *Gerlands Beitr. Geophys.*, **88** (1979).
- [73] K. PALANISWAMY and W. G. KNAUSS: *Mechanics Today*, edited by S. NEMAT-NASSER, Vol. 4 (Oxford, 1978), p. 87.
- [74] M. I. HUSSEINI, D. B. JAVANOVICH, M. J. RANDALL and L. B. FREUND: *Geophys. J. R. Astron. Soc.*, **43**, 367 (1975).
- [75] J. R. RICE and D. A. SIMONS: *J. Geophys. Res.*, **81**, 5322 (1976).
- [76] A. A. GRIFFITH: *Philos. Trans. R. Soc. London Ser. A*, **221**, 163 (1920).
- [77] B. K. ATKINSON: *Int. J. Rock Mech. Min. Sci. Geomech. Abstr.*, **16**, 49 (1979).
- [78] C-Y. KING, R. D. NASON and D. TOCHER: *Philos. Trans. R. Soc. London Ser. A*, **274**, 355 (1973).
- [79] B. K. ATKINSON: *Pure Appl. Geophys.*, **117**, 1011 (1979).
- [80] J. B. WACHTMAN jr.: *J. Am. Ceram. Soc.*, **57**, 509 (1974).
- [81] J. R. RICE: *J. Mech. Phys. Solids*, **26**, 61 (1978).
- [82] C. H. SCHOLZ: *J. Geophys. Res.*, **77**, 2104 (1972).
- [83] J. W. CRAGGS: *J. Mech. Phys. Solids*, **8**, 66 (1960).
- [84] B. V. KOSTROV and L. V. NIKITIN: *Arch. Mech. Stosow.*, **22**, 750 (1970).
- [85] F. ERDOGAN: *Fracture, an Advanced Treatise*, edited by H. LIEBOWITZ, Vol. 2 (New York, N. Y., 1968).
- [86] B. V. KOSTROV: orally-reported results, Bad Honnef, Germany (1978).
- [87] A. LINDH, G. FUIS and C. MANTIS: *Science*, **201**, 56 (1978).
- [88] K. B. BROBERG: *Ark. Fys.*, **18**, 159 (1960).
- [89] R. BURRIDGE and J. R. WILLIS: *Proc. Cambridge Philos. Soc.*, **66**, 443 (1969).
- [90] B. V. KOSTROV: *Appl. Math. Mech. (trans. PMM)*, **30**, 1241 (1966).
- [91] J. [†]D. ESHELBY: *J. Mech. Phys. Solids*, **17**, 177 (1969).
- [92] L. B. FREUND: *J. Mech. Phys. Solids*, **20**, 141 (1972).
- [93] A. F. FOSSUM and L. B. FREUND: *J. Geophys. Res.*, **80**, 3343 (1975).
- [94] R. BURRIDGE and G. S. HALLIDAY: *Geophys. J. R. Astron. Soc.*, **25**, 261 (1971).
- [95] G. I. BARENBLATT: *Adv. Appl. Mech.*, **7**, 55 (1962).
- [96] D. S. DUGDALE: *J. Mech. Phys. Solids*, **8**, 100 (1960).
- [97] J. R. WILLIS: *J. Mech. Phys. Solids*, **15**, 151 (1967).
- [98] Y. IDA: *J. Geophys. Res.*, **77**, 3796 (1972).
- [99] J. R. RICE and M. P. CLEARY: *Rev. Geophys. Space Phys.*, **14**, 227 (1976).
- [100] N. BARTON: *Int. J. Rock Mech. Min. Sci. Geomech. Abstr.*, **13**, 255 (1976); also *Eng. Geol. (Sacramento)*, **7**, 287 (1973).
- [101] W. F. BRACE: *Tectonophysics*, **14**, 189 (1972).
- [102] J. H. COULSON: *Proceedings of the XIII 1971 U.S. Symposium on Rock Mechanics*, edited by E. J. CORDING (Urbana, Ill., 1972), p. 77.
- [103] N. BARTON: *Int. J. Rock Mech. Min. Sci.*, **9**, 579 (1972).
- [104] J. H. DIETERICH: *J. Geophys. Res.*, **77**, 3690 (1972).
- [105] J. H. DIETERICH: *Pure Appl. Geophys.*, **116**, 790 (1978).
- [106] L. W. TEUFEL and J. M. LOGAN: *Pure Appl. Geophys.*, **116**, 840 (1978).
- [107] A. L. RUINA: Ph. D. Thesis research, Brown University (1979).
- [108] E. H. RUTTER and D. H. MAINPRICE: *Pure Appl. Geophys.*, **116**, 634 (1978); also, *Gerlands Beitr. Geophys.*, **88** (1979).
- [109] J. W. RUDNICKI and J. R. RICE: *J. Mech. Phys. Solids*, **23**, 371 (1975).
- [110] J. W. RUDNICKI: *J. Geophys. Res.*, **82**, 844 (1977).
- [111] R. HILL: *J. Mech. Phys. Solids*, **10**, 1 (1962).
- [112] J. MANDEL: *Rheology and Soil Mechanics*, edited by P. SIREYS *et al.* (New York, N. Y., 1964).
- [113] T. Y. THOMAS: *Plastic Flow and Fracture in Solids* (New York, N. Y., 1961).
- [114] J. R. RICE: *Theoretical and Applied Mechanics*, edited by W. T. KOITER, Vol. 1 (Amsterdam, 1976), p. 207.

- [115] J. R. RICE and J. W. RUDNICKI: *Int. J. Solids Struct.*, in publication (1980).
- [116] A. NEEDLEMAN and J. R. RICE: *Mechanics of Sheet Metal Forming*, edited by D. P. KOISTINEN and N. M. WANG (New York, N. Y., 1978), p. 237.
- [117] W. R. WAWERSIK and C. FAIRHURST: *Int. J. Rock Mech. Min. Sci.*, **7**, 561 (1970).
- [118] W. R. WAWERSIK and W. F. BRACE: *Rock Mech.*, **3**, 61 (1971).
- [119] A. W. SKEMPTON: *Proceedings of the I Congress, International Society for Rock Mechanics*, Vol. **I** (Lisbon, 1966), p. 329.
- [120] N. R. MORGENSTERN and J. S. TCHALENKO: *Geotechnique*, **17**, 309 (1967).
- [121] J. BYERLEE, V. MJACHKIN, R. SUMMERS and O. VOEVODA: *Tectonophysics*, **44**, 161 (1978).
- [122] G. MANDL, J. N. J. DEJONG and A. MALTHA: *Rock Mech.*, **9**, 95 (1977).
- [123] J. R. RICE and J. W. RUDNICKI: *J. Geophys. Res.*, **84**, 2177 (1979).
- [124] A. NUR and J. R. BOOKER: *Science*, **175**, 885 (1972).
- [125] J. R. BOOKER: *J. Geophys. Res.*, **79**, 2037 (1974).
- [126] S. K. GARG, D. H. BROWNELL and J. W. PRITCHETT jr.: *J. Geophys. Res.*, **82**, 855 (1977).
- [127] J. R. RICE, J. W. RUDNICKI and D. A. SIMONS: *Int. J. Solids Struct.*, **14**, 289 (1978).
- [128] M. A. BIOT: *J. Appl. Phys.*, **12**, 155 (1941); also, *J. Appl. Phys.*, **26**, 182 (1955).
- [129] M. A. BIOT: *J. Geophys. Res.*, **78**, 4924 (1973).
- [130] N. NUR and J. D. BYERLEE: *J. Geophys. Res.*, **76**, 6414 (1971).
- [131] S. K. GARG and A. NUR: *J. Geophys. Res.*, **78**, 5911 (1973).
- [132] R. J. O'CONNELL and B. BUDIANSKY: *J. Geophys. Res.*, **79**, 5412 (1974).
- [133] D. È. ANDERSON and J. H. WHITCOMB: *J. Geophys. Res.*, **80**, 1497 (1975).
- [134] R. L. KOVACH, A. NUR, R. L. WESSON and R. ROBINSON: *Geology*, **3**, 437 (1975).
- [135] J. R. RICE: *Proceedings of the VIII U.S. National Congress of Applied Mechanics*, edited by R. E. KELLY (North Hollywood, Cal., 1979).
- [136] R. NASON and J. WEERTMAN: *J. Geophys. Res.*, **78**, 7745 (1973).
- [137] C. H. SCHOLZ, L. R. SYKES and Y. P. AGGARWAL: *Science*, **181**, 803 (1973).
- [138] J. H. WHITCOMB, J. D. GARMANY and D. L. ANDERSON: *Science*, **180**, 632 (1973).
- [139] A. NUR: *Bull. Seismol. Soc. Am.*, **78**, 1217 (1972).
- [140] V. I. MYACHKIN, G. A. SOBOLEV, N. A. DOLBILKINA, V. N. MOROZOW and V. B. PREOBRAZENSKY: *Tectonophysics*, **14**, 287 (1972).
- [141] V. I. MYACHKIN, B. V. KOSTROV, G. A. SOBOLEV and O. G. SHAMINA: *Izv. Akad. Nauk SSSR Fiz. Zemli*, **10**, 107 (1974).
- [142] O. REYNOLDS: *Philos. Mag.* (1885); reprinted in *Papers on Mechanical and Physical Subjects* by O. REYNOLDS, Vol. **2** (New York, N. Y., 1901), p. 203.
- [143] W. F. BRACE and R. J. MARTIN: *Int. J. Rock Mech. Min. Sci.*, **5**, 415 (1968).
- [144] K. TERZAGHI: *Sitzungsber. Akad. Wiss. Wien Math. Naturwiss. Kl. Abt. 2A*, **132**, 105 (1923).
- [145] J. R. RICE: *Advances in Civil Engineering Through Engineering Mechanics*, ASCE (New York, N. Y., 1977), p. 295.
- [146] J. R. RICE: *J. Geophys. Res.*, **80**, 1531 (1975).
- [147] J. R. RICE: *Plasticity and Soil Mechanics*, edited by A. C. PALMER (Cambridge, 1973), p. 263.
- [148] H. MIZUTANI, T. ISHIDO, T. YOKOBURA and S. OHNISI: *Geophys. Res. Lett.*, **3**, 365 (1976).
- [149] R. DMOWSKA: *Geophys. Surveys*, **3**, 157 (1977).
- [150] J. C. SAVAGE and W. H. PRESCOTT: *J. Geophys. Res.*, **83**, 3369 (1978).
- [151] D. A. SPENCE and D. L. TURCOTTE: *Proc. R. Soc. London Ser. A*, **365**, 121 (1979).
- [152] A. NUR and G. MAVKO: *Science*, **183**, 204 (1974).
- [153] K. RYBICKI: *Bull. Seismol. Soc. Am.*, **61**, 79 (1971).

- [154] R. K. McCONNELL: *J. Geophys. Res.*, **73**, 7089 (1968).
- [155] L. M. CATHLES: *The Viscosity of the Earth's Mantle* (Princeton, N. J., 1975).
- [156] H. J. MELOSH: *J. Geophys. Res.*, **81**, 5621 (1976).
- [157] S. A. FEDOTOV: *Tr. Inst. Fiz. Zemli Akad Nauk SSSR*, **36**, 66 (1965).
- [158] K. MOGI: *J. Phys. Earth*, **16**, 30 (1968).
- [159] K. MOGI: *Bull. Earthquake Res. Inst.*, **46**, 53 (1968).
- [160] C. F. RICHTER: *Elementary Seismology* (San Francisco, Cal., 1958).
- [161] N. N. AMBRASEYS: *Tectonophysics*, **9**, 143 (1970).
- [162] J. C. SAVAGE: *J. Geophys. Res.*, **76**, 1954 (1971).
- [163] C. H. SCHOLZ: *Nature (London)*, **267**, 121 (1977).
- [164] W. H. ELSASSER: *J. Geophys. Res.*, **74**, 4744 (1971).
- [165] M. H. P. BOTT and D. S. DEAN: *Nature (London)*, **243**, 339 (1973).
- [166] F. K. LEHNER, V. C. LI and J. R. RICE: research in preparation for publication (1979).

Reprinted From

Physics of the Earth's Interior

© 1980, LXXVIII Corso

Soc. Italiana di Fisica - Bologna - Italy